Light quark fields in lattice gauge theories

Dissertation
zur Erlangung des Doktorgrades
des Fachbereiches Physik
der Universität Hamburg

vorgelegt von
Claus Gebert
aus Frankfurt am Main

Hamburg
2002

Gutachter der Dissertation:	PrivDoz. Dr. István Montvay Prof. Dr. Gerhard Mack
Gutachter der Disputation:	PrivDoz. Dr. István Montvay Prof. Dr. Klaus Fredenhagen
Datum der Disputation:	3. 12. 2002
Vorsitzender des Prüfungsausschusses:	Prof. Dr. Jochen Bartels
Vorsitzender des Promotionsausschusses:	Prof. Dr. Günter Huber
Dekan des Fachbereichs Physik:	Prof. Dr. Friedrich-Wilhelm Büßer

Abstract

We study different quantum field theories at small fermion masses on the lattice. For this the TSMB algorithm is used and its cost dependence on the quark mass and the physical volume are studied. We reach quark masses of roughly one sixth of the strange quark mass. Extentions of the TSMB and improvements of the updating sequence are discussed. The appearance of chiral logarithms and the dependence of the pion mass-squared m_π^2 and the pion decay constant f_π on the quark mass in Chiral Perturbation Theory is studied. In a supersymmetric theory it is shown that a recovery of the SUSY Ward identity can be achieved when going to the massless limit. Finally we discuss domain wall fermions as a possibility to reduce chiral symmetry breaking and show that their dynamical simulation with the TSMB is feasable on today's computers.

Zusammenfassung

Wir betrachten verschiedene Quanten-Feldtheorien bei kleinen Fermionmassen auf dem Gitter. Hierfür wird der TSMB Algorithmus benutzt, und seine Kosten in Abhängigkeit von der Quarkmasse und dem physikalischen Volumen werden untersucht. Wir erreichen dabei Quarkmassen von etwa einem Sechstel der Strange-Quarkmasse. Das Auftreten von chiralen Logarithmen und die Quarkmassen-Abhängigkeit der Pionmasse-Quadrat m_π^2 und der Pion-Zerfallskonstante f_π werden studiert. Erweiterungen des TSMB und Verbesserungen der Update Sequenz werden diskutiert. In einer supersymmetrischen Theorie wird gezeigt, daß eine Wiederherstellung der SUSY Ward-Identität erreicht werden kann, wenn man zum masselosen Limes geht. Abschließend besprechen wir Domain Wall Fermionen als Möglichkeit, die Brechung der chiralen Symmetrie auf dem Gitter zu reduzieren, und zeigen, daß ihre dynamische Simulation mit dem TSMB auf heutigen Computern möglich ist.

Contents

Introduction **1**

1 The lattice, updating algorithms and measurement methods **7**
1.1 The lattice . . . 7
1.2 Traditional updating algorithms . . . 9
1.2.1 The Metropolis algorithm . . . 10
1.2.2 The HMC algorithm . . . 11
1.3 The TSMB algorithm . . . 12
1.3.1 Multi-boson algorithms . . . 12
1.3.2 Correction step . . . 13
1.3.3 Reweighting factor . . . 17
1.3.4 TSMB with many fermion flavours . . . 18
1.3.5 The sign of the determinant . . . 20
1.4 Updating algorithms for boson and gauge fields . . . 21
1.4.1 The gauge part of the action . . . 21
1.4.2 The boson part of the action . . . 22
1.4.3 Even-odd preconditioning . . . 24
1.5 Measurement of basic quantities . . . 26
1.5.1 Smearing techniques . . . 26
1.5.2 Sommer scale parameter r_0 . . . 27
1.5.3 Hadronic observables and quark mass definitions . . . 30
1.5.4 Autocorrelations and error analysis . . . 33

2 QCD simulations with light quark masses **39**
2.1 Quark mass dependence . . . 40
2.1.1 Scaling behaviour in the light quark mass region . . . 43
2.1.2 Determinant breakup . . . 46
2.2 Volume dependence . . . 49
2.3 Behaviour of the eigenvalue spectrum . . . 51
2.3.1 Eigenvalues of the hermitean fermion-matrix and reweighting factors 52
2.3.2 Eigenvalues of the non-hermitean fermion-matrix . . . 54
2.3.3 Negative eigenvalues . . . 56
2.4 Chiral logarithms and the applicability of Chiral Perturbation Theory . . . 58
2.4.1 Chiral Perturbation Theory (χPT) . . . 59
2.4.2 Chiral logarithms at light quark masses . . . 60

3 $N = 1$ Supersymmetric Yang-Mills theory **63**
3.1 Introduction of the theory . . . 63
3.2 SYM on the lattice . . . 65
3.3 Simulations for the Ward identity . . . 66
3.3.1 The sign of the Pfaffian . . . 67
3.3.2 The finite temperature phase transition . . . 68
3.4 The SUSY Ward identity . . . 73
3.4.1 The Ward identity in the continuum . . . 73
3.4.2 The Ward identity on the lattice . . . 74
3.4.3 Numerical investigation of the Ward identity . . . 79

4 Dynamical domain wall fermions **85**
4.1 Shamir's formulation . . . 86
4.2 Domain wall fermions with the TSMB algorithm . . . 88
4.3 First exploratory studies . . . 89
4.4 Other applications of domain wall fermions . . . 91

Conclusions **93**

A Notations and conventions **97**
A.1 Gamma matrices . . . 97
A.2 Generators of the $SU(N_c)$ . . . 98
A.2.1 Generators for $N_c = 2$ . . . 98
A.2.2 Generators for $N_c = 3$ . . . 98

B Implementation issues and usage notes on the programs **101**

References **107**

Acknowledgements **117**

Introduction

Since ancient times mankind has been fascinated by the elementary structures of nature. As early as 400 BC the Greek philosophers Demokrit and Leukipp considered the question of whether all ingredients of matter are indivisible. They formulated the belief that all matter of the universe is built up from a certain number of distinct, elementary particles called atoms (from the Greek átomos = indivisible). It took more than 2000 years until in the nineteenth century John Dalton showed that there are indeed smallest recognizable building blocks of which every chemical element consists, which he called atoms, and that they remain unchanged in all chemical and physical processes. However, despite the name they were given, these atoms are not uncuttable. But at the beginning of the twentieth century, works by J. J. Thomson and Robert Millikan gave evidence of the existence of the electron, and until the 1930s further works by Ernest Rutherford, Niels Bohr and James Chadwick established a solar system-like atomic model with electrons orbiting around a nucleus. A theoretical explanation of this model was given by Erwin Schrödinger, Werner Heisenberg and Max Born with the theory of quantum mechanics.

For a while it was believed that protons, neutrons and electrons were the elementary particles. But very soon further particles were discovered: the neutrino, proposed by Wolfgang Pauli to keep energy conservation in the β decay; the muon, identical to the electron but 200 times heavier; pions, proposed by Hideki Yukawa as the particle to mediate the force between the nucleons, i. e. the protons and the neutrons; kaons, mesons similar to the pions, but somewhat "strange" due to their relatively long lifetime.

Paul Dirac proposed even more particles. He tried to combine Albert Einstein's theory of Special Relativity with Quantum Theory. But while Quantum Mechanics is a theory of a single particle this is no longer possible once the theory is combined with the theory of Relativity. This is due to the equivalence between energy and mass in the theory of Relativity, stated by the relation $E = mc^2$. According to this equivalence, particles can be created and annihilated and every known elementary particle acquires an antiparticle. Therefore quantum theory has to be a theory of many particles, and hence a theory of fields, Quantum Field Theory (QFT). The first antiparticle, which was discovered by Carl Anderson, was the positron.

The first success of Quantum Field Theory was Quantum Electrodynamics (QED), a Quantum Field Theory of electron and photon interactions. This theory was mainly developed by Richard Feynman, Julian Schwinger and Shinichiro Tomonaga. One of the many successes of QED was the precise prediction of the anomalous magnetic moment $g_e - 2$. In 1967 Steven Weinberg, and independently Abdus Salam and Sheldon Glashow were able to unify the weak interactions, that are responsible for the β-decay, with the electromagnetic interactions to a theory of electroweak interactions, the Glashow-Weinberg-Salam (GWS)

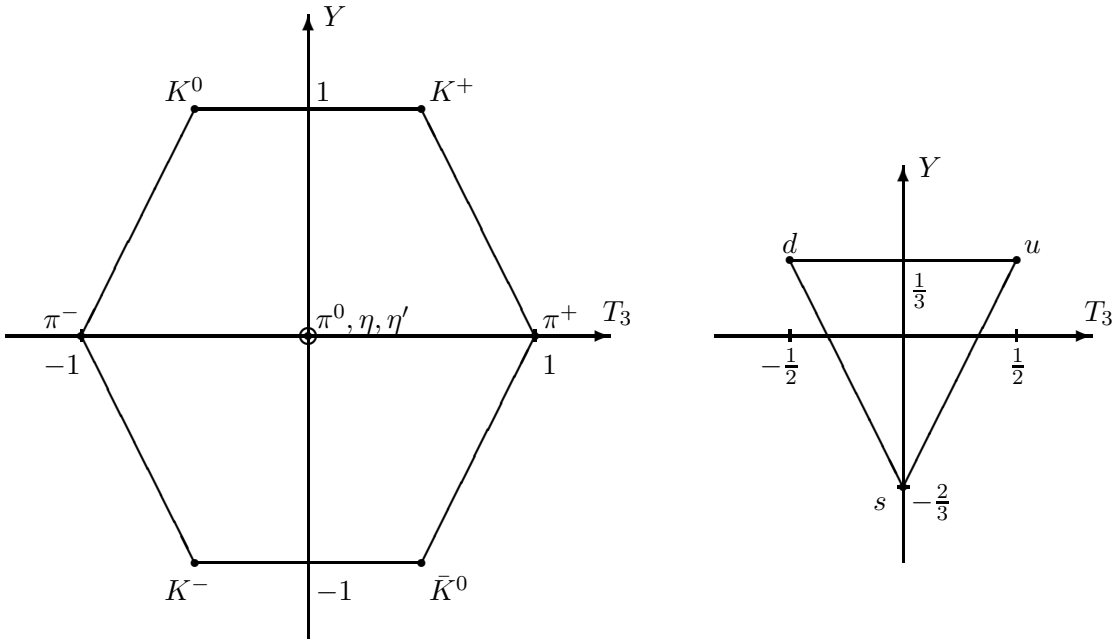

Figure 1: Left panel: Pseudoscalar meson octet together with the singlet η' classified by the strong hyper-charge Y and the isospin T_3. Right panel: The up, down and strange quarks as underlying particles of the Eightfold Way.

theory.

It was natural to hope that a Quantum Field Theory for the strong interactions between nucleons, pions, kaons and other hadronic particles was possible, too, and that it could order the particle zoo. A first step towards such a theory was made in 1955 by Murray Gell-Mann and Kazuhiko Nishijima by postulating new quantum numbers with corresponding conservation laws. In 1964 Murray Gell-Mann found, that all particles fall into families with properties mathematically the same as those of the "group of eight". The corresponding theory was called the Eightfold Way. In this theory the particles are organized into octets, e. g. the pseudoscalar meson octet in figure 1.

It was soon realized that the Eightfold Way could be explained by some underlying fundamental particles, the so-called quarks. Three of them were proposed, the up, down and strange quark. They have a new quantum number, called colour, and they interact through gluons. Requiring all free particles to be colourless allows for combining a quark with an antiquark, leading to the mesons, or combining three quarks, leading to the baryons. The corresponding Quantum Field Theory is Quantum Chromodynamics (QCD). Unlike QED, which is based on the Abelian group $U(1)$, QCD, as a theory of gauge fields, requires a more complicated group, the non-Abelian group $SU(3)$. The foundations to construct such Quantum Field Theories were laid by Chen-Ning Yang and Robert Mills.

The detection of the J/Ψ required to introduce a fourth quark called charm, which is heavier than the other three quarks. Later, even heavier quarks, the bottom and the top quark, also called beauty and truth, were proposed and found.

This theory of quarks and gluons, QCD, together with the GWS theory of the electroweak interactions and the so far undiscovered Higgs particle for the creation of electron,

neutrino and quark masses is the present Standard Model of elementary particle physics. The Standard Model has been tested down to distances of 10^{-16} cm, corresponding to energies of about 100 GeV. Up to now all experimental results are in agreement with the Standard Model.

Before the rise of Quantum Field Theories the principal technique for computations of particle interactions in relativistic quantum mechanics was time-dependent perturbation theory. This technique has been adapted for Quantum Field Theory to allow computations through Feynman diagrams. This perturbative treatment is very successful when applied to QED, and it is natural to try this for QCD, too. However in the late 1950s it was generally believed that the strong interactions cannot be described perturbatively. In fact it was recognized that a naive application of perturbation theory to a theory of mesons would fail because of the large coupling constant in the interactions between mesons and nucleons. In the framework of QCD this can be explained through quark confinement, the mechanism, due to which isolated quarks can never be seen in nature. Actually, this mechanism comes together with the asymptotic freedom, due to which the forces between quarks become small at small distances. Therefore one can use perturbation theory for small distances, i. e. high energies, but not for large distances or small energies, because in this strong coupling region non-perturbative effects dominate. Quark confinement and asymptotic freedom can be explained through the self-coupling of the gluons, an effect that doesn't exist for the photons in QED.

There are many questions in QCD that cannot be answered by perturbation theory. Thus, it is important to be able to calculate the observed hadron spectrum and decay rates from first principles. Such an approach would be very useful for finding out whether there are deviations in the spectrum or in the hadronic matrix elements that may indicate physics beyond the Standard Model. Furthermore one could check if QCD predicts further particles, e. g. particles only consisting of gluons. These and many other questions can only be answered in the strong coupling region. A tool for such non-perturbative calculations has been proposed in 1974 by Kenneth Wilson. The idea was to put Quantum Field Theory on a discretized Euclidean lattice, which leads to the correct results in the limit of vanishing lattice spacing. As Quantum Field Theory is related to Statistical Mechanics it is possible to compute observables on the lattice by performing Monte Carlo simulations on a computer. However it was soon realized, that with the computer power at the time, it was impossible to extract results of full QCD. Furthermore, there were technical problems with the representation of the quarks, the fermions of QCD. In a first approximation the fermions were therefore neglected from the lattice simulations, and in 2000 the CP-PACS collaboration was able to present a precise calculation in this so-called quenched approximation of the hadronic spectrum. These calculations confirmed the general structure of the observed spectrum, however with deviations of about 10%. Without further calculations including the fermions in the simulation, it cannot be decided if these deviations indicate a discrepancy between experiment and the theoretical framework of QCD, or if this is just a remnant of the quenched approximation.

With the Hybrid Monte Carlo (HMC) algorithm introduced in 1986 by Anthony Kennedy *et al.* it became possible to include the dynamical fermions, and another approach was presented by Martin Lüscher in 1994 with the multi-boson representation of fermions. However, simulations of full QCD are quite expensive, the computer power required is higher compared to quenched calculations by two or three orders of magnitude. In 1996 István Montvay invented the two-step multi-boson (TSMB) algorithm, which

promises to be more efficient especially at the phenomenologically important regime of light quark masses. Furthermore this algorithm unlike HMC allows the inclusion of any number of fermion flavours. And since the Eightfold Way with three quarks was so successful in describing the particle zoo it is natural to assume that three quarks are a good choice for the lattice simulations, too.

The study of this work is based on the TSMB algorithm. Therefore in the first chapter we will give more details on the lattice formulation, and the TSMB algorithm is explained in some detail along with new developments concerning this algorithm. In addition we explain how to extract some important masses of the hadron spectrum.

In the second chapter we study the performance of the algorithm in QCD at different quark masses and volumes. The physical masses of the up, down and strange quark are relatively light, and it is known that lattice algorithms suffer critical slowing down when approaching light quark masses. However this region is the important one because the scaling as predicted by Chiral Perturbation Theory (χPT) sets in at already light masses around a quarter of the strange quark mass, so that we put special emphasis on the scaling behaviour with the quark mass in this work. It has been proposed that the TSMB algorithm may have a less severe behaviour in this regime. We then apply χPT in this chapter to the next-to-leading order results for the pion mass-squared and the pion decay constant, where chiral logarithms appear.

Despite the great success of the Standard Model of elementary particle physics there are good reasons to believe in new physics beyond it. One reason is, that there is a general acceptance of the existence of a Grand Unified Theory (GUT). This follows the tradition of James Maxwell, who unified the electric and magnetic forces, and of the GWS theory of electroweak interactions. Apart from the Standard Model, which is valid in the microscopic regime, there is the theory of General Relativity by Albert Einstein, which is valid for cosmology. The best candidates for a GUT unifying the Standard Model and General Relativity are superstring theories, string theories that are based on supersymmetry. It is believed that supersymmetry may be crucial to these theories, because of the incompatibility of quantum mechanics and the General Theory of Relativity. Supersymmetry is a symmetry between bosons and fermions. Accordingly every known fermion has to have a bosonic partner, and every known boson needs a fermionic partner. Apart from their spin the supersymmetric partner should have the same properties. If nature can, indeed, be described by supersymmetry, then this symmetry has to be broken, because otherwise the supersymmetric partners would have the same masses and they would have already been discovered.

There are further important considerations that favour supersymmetric theories. The three gauge couplings of the Standard Model are running couplings, i. e. their strength depends on the energy scale. Extrapolating the known values of the coupling constants towards high energies as in figure 2, one sees that the three couplings never match simultaneously. This however would be desirable, because then a GUT with just one coupling above this scale can be expected. Due to less severe ultraviolet divergencies of supersymmetric theories such a matching could happen in these theories around $m_G \approx 2 \cdot 10^{16}$ GeV. Such a high scale however causes a further problem, the hierarchy problem. There is another scale $m_W \approx 100$ GeV, at which the breaking of the electroweak symmetry occurs. This scale is related to the mass of the Higgs particle, which is expected at a mass similar to m_W. But due to radiative corrections the Higgs should acquire a mass of the order of m_G, which is a contradiction to the much smaller scale m_W. It is still possible to fine

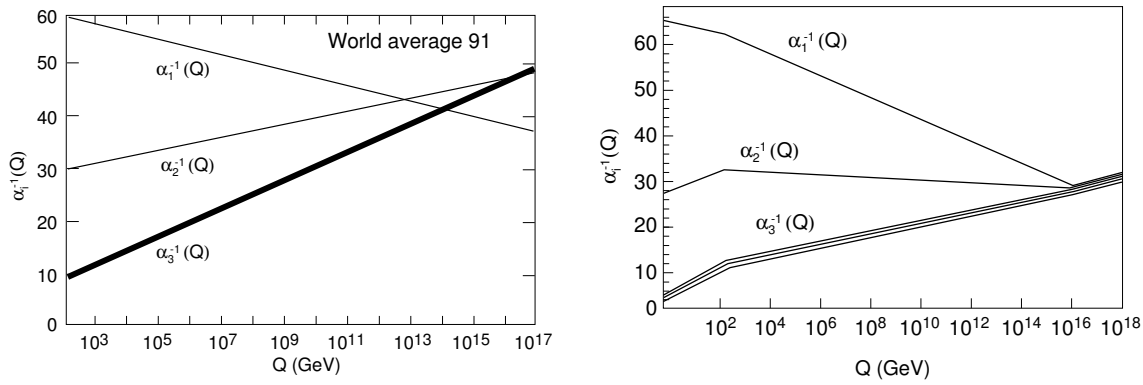

Figure 2: The running couplings in the Standard Model (left panel) and in a minimal supersymmetric Standard Model (right panel).

tune the Higgs mass towards the scale m_W. However, this would require fine tuning of the free parameters of the GUT up to 26 digits of precision in every order of perturbation theory, which is not regarded as a solution to the hierarchy problem. Supersymmetric theories, however, would show a better behaviour. Due to a non-renormalization theorem the radiative corrections of the order of m_G cancel each other and the free parameters of the GUT have to be fine tuned only once. This can be regarded as a partial solution of the hierarchy problem.

So far there are no experimental indications for supersymmetry. Indirect indications could be inferred from the measurement of the lifetime of a proton, where supersymmetric theories predict higher values than the Standard Model. However, the best evidence for supersymmetry would be the observation of a supersymmetric partner of an already known particle. There is hope that within a few years the new collider generation will find some of these supersymmetric particles. It is then to be decided which supersymmetric theory can be used to describe the new particle spectrum. As with the spectrum in QCD, this can only be done with lattice calculations. However, in the usual formulation supersymmetry is explicitly broken on the lattice, and it is only recovered for massless gluinos, the supersymmetric fermions. To keep supersymmetry breaking effects under control it is important to have a small gluino mass. The DESY-Münster-Roma Collaboration has explored the possibilities of simulating a simple supersymmetric model, the $N = 1$ Super-Yang-Mills theory. In chapter three we will report the results of this study, showing that it is feasable to approach supersymmetry on the lattice with sufficient precision by going close towards the massless limit.

Apart from the algorithmic problems of fermions on the lattice there is the further problem, that the most favoured formulation, the Wilson fermions, explicitly breaks chiral symmetry. Since in nature spontaneously broken chiral symmetry is a very important ingredient of the theory of low energy hadron interactions it would be advantageous to realize this symmetry at non-zero lattice spacings. There are now several possibilities to do this, but all of them are quite expensive, so they are usually only utilized in the quenched approximation. One way to restore chiral symmetry on the lattice is by using domain wall fermions, where a fifth dimension is introduced and the two chiralities of the lattice

fermions are exponentially bounded on the two boundaries in the fifth dimension. Since the extra cost of this formulation can be controlled by fixing the size in the fifth dimension, it is worthwhile trying to include dynamical domain wall fermions in the simulation of QCD. An exploratory study of this possibility is presented in the last chapter of this work.

In the appendices we give details on the computer programs that were used for the different steps needed for the lattice simulations of this work.

Chapter 1

The lattice, updating algorithms and measurement methods

In the first section of this chapter we will introduce the basic ingredients to formulate gauge theories on a lattice. After a short description of the Metropolis and the Hybrid Monte Carlo (HMC) algorithms we will explain the two-step multi-boson (TSMB) algorithm which is flexible enough to be used for the different theoretical models that are studied in this work. The TSMB algorithm represents the fermionic measure by means of bosonic fields, so we will further explain how to update the gauge and boson fields as required for the TSMB. Finally we explain how to extract some desired quantities from the configurations produced by the updating algorithm. To get reasonable results one should improve the signal-to-noise ratio by using different smearing techniques. These are described together with the measurement routines.

1.1 The lattice

The theory that was found to explain the hadron spectrum outlined in the introduction is the theory of quarks and gluons, Quantum Chromodynamics (QCD). The Lagrangian for this theory is given by

$$\mathcal{L}_{QCD}[A,\bar{\Psi},\Psi](x) = -\frac{1}{4}F^a_{\mu\nu}(x)F^{a,\mu\nu}(x) + \bar{\Psi}(x)\left(i\not{D} - m\right)\Psi(x). \tag{1.1}$$

Here the field strength tensor is

$$F^a_{\mu\nu} \equiv \partial_\mu A^a_\nu - \partial_\nu A^a_\mu + g f^{abc} A^b_\mu A^c_\nu, \tag{1.2}$$

Ψ and $\bar{\Psi}$ are the fields for N_f flavours of quarks and m is their mass. Furthermore $\not{D} = \gamma_\mu D_\mu$ is the covariant derivative.

In many ways this is a very formal statement. In perturbation theory, where an expansion in the gauge coupling g^2 is made, one encounters divergencies. These are handled by first regularizing the theory, e. g. by going to less than four dimensions $d - \epsilon$ and then subtracting the divergencies by some method, e. g. the $\overline{\text{MS}}$ scheme.

In 1974 Wilson proposed a new regulator, the lattice [1]. The lattice has proven to be a very useful tool because it allows to calculate non-perturbative effects, i. e. no expansion in

some parameter like the gauge coupling has to be made. The lattice regularizes the theory by discretizing a finite box of the Euclidean space-time. In this way one can compute expectation values of any observable $\mathcal{O}$, formally given by

$$\langle \mathcal{O} \rangle = \frac{\int \mathcal{D}[A]\mathcal{D}[\bar{\Psi}]\mathcal{D}[\Psi]\mathcal{O}e^{-S_{QCD}}}{\int \mathcal{D}[A]\mathcal{D}[\bar{\Psi}]\mathcal{D}[\Psi]e^{-S_{QCD}}}, \tag{1.3}$$

by using Monte Carlo techniques to generate ensembles of field configurations and calculate the observable $\mathcal{O}$ on them. In the limit of infinite volume and vanishing lattice spacing (continuum limit) the results from the lattice calculation will give a clearly non-perturbative determination of $\langle \mathcal{O} \rangle$.

While in the continuum the gauge field is given in terms of parallel transporters along infinitesimal distances this is no longer possible on a discretized Euclidean space-time (with pure imaginary time coordinates). Here the shortest possible distance is the lattice spacing a. This is the distance between a lattice point $x \in \Omega \subset \mathbb{Z}^4$ and its neighbour $x + \hat{\mu}$, where μ is one of the four directions of the lattice and $\hat{\mu}$ is a vector of length a in that direction. A parallel transporter connecting these two lattice points is given by the link $U_\mu(x) \in SU(N)$, with a link pointing in the other direction given by $U_\mu^\dagger(x)$. A link can be related to the gauge field through

$$U_\mu(x) \equiv e^{-aA_\mu(x)}. \tag{1.4}$$

The simplest gauge invariant object that can be formed out of such links is the plaquette, which is a closed loop in the $\mu\nu$-plane and with side length a. It is given by

$$U_{\mu\nu}(x) = U_\nu^\dagger(x) U_\mu^\dagger(x + \hat{\nu}) U_\nu(x + \hat{\mu}) U_\mu(x). \tag{1.5}$$

It can be used to describe the gauge part of the action. In [1] Wilson proposed to use

$$S_g[U] = \beta \sum_x \sum_{\mu\nu} \left(1 - \frac{1}{N} \mathrm{Re}\,\mathrm{Tr}\, U_{\mu\nu}(x) \right), \tag{1.6}$$

with the gauge coupling in a non-Abelian $SU(N)$ theory given by

$$\beta = \frac{2N}{g^2}. \tag{1.7}$$

For QCD we have $N = 3$.

The lattice formulation for the fermion fields causes more problems. Putting the fermions naively on the lattice one encounters more fermions in the continuum limit than originally asked for. This is the fermion doubling problem due to which there are $2^{d=4} = 16$ fermions, one at each corner of the Brillouin zone. This problem was already tackled by Wilson in his original work [1] by giving the additional fermions a mass at the order of the cutoff a^{-1}. In the continuum limit they decouple from the dynamics and they are localized in space-time. Hence only one fermion survives. This is achieved by

$$\begin{aligned} S_f[U, \bar{\Psi}, \Psi] &= \sum_x \bar{\Psi}^\dagger(x)\Psi(x) - \kappa \sum_x \sum_\mu \Big(\bar{\Psi}^\dagger(x + \hat{\mu}) U_\mu(x) (r + \gamma_\mu) \Psi(x) \\ &\qquad + \bar{\Psi}^\dagger(x - \hat{\mu}) U_\mu^\dagger(x - \hat{\mu}) (r - \gamma_\mu) \Psi(x) \Big) \qquad (1.8) \\ &= \sum_{xy} \bar{\Psi}^\dagger(y) \mathbf{Q}[U](y, x) \Psi(x), \qquad (1.9) \end{aligned}$$

the action for Wilson fermions. The Wilson-Dirac fermion matrix for the N_f fermion flavours is $\mathbf{Q}(y,x)$, and κ is the hopping parameter. The latter has to be tuned towards some critical value κ_{crit} if massless quarks are asked for, which is the best approximation for the lightest up and down quarks, and is still a good approximation to the strange quark because the natural scale is $\Lambda_{QCD} \simeq 200 - 300\,\mathrm{MeV}$. The need for this tuning with Wilson fermions is due to the fact that they break chiral symmetry. For a long time chiral symmetry breaking was considered to be unavoidable for any lattice fermion. This belief was formulated by Nielsen and Ninomiya in their famous no-go theorem [2]. However the last years brought progress in this direction, see chapter 4 for a possible solution and further remarks.

While it is relatively easy to simulate the pure gauge theory (1.6) there are further problems with the fermions when trying to find algorithms for them. This led the lattice community to neglect the fermions from the simulation and include them only in the process of measurement, i. e. when extracting the expectation values of observables. Hence only valence quarks are included but the virtual loops of the sea quarks are turned off. This is the so-called quenched approximation. This at first sight crude approximation is somewhat justified by good agreement with experiments for some results [3], where an agreement around 10% could be achieved. However there are other results where this approximation fails completely [4, 5], and for all the other quantities one would like to know if any deviation from the experiment is due to a bad theoretical model or just a remnant of the quenched approximation. Therefore the effort to include fermions in lattice simulations has been increased over the past years. In the next section we explain an algorithm that can be used for updating pure gauge theories and an algorithm, the HMC, that includes dynamical fermions, i. e. one that includes the virtual fermion loops. After that we will turn to the TSMB algorithm with the aim, that it allows a simulation of light quark fields.

1.2 Traditional updating algorithms

The aim of lattice simulations is to compute expectation values of observables formally given by (1.3). For any reasonable theory it is impossible to take all the possible field configurations and calculate the observables on them. By making a connection to statistical mechanics we can call e^{-S} the Boltzmann factor of the theory. Due to the large number of possible configurations only a small part of them will substantially contribute, namely those with a large Boltzmann factor. Since a consideration of all configurations is impossible, the Monte Carlo integration should make an importance sampling of the configurations, taking the Boltzmann factor as a weight. Updating algorithms for this importance sampling have to fulfill two important conditions. First of all they should fulfill detailed balance, a sufficient but not necessary condition. The transition probability for going from one configuration $[\varphi]$ to another $[\varphi']$ is given by $P([\varphi] \to [\varphi'])$. Detailed balance can then be formulated as

$$P([\varphi] \to [\varphi'])e^{-S[\varphi]} = P([\varphi'] \to [\varphi])e^{-S[\varphi']}. \tag{1.10}$$

The other important condition is ergodicity, i. e. it has to be possible to reach any other configuration with the updating step. For the transition probability this reads for any pair

of configurations

$$P([\varphi] \to [\varphi']) > 0. \tag{1.11}$$

This condition is called strong ergodicity. This doesn't mean that every elementary step has to fulfill this strong condition, because if enough of these elementary steps are combined to a bigger step, it is sufficient if this bigger step fulfills the strong ergodicity condition.

1.2.1 The Metropolis algorithm

The Metropolis algorithm was invented long before the lattice [6, 7]. The transition probablity for going from one configuration $[\varphi]$ to another $[\varphi']$ is given by

$$P([\varphi] \to [\varphi']) \propto F\left(\frac{e^{-S[\varphi']}}{e^{-S[\varphi]}}\right), \tag{1.12}$$

where $F:\ [0,\infty] \to [0,1]$ is a mapping that has to fulfill

$$\frac{F(x)}{F\left(\frac{1}{x}\right)} = x. \tag{1.13}$$

The usual choice is

$$F_1(x) = \min(1, x), \tag{1.14}$$

which gives the largest acceptance rate, an alternative choice is

$$F_2(x) = \frac{x}{1+x}, \tag{1.15}$$

where in general every new proposal $[\varphi']$ might be rejected. It is easily checked that this Metropolis algorithm fulfills detailed balance.

The procedure of the Metropolis algorithm is therefore to randomly choose some new trial configuration and according to (1.12) with the choice $F_1(x) = \min(1, x)$ accept the new configuration if the Boltzmann factor has increased, and otherwise accept only with a probability equal to the ratio of the Boltzmann factors. In practice not all possible trial configurations are considered but only those where the field is changed by a small amount on a single site. Strong ergodicity is then ensured by combining many elementary steps, i. e. repeating this local update several times over the complete lattice.

A generalization has been proposed in [8], where an arbitrary probability distribution $P_C([\varphi] \to [\varphi'])$ is allowed, and the acceptance probability

$$P_A([\varphi] \to [\varphi']) \propto \min\left(1, \frac{P_C([\varphi'] \to [\varphi])e^{-S[\varphi']}}{P_C([\varphi] \to [\varphi'])e^{-S[\varphi]}}\right) \tag{1.16}$$

compensates for P_C. The total transition probability is then given by $P = P_A P_C$.

Sometimes one can use special versions of the Metropolis algorithm, e. g. the heatbath [9,10] or the overrelaxation [11–14] algorithms. If applicable they are usually more efficient than the Metropolis algorithm in decorrelating the field configurations.

1.2.2 The HMC algorithm

In general the Metropolis algorithm can be applied to simulations including dynamical fermions. However a straightforward implementation would by highly inefficient due to the many calls to the fermion matrix multiplication. This difficulty led to developments of a completely different kind of upating algorithms based on difference equations (discretized differential equations). These algorithms work by integrating the difference equations with some finite step size $\Delta\tau$ and they require an extrapolation to zero step size. This extrapolation is very expensive and a possible source for systematic errors. Therefore it is advised to complement the difference equation integration by some correction scheme. This is the idea of the Hybrid Monte Carlo (HMC) algorithms [15].

HMC algorithms are based on the Hamiltonian

$$H[P,\pi,U,\phi] = \frac{1}{2}\sum_{x\mu j} P_{x\mu j}^2 + \frac{1}{2}\sum_x \pi_x^\dagger \pi_x + S[U,\phi], \tag{1.17}$$

with ϕ_x a pseudofermion field and

$$S[U,\phi] = S_g[U] + \phi^\dagger [Q^\dagger Q]^{-1}\phi \tag{1.18}$$

being the lattice action after performing the Gaussian integrals over the fermionic variables leading to a bosonic term in the action. The conjugate momentum of ϕ_x is π_x, and for the gauge field $U_{x\mu}$ it is an element of the Lie algebra $P_{x\mu} \in \mathcal{L}SU(N_c)$. Expectation values are then given by

$$\langle F\rangle = Z^{-1}\int [\mathrm{d}P\mathrm{d}U\,\mathrm{d}\pi\mathrm{d}\pi^\dagger\mathrm{d}\phi\mathrm{d}\phi^\dagger] e^{-H[P,\pi,U,\phi]} F[U,\phi]. \tag{1.19}$$

Performing e. g. leapfrog integrations of the discretized Hamiltonian equations a new configuration can be generated following the general ideas of algorithms based on molecular dynamics. This is done starting the conjugate momenta from a Gaussian distribution. The endpoint of a classical trajectory can be considered as a new trial configuration for a global accept-reject Metropolis step as in (1.16). The acceptance probability for the HMC is

$$P_A([P,U,\pi,\phi]\to[P',U',\pi',\phi']) \propto \min\left(1, e^{-H[P',U',\pi',\phi']+H[P,U,\pi,\phi]}\right). \tag{1.20}$$

The advantage of the algorithm is, that due to the underlying difference equation algorithm a global change of the configuration is possible that keeps the action in the vicinity of its minimum. Therefore the global Metropolis step can have a good acceptance rate, depending on the chosen step size $\Delta\tau$ of the integration.

In principle this algorithm can simulate QCD with dynamical fermions. However, it seems that its critical slowing down for small quark masses is too extreme, because apart from the usual critical slowing down there are indications for spikes in the quark force when going to lighter masses [16]. For the limited numerical precision of the calculations on a computer these spikes violate the important condition of reversability of the molecular dynamics integration and much smaller step sizes than without these spikes are needed. This increases the computing time for a new independent configuration. Therefore in the next section we turn towards the TSMB algorithm, which is based on the multi-boson representation of the fermion determinant and which is believed to have a better behaviour at small quark masses.

1.3 The TSMB algorithm

1.3.1 Multi-boson algorithms

The lattice version of the QCD action with Wilson fermions is

$$S[U,\bar{\Psi},\Psi] = S_g[U] + S_f[U,\bar{\Psi},\Psi], \tag{1.21}$$

with $S_g[U]$ given in (1.6) and $S_f[U,\bar{\Psi},\Psi]$ given in (1.9). After performing the Grassmann integration over $\bar{\Psi}$ and Ψ this action can be written as

$$S_{eff}[U] = S_g[U] - \log\det \mathbf{Q}[U]. \tag{1.22}$$

For N_f identical flavours, i. e. for degenerate masses, the fermion determinant $\mathbf{Q}$ is block diagonal and we can write

$$|\det \mathbf{Q}| = |\det Q|^{N_f}\,. \tag{1.23}$$

This is the starting point for all multi-boson algorithms. The inclusion of the fermion determinant is the most demanding task for a Monte-Carlo algorithm from the computational point of view. A first step towards the solution of this problem is the bosonisation of the determinant

$$\det(Q^\dagger Q) = \int \mathcal{D}[\phi^\dagger]\mathcal{D}[\phi] \exp\left(-\sum_{xy}\phi_y^\dagger \left[Q^\dagger Q\right]^{-1}_{yx}\phi_x\right), \tag{1.24}$$

where we can use the hermitean Wilson-Dirac fermion matrix $\tilde{Q} \equiv \gamma_5 Q = \tilde{Q}^\dagger$, with $\tilde{Q}^2 = Q^\dagger Q$ being positive definite (and bounded). However, this bosonisation cannot be the final solution since the effort to compute $[\tilde{Q}^2]^{-1}$ is prohibitively large. The idea of multi-boson algorithms as introduced by Lüscher [17] is to approximate the matrix inversion by some suitable polynomial $P^{(1)}_{n_1}$ of degree n_1

$$\begin{aligned} |\det Q|^{N_f} = \frac{1}{\det(\tilde{Q}^2)^{-N_f/2}} &\simeq \frac{1}{\det P^{(1)}_{n_1}(\tilde{Q}^2)} \\ &= \int \mathcal{D}[\phi^\dagger]\mathcal{D}[\phi] \exp\left(-\sum_{xy}\phi_y^\dagger P^{(1)}_{n_1}(\tilde{Q}^2)_{yx}\phi_x\right). \end{aligned} \tag{1.25}$$

The polynomial $P^{(1)}_{n_1}$ has to approximate the function $x^{-N_f/2}$ good enough for all eigenvalues of $\tilde{Q}^2$. With ε and λ being the smallest and largest ones of these eigenvalues the polynomial has to satisfy

$$\lim_{n_1\to\infty} P^{(1)}_{n_1}(x) = x^{-N_f/2} \qquad \forall x \in [\varepsilon,\lambda]. \tag{1.26}$$

The polynomial can always be written as a product of monomials

$$P^{(1)}_{n_1}(\tilde{Q}^2) = c_0 \prod_{i=1}^{n_1}(\tilde{Q}^2 - z_i), \tag{1.27}$$

where for even n_1 the roots z_i appear in complex conjugate pairs. Therefore one can write

$$P^{(1)}_{n_1}(\tilde{Q}^2) = r_0 \prod_{i=1}^{n_1}(\tilde{Q} - \rho_i^*)(\tilde{Q} - \rho_i), \tag{1.28}$$

which allows to write the fermion determinant as a multi-bosonic path integral

$$\left|\det(\tilde{Q}^2)\right|^{\frac{N_f}{2}} \overset{n_1\to\infty}{=} \int \mathcal{D}[\phi^\dagger]\mathcal{D}[\phi] \exp\left(-\sum_{xy}\sum_{i=1}^{n_1} \phi_y^{(i)\dagger}\left[(\tilde{Q}-\rho_i^*)(\tilde{Q}-\rho_i)\right]_{yx}\phi_x^{(i)}\right). \quad (1.29)$$

This is a major improvement compared to (1.24), the fermion matrix inversion could be traded off for a polynomial approximation. For very small condition numbers λ/ε one could try to run a Monte Carlo simulation applying this prescription. This has been tried in [18]. However, simulations should preferably be done in the vicinity of the physical light quark masses. Due to the relation

$$\sqrt{\lambda/\varepsilon} \propto (am_0)^{-1} \quad (1.30)$$

this implies very large condition numbers ($\sim 10^{5-6}$) and the simulation will become very costly or even impossible. It could become very costly because a very high polynomial order n_1 may be needed before the results loose their dependence on the polynomial approximation. This can be seen from the expression for the quadratically averaged error of the approximation:

$$\delta_{n_1}(\varepsilon,\lambda) \simeq \exp\left(-Cn_1\sqrt{\frac{\varepsilon}{\lambda}}\right). \quad (1.31)$$

Such large polynomial orders n_1 are, however, impossible, because the polynomial in its root-factorized representation as needed in this algorithm cannot be evaluated with the given 64 bit precision of today's computers. Another obstacle is the autocorrelation of configurations which dramatically increases with n_1.

1.3.2 Correction step

There exist several modifications of the multi-boson algorithm that allow simulations at quark masses around the strange quark mass. Here we will present the one which still allows for any number of fermions and is believed to allow for the smallest masses due to the fact that it does not rely on inversion routines, since these become slow or unstable for small masses.

With these modifications we want to reduce the polynomial order n_1 without increasing the error of our approximation. This seeming contradiction can be achieved by introducing a global Metropolis step to correct the error of the approximation of the first polynomial $P_{n_1}^{(1)}$ as proposed in [19]. In this way the quality of the approximation and therefore its polynomial order n_1 can be reduced to any value at the price of lower acceptance rates in the global correction step but without changing the quality of the final result. Indeed, the idea is to reduce n_1 just by so much that the acceptance rate is still reasonably high. We tried to aim at acceptance rates of 50% to 60%.

For going from one field configuration $[U]$ to another $[U']$ an exact updating sequence has to fulfill the following condition of detailed balance:

$$\frac{P(U\to U')}{P(U'\to U)} = \frac{e^{-S[U',\bar{\Psi},\Psi]}}{e^{-S[U,\bar{\Psi},\Psi]}} = \frac{\det\left(\tilde{Q}^{N_f}[U']P_{n_1}^{(1)}(\tilde{Q}^2[U'])\right)}{\det\left(\tilde{Q}^{N_f}[U]P_{n_1}^{(1)}(\tilde{Q}^2[U])\right)} \frac{e^{-S^{(n_1)}[U',\phi^\dagger,\phi]}}{e^{-S^{(n_1)}[U,\phi^\dagger,\phi]}}. \quad (1.32)$$

Since the updating with the polynomial $P_{n_1}^{(1)}$ fulfills

$$\frac{P_\phi(U \to U')}{P_\phi(U' \to U)} = \frac{e^{-S^{(n_1)}[U',\phi^\dagger,\phi]}}{e^{-S^{(n_1)}[U,\phi^\dagger,\phi]}} \tag{1.33}$$

we can use

$$P_{NC}(U \to U') = \min\left(1, \frac{\det\left(\tilde{Q}^{N_f}[U']P_{n_1}^{(1)}(\tilde{Q}^2[U'])\right)}{\det\left(\tilde{Q}^{N_f}[U]P_{n_1}^{(1)}(\tilde{Q}^2[U])\right)}\right) \tag{1.34}$$

as an acceptance probability in the global Metropolis correction step.

With this correction step we are now able to correct any inaccuracy of the polynomial approximation. However, we have explicitly reintroduced a determinant not much different in its form from the original fermion determinant. It is therefore clear that a direct computation of this determinant is impossible. Following the idea of the multi-boson algorithm we will approximate this new determinant by another polynomial $P_{n_2}^{(2)}$:

$$\left(\det\tilde{Q}^2\right)^{\frac{N_f}{2}} \det P_{n_1}^{(1)}(\tilde{Q}^2) \simeq \frac{1}{\det P_{n_2}^{(2)}(\tilde{Q}^2)} = \int\mathcal{D}[\eta^\dagger]\mathcal{D}[\eta]e^{-\eta^\dagger P_{n_2}^{(2)}(\tilde{Q}^2)\eta}, \tag{1.35}$$

and this second polynomial $P_{n_2}^{(2)}$ has to fulfill

$$\lim_{n_2\to\infty} P_{n_2}^{(2)}(x) = x^{-N_f/2}P_{n_1}^{(1)}(x)^{-1} \qquad \forall x \in [\varepsilon, \lambda]. \tag{1.36}$$

Therefore we have

$$\lim_{n_2\to\infty} P_{n_1}^{(1)}(x)P_{n_2}^{(2)}(x) = x^{-N_f/2} \qquad \forall x \in [\varepsilon, \lambda], \tag{1.37}$$

and we call this multi-boson updating sequence with global Metropolis correction step the "*two-step multi-boson*" (TSMB) algorithm [19]. The required probability can be calculated from the normalized Gaussian random distribution

$$\mathrm{d}\rho(\eta) = \frac{e^{-\eta^\dagger P_{n_2}^{(2)}(\tilde{Q}^2)\eta}}{\int\mathcal{D}[\tilde{\eta}^\dagger]\mathcal{D}[\tilde{\eta}]e^{-\tilde{\eta}^\dagger P_{n_2}^{(2)}(\tilde{Q}^2)\tilde{\eta}}}. \tag{1.38}$$

The acceptance rate in the Metropolis step is then given by

$$P_{NC}^{(n_2)}(U \to U') = \min\left(1, A^{(n_2)}(\eta, U \to U')\right) \tag{1.39}$$

with

$$A^{(n_2)}(\eta, U \to U') = \exp\left(-\eta^\dagger\left[P_{n_2}^{(2)}(\tilde{Q}[U']^2) - P_{n_2}^{(2)}(\tilde{Q}[U]^2)\right]\eta\right). \tag{1.40}$$

Of course the result from only one noisy estimator η may differ drastically from the result obtained from calculating the determinants exactly. However, since every transition $U \to U'$ may happen numerous times in each trajectory, on an average every configuration is accepted correctly. Therefore it is sufficient to use only one estimator η. We will discuss determinant breakup as a possible improvement of this situation in section 2.1.2, see also the end of this section.

Now, the remaining task is to generate Gaussian vectors with a normalization as in (1.38). It is very easy to generate Gaussian random vectors with a normal distribution

$$\mathrm{d}\rho(\bar{\eta}) = \frac{e^{-\bar{\eta}^\dagger \bar{\eta}}}{\int \mathcal{D}[\tilde{\eta}^\dagger]\mathcal{D}[\tilde{\eta}] e^{-\tilde{\eta}^\dagger \tilde{\eta}}}, \tag{1.41}$$

and from these one derives Gaussian random vectors according to (1.38) with

$$\eta = P_{n_2}^{(2)}(\tilde{Q}^2)^{-\frac{1}{2}}\bar{\eta}. \tag{1.42}$$

In principle $P_{n_2}^{(2)^{-\frac{1}{2}}}$ can be obtained by a generalization of the conjugate gradient inversion algorithm [20] but this needs multiple applications of $P_{n_2}^{(2)}(\tilde{Q}^2)$ on a vector. Therefore another polynomial $P_{n_3}^{(3)}$ is introduced for the inverse square root of $P_{n_2}^{(2)}$:

$$\lim_{n_3\to\infty} P_{n_3}^{(3)}(x) = P_{n_2}^{(2)}(x)^{-\frac{1}{2}} \qquad \forall x \in [\varepsilon', \lambda], \quad \varepsilon' \leq \varepsilon. \tag{1.43}$$

In order to avoid systematic errors the precision of this third polynomial should be very good. For the same reason it is preferable to choose a smaller lower limit ε' for the approximation. We usually choose to work with $\varepsilon' = \frac{1}{100}\varepsilon$ to be sure that the inverse square root of $P_{n_2}^{(2)}$ remains exact even if the smallest eigenvalue of $\tilde{Q}^2$ drops below ε occasionally. A practical way to obtain this polynomial is by Newton iteration:

$$P_{k+1}^{(3)} = \frac{1}{2}\left(P_k^{(3)} + \frac{1}{P_k^{(3)} P_{n_2}^{(2)}}\right) \qquad k = 0, 1, 2, \ldots. \tag{1.44}$$

Using this third polynomial the acceptance rate (1.40) can be written in terms of Gaussian normal vectors $\bar{\eta}$:

$$A^{(n_2)}(\bar{\eta}, U \to U') = \exp\left(-\left(P_{n_3}^{(3)}(\tilde{Q}[U]^2)\bar{\eta}\right)^\dagger P_{n_2}^{(2)}(\tilde{Q}[U']^2)\left(P_{n_3}^{(3)}(\tilde{Q}[U]^2)\bar{\eta}\right) + \bar{\eta}^\dagger\bar{\eta}\right). \tag{1.45}$$

Detailed balance

We will now comment further on the question in which situations the TSMB algorithm – as presented in this section – fulfills the condition of detailed balance. First remarks concerning the noisy estimator in the correction step were already made in the paragraph after equation (1.40).

In the Monte Carlo updating process we want to generate the canonical gauge field distribution

$$\omega[U] = \frac{e^{-S_g[U]}}{\det\left(P_{n_1}^{(1)}\left(\tilde{Q}[U]^2\right)\right)\det\left(P_{n_2}^{(2)}\left(\tilde{Q}[U]^2\right)\right)}. \tag{1.46}$$

The distribution for the gauge and the boson field is then given by

$$\omega[U, \phi] = \frac{e^{-S[U,\phi]}}{\det\left(P_{n_2}^{(2)}\left(\tilde{Q}[U]^2\right)\right)}. \tag{1.47}$$

A sufficient condition to make sure that this distribution is reproduced is the condition of detailed balance. This condition is fulfilled if the transition probability $P([U,\phi] \to [U',\phi'])$ of the Markov process behaves as follows:

$$\frac{P([U,\phi] \to [U',\phi'])}{P([U',\phi'] \to [U,\phi])} = \frac{e^{-S[U',\phi']} \det\left(P_{n_2}^{(2)}\left(\tilde{Q}[U]^2\right)\right)}{e^{-S[U,\phi]} \det\left(P_{n_2}^{(2)}\left(\tilde{Q}[U']^2\right)\right)}. \tag{1.48}$$

The transition probability can be devided into two parts, i. e. into the transition probability $P_{up}([U,\phi] \to [U',\phi'])$, which is realized by the local updates for the gauge and the boson fields and by the global heatbath for the boson fields, and into the transition probability $P_{NC}([U,\phi] \to [U',\phi'])$, which is the acceptance probability of the correction step. It thus follows that

$$P([U,\phi] \to [U',\phi']) = P_{up}([U,\phi] \to [U',\phi'])P_{NC}([U,\phi] \to [U',\phi']). \tag{1.49}$$

As far as $P_{up}([U,\phi] \to [U',\phi'])$ is concerned, it is known how to implement the updates so that detailed balance is satisfied for the action $S[U,\phi]$:

$$\frac{P_{up}([U,\phi] \to [U',\phi'])}{P_{up}([U',\phi'] \to [U,\phi])} = \frac{e^{-S[U',\phi']}}{e^{-S[U,\phi]}}. \tag{1.50}$$

To satisfy this condition we prefer to do double sweeps with opposite orders in the local updates. Other possibilities are to choose the order of the updates randomly or to use chequerboard decomposition.

Putting equations (1.49) and (1.50) into (1.48) we find the condition for detailed balance for the acceptance rate of the correction step

$$\frac{P_{NC}([U,\phi] \to [U',\phi'])}{P_{NC}([U',\phi'] \to [U,\phi])} = \frac{\det\left(P_{n_2}^{(2)}\left(\tilde{Q}[U]^2\right)\right)}{\det\left(P_{n_2}^{(2)}\left(\tilde{Q}[U']^2\right)\right)}. \tag{1.51}$$

This can be achieved if the new configuration $[U',\phi']$ is accepted with the probability

$$P_{NC}([U,\phi] \to [U',\phi']) \propto \min\left(1, \frac{\det\left(P_{n_2}^{(2)}\left(\tilde{Q}[U]^2\right)\right)}{\det\left(P_{n_2}^{(2)}\left(\tilde{Q}[U']^2\right)\right)}\right), \tag{1.52}$$

which is a global Metropolis step as discussed in section 1.2.1.

This proof of detailed balance was first given in [19]. Here we would like to make some further remarks about its implementation. A straightforward implementation would generate a new field configuration $[U',\phi']$, i. e. both new boson and gauge fields. If this new field configuration is accepted by the correction step then one proceeds with the update, otherwise the fields have to be restored to their respective values $[U,\phi]$ before the update can be continued. This, however, has one major drawback. There is no way to avoid the resetting of the gauge field, but it would cause a bottleneck of the algorithm if the boson fields had to be reset, too. The boson fields are represented by 12 complex numbers at each lattice point, the gauge field by 36. Therefore already at small numbers n_1 of boson fields the memory requirement of the program is dominated by the boson field ϕ,

and storing it twice would not be possible on many systems where memory is the limiting factor. It is therefore desired to avoid the setting back of the boson field.

Indeed, it is obvious that a gauge update together with the correction step still fulfills the condition of detailed balance because the proof given above works for this situation, too. Therefore, we have an algorithm that allows to update the boson fields with respect to detailed balance, and we have such an algorithm for the gauge field. However, one has to be careful because it is not true that every combination of algorithms that fulfill detailed balance is again an exact updating algorithm. An example for this is the updating of a field at two lattice points x and y. If we take an algorithm that can make an update on one of these points respecting detailed balance, then it is wrong to do the update in a simple alternating order. A correct way is to update x once, then y twice and then again x once. This is equivalent to making two consecutive updates on x followed by two consecutive updates on y and then repeating this procedure.

This argument can be used for the TSMB algorithm, too. Knowing how to do an exact update both for the boson and the gauge field, we can combine them by doing two updates on the boson field followed by two updates with correction step on the gauge field. This is what is done throughout the simulations used in this work.

Usually these two boson field updates, each of them consisting of some number of boson heatbath and overrelaxation sweeps, completely decorrelate the boson field. If no new gauge field is accepted in the two consecutive gauge updates one may try to gain some computer time by skipping the boson field updates until a new gauge field is accepted. Due to the decorrelation of the boson field this should still fulfill the condition of detailed balance, but the effect on the autocorrelation remains to be seen.

1.3.3 Reweighting factor

The correction step introduced in section 1.3.2 allows to keep n_1 fixed and the algorithm becomes exact in the limit of infinitely high polynomial order n_2. But this is still not convenient for a practical simulation, because this would require several simulations with different values of n_2 in order to be able to extrapolate to $n_2 \to \infty$. It is better to fix n_2 to some relatively high order and correct for the remaining approximation errors in the measurements. This indeed can be done by reweighting the configurations [21], here $N_f = 2$ was used. In [22] it was shown how to get it for general flavour number N_f.

With this reweighting factor $R[U]$ the reweighted expectation value $\langle \mathcal{O} \rangle$ can be calculated as follows:

$$\langle \mathcal{O} \rangle = \frac{\langle \mathcal{O} R[U] \rangle}{\langle R[U] \rangle}. \tag{1.53}$$

Again one has several ways to compute the reweighting factor. Calculating all eigenvalues explicitly or to use preconditioned inversions is either impossible or problematic, so again we calculate it using another polynomial:

$$\lim_{n_4 \to \infty} P^{(1)}_{n_1}(x) P^{(2)}_{n_2}(x) P^{(4)}_{n_4}(x) = x^{-N_f/2} \qquad \forall x \in [\varepsilon, \lambda]. \tag{1.54}$$

The reweighting factor $R[U]$ is then given by

$$R[U] = \frac{1}{\det P^{(4)}_{n_4}(\tilde{Q}^2)} = \frac{\int \mathcal{D}[\eta^\dagger] \mathcal{D}[\eta] e^{-\eta^\dagger P^{(4)}_{n_4}(\tilde{Q}^2) \eta}}{\int \mathcal{D}[\eta^\dagger] \mathcal{D}[\eta] e^{-\eta^\dagger \eta}}. \tag{1.55}$$

Using this representation the reweighting factor can be determined stochastically using noisy estimators, as can be seen by considering an extended update procedure on a set of variables including η. With the same argument as for the case of the noisy estimator in the correction step any fixed number of noisy estimators will lead to a correct determination. Here we took four to six estimators. Unlike with the correction step any number of noisy estimators is allowed for the reweighting factor, detailed balance will always be satisfied.

It is now sufficient to measure quantities $\mathcal{O}$ from only one simulation but with different sets of reweighting factors corresponding to sets of polynomials with different polynomial orders n_4. In practice n_2 is already so large that the inclusion of the reweighting factor has only a negligible effect, and therefore only one set of reweighting factors is used.

There might be some exceptional configurations with very small eigenvalues of $\tilde{Q}^2$ below 10^{-7}. In this case the polynomial $P_{n_4}^{(4)}(x)$ cannot approximate the desired behaviour if reasonable polynomial orders should be used. In addition the value of $R[U]$ will be very noisy if few noisy estimators are used. Therefore it is very helpful to augment this reweighting factor determination with the explicit calculation of some of the smallest eigenvalues. For this some ε', typically chosen slightly above ε, is fixed and all eigenvalues with corresponding eigenvectors of $\tilde{Q}^2$ are calculated that are below this ε'. For these eigenvalues the exact reweighting is given by $P_{n_1}^{(1)}(\lambda)P_{n_2}^{(2)}(\lambda)\lambda^{N_f/2}$ and the reweighting factor takes the form

$$R[U] \simeq \prod_{\lambda<\varepsilon'} P_{n_1}^{(1)}(\lambda)P_{n_2}^{(2)}(\lambda)\lambda^{\frac{N_f}{2}} \prod_{\lambda>\varepsilon'} P_{n_4}^{(4)}(\lambda)^{-1}. \tag{1.56}$$

The second factor can be calculated as before, but the eigenspace of the set of smallest eigenvalues that are taken into account with the first factor has to be projected out from the considered noisy estimators.

1.3.4 TSMB with many fermion flavours

So far we were making use of the fact that the fermion matrix $\mathbf{Q}$ for N_f fermion flavours is block-diagonal, with each of its blocks consisting out of the fermion matrix Q for one flavour.

In the physical situation the up and down quark are very light, while the strange quark mass is somewhat heavier. As lattice simulations manage to run at increasingly light quark masses it becomes desireable to give the different quarks different masses. This is possible with a minor extension of the TSMB algorithm.

Let's assume two different quark masses, $N_f^{(1)}$ quark flavours of the one mass and $N_f^{(2)}$ flavours of the other mass. The fermion determinant can then be written as

$$|\det \mathbf{Q}| = \left|\det Q_{(1)}\right|^{N_f^{(1)}} \left|\det Q_{(2)}\right|^{N_f^{(2)}}. \tag{1.57}$$

The original multi-boson algorithm without correction step can be applied to this measure in a straightforward way:

$$\frac{1}{\det(\tilde{Q}_{(1)}^2)^{-N_f^{(1)}/2}} \frac{1}{\det(\tilde{Q}_{(2)}^2)^{-N_f^{(2)}/2}} \simeq \frac{1}{\det P_{n_1}^{(1,1)}(\tilde{Q}_{(1)}^2)} \frac{1}{\det P_{n_1}^{(1,2)}(\tilde{Q}_{(2)}^2)}. \tag{1.58}$$

The polynomials now have to approximate the function $x^{-N_f^{(1,2)}/2}$ good enough for all eigenvalues of the corresponding fermion matrix $\tilde{Q}^2_{(1,2)}$ with a similar definition as before (1.26).

A second approximation that will be realized by the correction step can be used, too:

$$\frac{1}{\det(\tilde{Q}^2_{(1)})^{-N_f^{(1)}/2}}\frac{1}{\det(\tilde{Q}^2_{(2)})^{-N_f^{(2)}/2}} \simeq \prod_{f=1}^{2}\frac{1}{\det P_{n_1}^{(1,f)}(\tilde{Q}^2_{(f)})\det P_{n_2}^{(2,f)}(\tilde{Q}^2_{(f)})}. \tag{1.59}$$

Instead of (1.46) the gauge field distribution is now

$$\omega[U] = \frac{e^{-S_g[U]}}{\prod_{f=1}^{2}\det\left(P_{n_1}^{(1,f)}\left(\tilde{Q}_{(f)}[U]^2\right)\right)\det\left(P_{n_2}^{(2,f)}\left(\tilde{Q}_{(f)}[U]^2\right)\right)}. \tag{1.60}$$

The condition of detailed balance for the correction step acceptance (1.51) translates to

$$\frac{P_{NC}([U,\phi]\to[U',\phi'])}{P_{NC}([U',\phi']\to[U,\phi])} = \prod_{f=1}^{2}\frac{\det\left(P_{n_2}^{(2,f)}\left(\tilde{Q}_{(f)}[U]^2\right)\right)}{\det\left(P_{n_2}^{(2,f)}\left(\tilde{Q}_{(f)}[U']^2\right)\right)} \tag{1.61}$$

$$= \frac{\int\mathcal{D}[\eta_1^\dagger]\mathcal{D}[\eta_1]\mathcal{D}[\eta_2^\dagger]\mathcal{D}[\eta_2]e^{-\sum_{f=1}^{2}\eta_f^\dagger P_{n_2}^{(2,f)}(\tilde{Q}_{(f)}[U']^2)\eta_f}}{\int\mathcal{D}[\eta_1^\dagger]\mathcal{D}[\eta_1]\mathcal{D}[\eta_2^\dagger]\mathcal{D}[\eta_2]e^{-\sum_{f=1}^{2}\eta_f^\dagger P_{n_2}^{(2,f)}(\tilde{Q}_{(f)}[U]^2)\eta_f}}. \tag{1.62}$$

For a noisy Metropolis acceptance step we therefore need a Gaussian distribution

$$\mathrm{d}\rho(\eta_1,\eta_2) = \frac{e^{-\sum_{f=1}^{2}\eta_f^\dagger P_{n_2}^{(2,f)}(\tilde{Q}_{(f)}[U]^2)\eta_f}}{\int\mathcal{D}[\tilde{\eta}_1^\dagger]\mathcal{D}[\tilde{\eta}_1]\mathcal{D}[\tilde{\eta}_2^\dagger]\mathcal{D}[\tilde{\eta}_2]e^{-\sum_{f=1}^{2}\eta_f^\dagger P_{n_2}^{(2,f)}(\tilde{Q}_{(f)}[U]^2)\eta_f}} \tag{1.63}$$

and the acceptance rate is then given by

$$P_{NC}^{(n_2)}(U\to U') = \min\left(1, A^{(n_2)}(\eta_1,\eta_2,U\to U')\right) \tag{1.64}$$

with

$$A^{(n_2)}(\eta_1,\eta_2,U\to U') = \exp\left(-\sum_{f=1}^{2}\eta_f^\dagger\left[P_{n_2}^{(2,f)}(\tilde{Q}_{(f)}[U']^2) - P_{n_2}^{(2,f)}(\tilde{Q}_{(f)}[U]^2)\right]\eta_f\right). \tag{1.65}$$

With these modifications it is possible to run simulations with quark flavours that have different masses, i. e. with several κ values. In [23] it was proposed to do simulations with $N_f = 2+1$ quark flavours instead of $N_f = 3$. This should speed up the simulations if the single quark is kept fixed at a much larger quark mass around the strange quark mass. Furthermore this is closer to the physical situation, something that is not needed for chiral perturbation theory, but might be useful otherwise.

Besides the benefits of $N_f = 2+1$ this modification of the algorithm can be used in other promising ways. In [24, 25] a similar method was used for a determinant breakup to reduce the variance of the noisy estimator in the correction step. Although this increases the costs of each update cycle they find in their algorithm that in this way the total autocorrelation length is reduced significantly. We study this determinant breakup in the context of the TSMB algorithm in section 2.1.2.

1.3.5 The sign of the determinant

According to (1.25) the TSMB algorithm simulates a theory with a fermionic measure $|\det Q|^{N_f}$ and therefore neglects the sign of the determinant for odd N_f. To have the correct measure this sign has to be included somewhere in the measurement process, and a natural way is in the reweighting factor. This is of course only needed if N_f is odd while for an even number of fermion flavours the fermionic measure will always be positive. Since the best description of the physical situation is with either $N_f = 3$ or better with $N_f = 2+1$ this sign will play a role, and a priori it is not known how many configurations will have different signs and what influence that will have. This sign has to be considered in other applications of the TSMB algorithm, too, e. g. in the $N = 1$ supersymmetric Yang-Mills theory as considered in chapter 3 or in two-colour QCD with a chemical quark potential μ [26, 27].

One efficient method to determine the sign of the determinant is to consider the spectral flow of the smallest eigenvalues. It is known that at $\kappa_{val} < \frac{1}{8}$ and for $r = 1$ the fermion determinant has a positive sign [28]. By increasing κ_{val} in small steps up to the simulation parameter κ_{sea} one can count the number of zero level crossings of the smallest eigenvalues. The sign of the fermion determinant is given by

$$\operatorname{sign}(\det Q) = (-1)^{\#\{\text{zero-level crossings}\}}. \tag{1.66}$$

Therefore the sign does not cause many problems from the theoretical point of view. However, there could occur a practical problem. If there is some clearly non-zero fraction of configurations that has a negative sign, then it could be that for some quantities the expectation value for that observable on the subset of configurations with positive sign is of the same order as on the subset of configurations with negative sign. The correct expectation value will then be the difference of these two results. This will lead to large statistical uncertainties in the final result due to the effect of cancellation even if the determinations on the two different subsets were quite precise. In this case it would be practically impossible to do measurements.

Luckily practice has shown that nearly always the configurations with negative sign of the determinant come with very small reweighting factors and are so few that their sign can be neglected completely [29, 30]. A significant number of configurations with negative sign seems to be connected to the appearance of phase transitions. Indeed it was shown that in these cases it is crucial to include the sign, and that only then a correct result was obtained, while this was not the case when using other algorithms where sign changes seem to be highly surpressed [27]. However, in that study they suffer from the effect of cancellation.

Throughout all the considered cases in this work no sign problem is expected. However, one cannot rely on that and therefore it has to by checked carefully in every simulation. For this the spectral flow method is used, and in section 2.3.3 this method is compared with a direct computation of the eigenvalues of the non-hermitean fermion matrix.

The spectral flow method suggests that a negative sign is related to exceptionally small eigenvalues due to the needed zero level crossing. It is therefore not needed to compute the sign of the determinant on every configuration. Instead one should pick a small subsample together with all those configurations that have exceptionally small eigenvalues. If on this subsample the number of configurations with negative sign is statistically insignificant then the sign doesn't have to be calculated for the remaining configurations.

1.4 Updating algorithms for boson and gauge fields

The TSMB algorithm presented in section 1.3 trades off the fermion determinant at the price of introducing pseudofermionic boson fields. In this section we will present the updating algorithms for these fields as they are used in this work. We will especially emphasise on the peculiarities that have to be considered if these algorithms are to be used in the context of the TSMB algorithm. In addition we will have a look at the updating of the gauge fields.

The algorithms presented here are local updates, and therefore they are not affected by the accumulation of roundoff errors leading to possible violations of the reversibility of the HMC algorithm. Despite being a global update this is also true for the global heatbath algorithm.

1.4.1 The gauge part of the action

There are quite a few algorithms that can be used to update the gauge field in a pure gauge theory. One of the first algorithms that has been introduced is the Metropolis algorithm [6], see also section 1.2.1, which is applicable under nearly all circumstances that are relevant in field theory. Its idea is to propose a new gauge field $U'_{x,\mu}$ and to accept it with probability

$$P_{acc}(U'_{x,\mu} \leftarrow U_{x,\mu}) = \min(1, \exp(S[U] - S[U'])). \tag{1.67}$$

It would be a waste of time to calculate the action completely for every link that has to be updated. Instead one computes only that part of the action that may change with the specific link. In case of the Wilson gauge action this term can be written as a product of that link with the so-called staple $\Delta S_{x,\mu}$. The acceptance rate is then given by:

$$P_{acc}(U'_{x,\mu} \leftarrow U_{x,\mu}) = \min(1, \exp((U_{x,\mu} - U'_{x,\mu})\Delta S_{x,\mu})). \tag{1.68}$$

In this way one can perform e. g. a N-step multihit Metropolis update while the corresponding staple has to be calculated only once. Other algorithms that can be used efficiently with the staples description are the gauge heatbath algorithm [9, 10] and the gauge overrelaxation algorithm [13]. For the gauge heatbath the acceptance rate of the original heatbath as introduced by Creutz [9] would be very low due to the large fermionic force and the resulting bad approximation of the square root. Therefore the heatbath as proposed by Kennedy and Pendleton [10] should be used, which gives nearly 100% acceptance rate.

For the TSMB algorithm it is important that we have a similar efficient formulation for the boson part of the action as we have it with the staples for the gauge part. Indeed it is possible to write the dependence on the gauge field $U_{x,\mu}$ as follows:

$$\Delta S_\phi(U_{x,\mu}, \phi) = \mathrm{ReTr}\left(U_{x,\mu}\Delta S^{(1)}_{x,\mu}(\phi) + U_{x,\mu}\Delta S^{(2)}_{x,\mu}(\phi)\right). \tag{1.69}$$

The terms in $S^{(1)}_{x,\mu}(\phi)$ give the dependence on the nearest neighbour contributions and $S^{(2)}_{x,\mu}(\phi)$ the dependence on the next-to-nearest neighbour contributions. In $S^{(1)}_{x,\mu}(\phi)$ there is no further dependence on the gauge fields. Therefore it is possible to calculate this term after the update of the boson fields and use it throughout the following gauge updates.

Due to the next-to-nearest neighbour interactions in $S^{(2)}_{x,\mu}(\phi)$ this term has to depend on the gauge field. However, it can be written as

$$S^{(2)}_{x,\mu}(\phi) = \sum_{\substack{\nu=1 \\ \nu\neq\mu}}^{4} \left(f^{++}_{x,\mu\nu} U_{x+\hat{\mu},\nu} + f^{+-}_{x,\mu\nu} U^{\dagger}_{x+\hat{\mu}-\hat{\nu},\nu} + U^{\dagger}_{x,\nu} f^{-+}_{x+\hat{\nu},\nu\mu} + U_{x-\hat{\nu},\nu} f^{++}_{x-\hat{\nu},\nu\mu} \right). \quad (1.70)$$

Here the terms f^{++}, f^{+-} and f^{-+} don't depend on the gauge field. Therefore it is again possible to calculate them after the boson fields have been updated. This greatly reduces the time needed for the gauge update, because the spinor indices and the polynomial indices can be summed over before the gauge update is started. The results from the summation can be regarded as an auxiliary field. Of course this field has to be stored in the memory, which takes additional space. The memory needed for the auxiliary fields corresponds to 40 gauge fields, which in the case of QCD corresponds to roughly 13 boson fields.

1.4.2 The boson part of the action

The boson part of the action associated with the pseudo-fermionic boson fields $\phi^{(i)}$ can be read off directly from (1.29). For the practical calculation of this action a slightly different representation of the polynomial $P^{(1)}_{n_1}$ is used:

$$P^{(1)}_{n_1}(\tilde{Q}^2) = r_0 \prod_{i=1}^{n_1} \left(\left(\tilde{Q}^2 \pm \mu_i \right)^2 + \nu_i^2 \right). \quad (1.71)$$

This relates to (1.28) by $\rho_j = \mu_j + i\nu_j$ and to (1.27) by $z_j = (\mu_j + i\nu_j)^2$.

Writing out the action allows to write the boson action as

$$S_{\phi}[U,\phi,\phi^{\dagger}] = \sum_{x} \sum_{i=1}^{n_1} \left({\phi^{(i)}_x}^{\dagger} A^{(i)} \phi^{(i)}_x + \left[{\phi^{(i)}_x}^{\dagger} b^{(i)}_x + h.c. \right] \right), \quad (1.72)$$

with a term classifying the local part of the interaction

$$A^{(i)} = 1 + 16\kappa^2 + \mu_i^2 + \nu_i^2 + 2\mu_i\gamma_5 \quad (1.73)$$

and a term with nearest neighbour and next-to-nearest neighbour interactions

$$\begin{aligned} b^{(i)}_x &= -\kappa \sum_{\mu} \left(1 + \mu_i(\gamma_5 - \gamma_5\gamma_\mu)\right) U^{\dagger}_{x,\mu} \phi^{(i)}_{x+\hat{\mu}} \\ &\quad + \kappa^2 \sum_{\substack{\mu,\nu=\pm 1 \\ \mu\neq\pm\nu}}^{\pm 4} \left(1 + \gamma_\mu - \gamma_\nu - \gamma_\mu\gamma_\nu\right) U^{\dagger}_{x,\mu} U^{\dagger}_{x+\hat{\mu},\nu} \phi^{(i)}_{x+\hat{\mu}+\hat{\nu}}. \end{aligned} \quad (1.74)$$

This is precisely in such a form that local updates like the heatbath algorithm or the overrelaxation algorithm are applicable. For the boson heatbath a Gaussian random spinor χ is generated and the boson field is replaced according to the following prescription:

$$\phi^{(i)}_x \leftarrow {A^{(i)}}^{-\frac{1}{2}} \chi - {A^{(i)}}^{-1} b^{(i)}_x. \quad (1.75)$$

Even more efficient is the overrelaxation algorithm, which, however, leaves the action invariant and therefore is not ergodic. Still it can be used, either by combining it with the heatbath algorithm, or by using an ergodic updating algorithm for the gauge field, which would be enough since the gauge field and the boson field interact. The prescription for the boson overrelaxation is:

$$\phi_x^{(i)} \leftarrow -\phi_x^{(i)} - 2{A^{(i)}}^{-1} b_x^{(i)}. \tag{1.76}$$

Due to the specific form of the boson action there exists another way to create a new boson field starting from a Gaussian random spinor χ:

$$\phi_x^{(i)} \leftarrow \sum_y (Q-\rho_i)^{-1}_{xy} \chi_y^{(i)}. \tag{1.77}$$

This is called a global heatbath. It is very costly due to the matrix inversion needed for the generation of the boson field ϕ, but it has the advantage of perfectly decorrelating the boson field in one step.

There is a method to reduce the costs of the global heatbath [31]. Here the global heatbath is applied on the spinor

$$\eta_x^{(i)} = \chi_x^{(i)} + (Q-\rho_i)_{xy}\phi_x^{(i)}, \tag{1.78}$$

and a new boson field is proposed as

$$\phi_x^{(i)\prime} = (Q-\rho_i)^{-1}_{xy}\eta_y^{(i)} - \phi_x^{(i)}. \tag{1.79}$$

Performing the global heatbath in this way has the advantage that we have the choice of doing the inversion $\zeta_x^{(i)} = (Q-\rho_i)^{-1}_{xy}\eta_y^{(i)}$ less precise. As a compensation for this error one has to make a Metropolis step that accepts or rejects the proposed $\phi_x^{(i)\prime}$ with

$$P_{acc}(\phi_x^{(i)\prime} \leftarrow \phi_x^{(i)}) = \min(1, \exp(-\Delta S^{(i)})) \tag{1.80}$$

and

$$\Delta S^{(i)} = 2\mathrm{Re}\left(\left((Q-\rho_i)_{xy}\zeta_y^{(i)} - \eta_x^{(i)}\right)\left((Q-\rho_i)_{xy}\phi_y^{(i)} - Q_{xy}\phi_y^{(i)\prime}\right)\right). \tag{1.81}$$

Following this global quasi-heatbath it is possible to do a very lazy computation of the matrix inversion. However, the proposed field should be accepted often enough so that this expensive update still makes sense, and in addition a very unprecise computation of the inversion may give some correlations on the original field even if the new field is accepted. We have implemented this algortihm in such a way that the residuum for the inversion is adjusted according to the quality of the previous global quasi-heatbath results. The acceptance rate that we were aiming for was set to 80%-90%.

In the literature it is claimed that by using this global quasi-heatbath one can gain a factor of 2-3 [31]. Indeed we found that the number of iterations needed for the matrix inversion is greatly reduced. However, there is additional overhead for the setup of the spinor η and for the Metropolis step so that the benefit of this method is highly dependent on implementation details.

The property that it perfectly decorrelates the boson field makes this global heatbath very attractive. But even with the improvements of the global quasi-heatbath it remains

a very expensive updating algorithm. For these reasons we have decided to use the local updating algorithms, and only after some updates a global quasi-heatbath is done. There were usually $8-15$ updates between two calls to the global quasi-heatbath. This way the time spent for the local updates was comparable to the time for the global updates, and the frequency of global updates is still high enough so that the long tail in the autocorrelation is reduced.

1.4.3 Even-odd preconditioning

Most of the computer time in the simulations is spent on some variant of the inversion of the fermion matrix Q or its hermitean version $\tilde{Q}$. This inversion is done either explicitly in the conjugate gradient inversion for the measurement of correlators or implicitly by the polynomials of the multi-boson algorithm. The number of needed iterations for the conjugate gradient inverter is directly related to the condition number $\frac{\lambda}{\varepsilon}$ of the fermion matrix $\tilde{Q}^2$, and the polynomial order is determined by that factor due to equation (1.31), too.

It is therefore advantageous to find some other matrix $\bar{Q}$ as a replacement for Q that has a smaller condition number but the same determinant

$$|\det Q|^{N_f} = \det\left(\tilde{Q}^2\right)^{\frac{N_f}{2}} = \det\left(\tilde{\bar{Q}}^2\right)^{\frac{N_f}{2}}. \tag{1.82}$$

Indeed this can be done by using the following representation of the Wilson-fermion matrix

$$Q = 1 - \kappa \begin{pmatrix} 0 & D_{eo} \\ D_{oe} & 0 \end{pmatrix}, \tag{1.83}$$

where D_{eo} acts only on odd sites and D_{oe} only on even sites. Together with the identity

$$\det \begin{pmatrix} A & B \\ C & D \end{pmatrix} = \det A \det\left(D - CA^{-1}B\right) \tag{1.84}$$

we find for the fermion determinant

$$\det Q = \det\left(1 - \kappa^2 D_{oe} D_{eo}\right). \tag{1.85}$$

Another possible matrix that has this determinant is

$$\tilde{\bar{Q}} = 1 - \kappa^2 \begin{pmatrix} 0 & 0 \\ 0 & D_{oe} D_{eo} \end{pmatrix}. \tag{1.86}$$

Half of the eigenvalues of this matrix $\tilde{\bar{Q}}$ are equal to one. The other half of the eigenvalues can be related to the eigenvalues of Q. If $v = (v_e, v_o)$ is an eigenvector of Q with eigenvalue λ then it satisfies

$$(\lambda v_e, \lambda v_o) = (v_e - \kappa D_{eo} v_o, v_o - \kappa D_{oe} v_e). \tag{1.87}$$

Then we get from

$$(1 - \kappa^2 D_{oe} D_{eo}) v_o = v_o - (1-\lambda)^2 v_o = \lambda(2-\lambda) v_o \tag{1.88}$$

that the eigenvalues of $\bar{Q}$ are either one (in the even subspace) or they satisfy

$$\bar{\lambda} = \lambda(2-\lambda). \tag{1.89}$$

For very small eigenvalues we see that the eigenvalues of $\tilde{\bar{Q}}$ are roughly twice as large as those of Q. This speeds up the matrix inversion by roughly a factor of two, and the polynomial orders can be chosen smaller by more than a factor of two, also.

However the matrix $\tilde{\bar{Q}}$ already contains next-to-nearest neighbour interactions and therefore the square of this matrix as it appears in the local boson action is quite complicated. In general this should be no reason to abandon this preconditioning, but unfortunately the implementation on parallel computers becomes impossible due to the large distance interactions of $\tilde{\bar{Q}}^2$. This can be avoided by applying (1.84) directly on (1.29), as was proposed in [32]. The bosonic action can then be written as

$$S_{f,eo}^{(n_1)}[U,\phi] = \sum_{j=1}^{n_1} \phi^{(j)\dagger} \left(\tilde{Q} - P_o\rho_j^*\right)\left(\tilde{Q} - P_o\rho_j\right)\phi^{(j)}, \tag{1.90}$$

with P_o being the projector on the odd subspace

$$P_o = \begin{pmatrix} 0 & 0 \\ 0 & 1 \end{pmatrix}. \tag{1.91}$$

This action again has to be written in the form (1.72), and comparing the result with (1.73) and (1.74) we find that only small changes are needed in the local bosonic action. The term $A^{(i)}$ from equation (1.73) has to be replaced by a term that depends on the parity of the site

$$\begin{aligned} A_{ee}^{(i)} &= 1 + 16\kappa^2 \\ A_{oo}^{(i)} &= 1 + 16\kappa^2 + |\rho_i|^2 - (\rho_i + \rho_i^*)\gamma_5, \end{aligned} \tag{1.92}$$

and in equation (1.74) in the term $b^{(i)}$ the μ_i has to be replaced by $-\frac{1}{2}\rho_i$ or $-\frac{1}{2}\rho_i^*$ depending on the interaction and the parity of the site.

These are minor modifications and the form of the bosonic action remains unchanged. In this way the even-odd preconditioned matrix is as easy to use as the non-preconditioned matrix from the point of view of the implementation.

The matrix $\bar{Q}$ might have the same determinant as Q, but it is not obvious how to relate $\bar{Q}^{-1}$ to Q^{-1} as needed in the computation of fermionic correlators. There is, however, a simple decomposition of Q into $\bar{Q}$:

$$Q = L\bar{Q}R = \begin{pmatrix} 1 & 0 \\ -\kappa D_{oe} & 1 \end{pmatrix} \begin{pmatrix} 1 & 0 \\ 0 & 1 - \kappa^2 D_{oe}D_{eo} \end{pmatrix} \begin{pmatrix} 1 & -\kappa D_{eo} \\ 0 & 1 \end{pmatrix}. \tag{1.93}$$

For the matrices L and R the inverse is easily found:

$$L^{-1} = \begin{pmatrix} 1 & 0 \\ \kappa D_{oe} & 1 \end{pmatrix}, \tag{1.94}$$

$$R^{-1} = \begin{pmatrix} 1 & \kappa D_{eo} \\ 0 & 1 \end{pmatrix}. \tag{1.95}$$

When asking for the inverse of the matrix Q we are actually only interested in the solution z of the equation

$$Qz = s, \tag{1.96}$$

with s being some source vector. Since the standard conjugate gradient works only on matrices that are hermitean and positive definite we apply it for $\tilde{Q}^2$ on the source $Q^\dagger s$:

$$\tilde{Q}^2 z = Q^\dagger s. \tag{1.97}$$

Using the relations given above for the matrices Q, L and R we find that the solution z can also be written as

$$z = R^{-1}\gamma_5 \left(\tilde{\tilde{Q}}^2\right)^{-1} \tilde{\tilde{Q}} L^{-1} s. \tag{1.98}$$

The source s therefore has to be multiplied by L^{-1} and by $\tilde{\tilde{Q}}$, and then the much faster conjugate gradient on the preconditioned matrix $\tilde{\tilde{Q}}^2$ can be applied. The result has to be multiplied further by γ_5 and R^{-1}, which gives the original result z.

With the explanations given in this section the even-odd preconditioning can be applied in the local updates, in the correction step and in the measurement of the correlators. This should be done because the effort is not much larger than before while the polynomial orders and the conjugate gradient iterations are greatly reduced. There is unfortunately one remaining place where we are forced to use the non-preconditioned fermion matrix. This is the global heatbath algorithm for the boson fields, where (1.90) has to be used. Due to the efficiency of the global heatbath it is still worthwhile to use it, although without preconditioning.

1.5 Measurement of basic quantities

When running the simulations we have the gauge coupling β and the fermion coupling κ as tuning parameters. These are not very physical parameters. What we actually want to fix is e. g. the physical volume $L^3 \cdot T$ and the quark or pion mass. Therefore we have to measure the volume, which is usually done by measuring the Sommer scale parameter r_0 [33, 34], and we have to measure the masses. Then we can tune the parameters β and κ until the volume and the quark mass are at the desired values.

Since this is a generic procedure to be applied for nearly every model with gauge fields we will give the basic definitions and some explanations on how to measure these quantities in this section before going to some applications in the next chapters.

1.5.1 Smearing techniques

The quantities we want to measure are either gluonic, in which case they can be represented on the lattice by closed loops of gauge links, the Wilson loops, or they are fermionic. In the latter case they are calculated from propagators, i. e. inversions of the fermion matrix as described in section 1.4.3. In any case we want to get the best possible result, i. e. smallest errors with least effort. For this purpose it is useful to apply smearing. This usually increases the signal to noise ratio or the projection on the ground state is increased. The smearing technique we will use for the gauge fields is the APE smearing [35]. For the fermionic quantities we will use Jacobi smearing [36].

APE smearing

With one iteration of APE smearing every spatial link is replaced by the sum of itself and the weighted sum of the four orthogonal space-like staples perpendicular to the direction of the original link:

$$U_k^s(x) = \mathcal{P}_{SU(N)} \left(U_k(x) + \alpha \sum_{\substack{j=\pm 1 \\ j \neq \pm k}}^{\pm 3} U_j^\dagger(x+\hat{k}) U_k(x+\hat{j}) U_j(x) \right). \tag{1.99}$$

The operator $\mathcal{P}_{SU(N)}$ denotes the projection back into the group $SU(N)$. This projection is straightforward for the case of two colours as considered in chapter 3, but for $N = 3$ one has several choices. In that case we are projecting back A to $M = \mathcal{P}_{SU(3)}(A)$ by maximizing $\mathrm{Tr}(M^\dagger A)$ using $\mathcal{O}(10)$ Cabibbo-Marinari hits on the $SU(2)$ subgroups of $SU(3)$. It can easily be checked that this smearing algorithm is gauge covariant. Usually it is iterated many times. Both the staple to link ratio α and the number of iterations N_{APE} have to be optimized to get the best results.

There are other smearing algorithms for the gauge fields that are roughly as efficient, e. g. Teper blocking [37]. However, APE smearing is much easier to implement on parallel computers, which is why we have decided to use this method.

Jacobi smearing

For analytical calculations it is easiest to take pointlike sources and sinks when inverting the fermion matrix. This, however, doesn't resemble the physical states of the fermion in an optimal way. To improve this situation one can use the intuition given from shell model wavefunctions for the approximation of the ground state. This means that a smearing technique for the fermion fields can be found by starting from the solution to a three dimensional Klein-Gordon equation. Hence a spinor ψ is smeared as

$$\bar{\psi}(\mathbf{x}, t) = \sum_{\mathbf{x}'} F(\mathbf{x}, \mathbf{x}') \psi(\mathbf{x}', t), \tag{1.100}$$

with the Jacobi smearing defined through

$$F^{ab}(\mathbf{x}, \mathbf{x}') = \delta^{ab} \delta_{\mathbf{x}\mathbf{x}'} + \sum_{i=1}^{N_J} \left(\kappa_J \sum_{j=1}^{3} \left(\delta_{\mathbf{x}', \mathbf{x}+\hat{j}} U_j^{ab}(x) + \delta_{\mathbf{x}'+\hat{j}, \mathbf{x}} U_j^{\dagger\, ab}(x) \right) \right)^i. \tag{1.101}$$

Again this smearing algorithm is gauge covariant. This smearing technique has two parameters κ_J and N_J that have to be tuned to get the optimal results.

1.5.2 Sommer scale parameter r_0

Of course we know the dimensionless parameter $\frac{L}{a}$ from our simulations, which is just the number of lattice sites in one direction. Therefore we need to relate the lattice spacing a to some physical quantity which then gives us the lattice extension and of course relates all other quantities given in lattice units to physical units. In quenched QCD the string tension σ is often used. However, this is a quantity that should be measured at large

distances, and with dynamical quarks string breaking effects might take place. In [33] Sommer proposes a new method to set the scale for a. This is done by computing $\frac{r_0}{a}$ from the static potential, which should be done at medium distances, and which can be related to phenomenological models like the Cornell [38] or the Richardson [39] model.

The Sommer scale parameter as proposed in [33] is defined through the relation

$$r^2 F(r)\big|_{r=R(c)} = c, \tag{1.102}$$

where $F(r)$ is the force between static quarks and the hadronic length scale $R(c)$ as usually used for the definition of the Sommer parameter is

$$R(1.65) \equiv r_0 \simeq 0.49 \text{ fm}. \tag{1.103}$$

On the lattice r_0/a can be calculated from the static quark potential, which is in turn determined from Wilson loops. The basic idea is simple, but since we want to match all our results to this parameter it is crucial to get a precise determination. To achieve this we follow the method proposed by Michael and collaborators [40,41] and some details in [42].

Using the variational approach of [43] we get matrices $W_{ij}(r,t)$ consisting of $r \cdot t$ loops of smeared gauge links, where our smearing technique of choice is APE-smearing, and the indices i, j label the level of smearing.

From the solutions to

$$W_{ij}(\mathbf{r},t)\phi(\mathbf{r})_j^{(k)} = \lambda^{(k)}(\mathbf{r};t,t_0)W_{ij}(\mathbf{r},t_0)\phi(\mathbf{r})_j^{(k)} \tag{1.104}$$

one gets the eigenvector $\phi(\mathbf{r})_j^{(0)}$ for the largest eigenvalue $\lambda^{(0)}(\mathbf{r};t = t_0+1,t_0)$. This equation is solved by transforming it into an ordinary eigenvalue equation, where several ways are possible:

$$W(\mathbf{r},t_0)^{-1}W(\mathbf{r},t)\phi = \lambda\phi \tag{1.105}$$

$$W(\mathbf{r},t)W(\mathbf{r},t_0)^{-1}(W(\mathbf{r},t_0)\phi) = \lambda(W(\mathbf{r},t_0)\phi) \tag{1.106}$$

$$W(\mathbf{r},t_0)^{-1/2}W(\mathbf{r},t)W(\mathbf{r},t_0)^{-1/2}(W(\mathbf{r},t_0)^{1/2}\phi) = \lambda(W(\mathbf{r},t_0)^{1/2}\phi). \tag{1.107}$$

In the literature [43] the third version has been used. However this can only be done with extremely good statistics. Otherwise it is possible that, due to statistical fluctuations, the matrix W_{ij} gets negative eigenvalues making the (real) square root impossible. We checked that the first two versions give numerically exactly the same result. For the final determinations we choose the first version (1.105), where one has to be careful about the fact that $W(\mathbf{r},t_0)^{-1}W(\mathbf{r},t)$ no longer has to be symmetric, complicating the calculation of the corresponding eigenvectors.

Once the eigenvector $\phi(\mathbf{r})_j^{(0)}$ has been obtained, we can project the matrix W_{ij} to the ground state:

$$\tilde{W}_0(\mathbf{r},t) = \phi(\mathbf{r})_i^{(0)}W_{ij}(\mathbf{r},t)\phi(\mathbf{r})_j^{(0)}. \tag{1.108}$$

This correlator leads to good estimates of the ground state energy

$$\tilde{E}_0(\mathbf{r},t) = \ln\left(\frac{\tilde{W}_0(\mathbf{r},t)}{\tilde{W}_0(\mathbf{r},t+1)}\right). \tag{1.109}$$

The potential $V(\mathbf{r})$ is estimated by averaging $E_0(\mathbf{r},t)/t$ over time extensions t with $t \geq 1$ and weight given by the Jackknife error. Compared to some other methods this way of extracting the potential seems to give the most reliable estimates with smallest error bars.

Rewriting the force in (1.102) the Sommer scale parameter is given in terms of the potential as

$$r_0^2 \left.\frac{\mathrm{d}V}{\mathrm{d}r}\right|_{r_0} = 1.65. \tag{1.110}$$

Having a reliable static quark potential we can follow [44] by fitting the potential to

$$V(\mathbf{r}) = V_0 + \sigma r - e[\frac{1}{\mathbf{r}}] \tag{1.111}$$

with $r = |\mathbf{r}|$ and $[\frac{1}{\mathbf{r}}]$ being the tree-level lattice Coulomb term

$$[\frac{1}{\mathbf{r}}] = 4\pi \int_{-\pi}^{\pi} \frac{\mathrm{d}^3\mathbf{k}}{(2\pi)^3} \frac{\cos(\mathbf{k}\cdot\mathbf{r})}{4\sum_{j=1}^{3}\sin^2(k_j/2)}. \tag{1.112}$$

Due to the small lattice size we had to drop in (1.111) the additional correction term $f\cdot\big([\frac{1}{\mathbf{r}}] - \frac{1}{r}\big)$, which could have been used to estimate $\mathcal{O}(a)$ effects, fixing $e = \pi/12$. Bringing together the above equations (1.110) and (1.111) we extract r_0 from

$$r_0 = \sqrt{\frac{1.65 - e}{\sigma}}. \tag{1.113}$$

Another reliable estimate of the Sommer scale parameter can be obtained from interpolating the force as it appears in (1.102). This is the original method proposed in [33] and emphasized again in [34]. For this method the force is needed. At distance r_I this can be estimated as

$$F(r_I) = V(\mathbf{r}) - V(\mathbf{r} - \frac{\mathbf{r}}{|\mathbf{r}|}), \tag{1.114}$$

where the argument r_I is defined from (1.112) as

$$r_I = [\frac{1}{\mathbf{r}}] - [\frac{1}{\mathbf{r} - \frac{\mathbf{r}}{|\mathbf{r}|}}]. \tag{1.115}$$

The two points neighbouring the estimated value of r_0 are interpolated to the function

$$F_1(r) = f_1 + f_2\frac{1}{r^2}. \tag{1.116}$$

For not too small values of r this is locally an excellent approximation to the r dependence of the force. Therefore this function can be used to estimate the force as needed for (1.102), leading to an alternative determination of the Sommer scale parameter. The systematic errors of this method can be estimated by further interpolating the force to the function

$$F_s(r) = f_1 + f_2\frac{1}{r^2} + f_3\frac{1}{r^4}. \tag{1.117}$$

For small values of r_0 we found the systematic errors to be larger than the statistical ones, but for values of $\frac{r_0}{a} > 3$ they become negligible.

The results for $\frac{r_0}{a}$ determined from the two methods show a disagreement slightly beyond the statistical uncertainty. This, however, is to be expected, since the two determinations may differ by $\mathcal{O}(a)$ effects. Any determination can be taken, but when performing a continuum extrapolation one should stick to one definition to allow for a smoother extrapolation.

Routinely we are using both methods to determine $\frac{r_0}{a}$ from the potential obtained from (1.109), from the generalized eigenvalues of (1.104) and from Wilson loops with fixed APE smearing level. We have found that by interpolating the force an estimate for $\frac{r_0}{a}$ can be given with less statistics. Nevertheless once enough statistics is available for both methods they give $\frac{r_0}{a}$ with roughly the same precision.

1.5.3 Hadronic observables and quark mass definitions

The masses and amplitudes can be computed from zero-momentum two-point functions of the time-slice distance $(x_0 - y_0)$

$$C_{XY}(x_0 - y_0) = \frac{1}{V_s} \sum_{\mathbf{x},\mathbf{y}} \left\langle X^\dagger(x) Y(y) \right\rangle , \tag{1.118}$$

where $x \equiv (x_0, \mathbf{x})$, V_s is the spatial volume and in our case the operators X and Y are one of

$$\begin{array}{lll} X(x) = Y(x) = P_5(x) \equiv \bar{q}'(x)\gamma_5 q(x) & \longrightarrow & C_{PP}(x_0 - y_0), \\ X(x) = Y(x) = A_0(x) \equiv \bar{q}'(x)\gamma_5\gamma_0 q(x) & \longrightarrow & C_{AA}(x_0 - y_0), \\ X(x) = Y(x) = V_i(x) \equiv \bar{q}'(x)\gamma_i q(x) & \longrightarrow & C_{V_iV_i}(x_0 - y_0). \end{array} \tag{1.119}$$

Furthermore we consider the mixed correlator

$$X(x) = A_0(x), \qquad Y(x) = P_5(x) \qquad \longrightarrow \qquad C_{AP}(x_0 - y_0). \tag{1.120}$$

The correlators, e. g. the pion correlator $C_{PP}(x_0 - y_0)$ may then be written as

$$C_{PP}(x_0 - y_0) = \frac{1}{V_s} \sum_{\mathbf{x},\mathbf{y}} \mathrm{Tr} \left({Q^\dagger_{xy}}^{-1} Q^{-1}_{yx} \right) \tag{1.121}$$

using $q(x)\bar{q}(y) = Q^{-1}_{xy}$ and $\gamma_5 Q^{-1}_{xy} \gamma_5 = {Q^\dagger_{yx}}^{-1}$. With the relation (1.121) we can compute the correlator using a conjugate gradient algorithm with the source at site $y \equiv (y_0, \mathbf{y})$. This conjugate gradient algorithm has to be applied twelve times (in the case of QCD) to get all needed combinations of the colour and spinor indices. The other correlators can be calculated from the same results of the inversion, they only have to be multiplied by some additional γ-matrices.

Of course we want to get results for these correlators with computational costs as low as possible, i. e. we want to get some small final statistical error with the lowest possible number of measurements and the fewest updates between the measurements. We have found that this can be achieved by picking the source y in (1.121) at random over the lattice. This reduces the final statistical error for hadronic observables and furthermore reduces the autocorrelation of these quantities to values clearly below the plaquette autocorrelation [29], see chapter 2.

Once the correlators are known one can extract masses and amplitudes from the asymptotic behaviour:

$$C_{XY}(t) = \frac{\xi_{XY}^2}{2m_p}\left(e^{-m_p t} + (-1)^{X+Y} e^{-m_p(L_t-t)}\right), \tag{1.122}$$

$$\xi_{XY} = \sqrt{\langle 0\,|X(0)|\,p\rangle\,\langle 0\,|Y(0)|\,p\rangle}. \tag{1.123}$$

Here $|p\rangle$ is the zero-momentum state of the particle that is associated with the operators $X(x)$ and $Y(x)$, m_p is the corresponding mass and $(-1)^X$ is the time-parity of the operator $X(x)$. There is an obvious symmetry around $\frac{L_t}{2}$, which we use to reduce the noise of the correlators by time-symmetrization. The best results for m_p and ξ_{XY} can be achieved by a global fit over some range of time-slice distances $t \in [T_{min}, \frac{L_t}{2}]$. The optimal value of T_{min} is to be determined by checking the effective local mass $m_{eff}(t)$ for the beginning of the plateau. The effective local mass is implicitly defined by

$$\frac{C_{XY}(t)}{C_{XY}(t+1)} = \frac{e^{-m_{eff}(t)t} + (-1)^{X+Y} e^{-m_{eff}(t)(L_t-t)}}{e^{-m_{eff}(t)(t+1)} + (-1)^{X+Y} e^{-m_{eff}(t)(L_t-t-1)}}. \tag{1.124}$$

Actually the effective mass could be used as a mass estimate, and indeed it agrees very well with the result from the global mass fit. However, the latter gives a more precise determination of the mass and is therefore used.

In general the determination of the pion mass m_π or the ρ meson mass m_ρ is possible without further complications. However, for small quark masses we find that we need larger values of T_{min} because the asymptotic behaviour of the correlators sets in later. This results in larger errors for the hadronic observables. We have tried Jacobi smearing [36] both on the source and the sink and as expected the overlap of the operators with the ground state is improved.

Hadronic observables that we monitor are the pion mass m_π, the ρ meson mass m_ρ, the pion amplitude g_π and the pion decay constant f_π. The pion mass is determined from the asymptotic behaviour of the correlator $C_{PP}(t)$, and the ρ mass from the correlator

$$C_{VV}(t) = \frac{1}{3}\sum_{i=1}^{3} C_{V_iV_i}(t). \tag{1.125}$$

The amplitude

$$g_\pi \equiv \langle 0\,|P_5(0)|\,\pi\rangle \tag{1.126}$$

can be extracted from $C_{PP}(t)$ by identifying $g_\pi = \xi_{PP}$. For the pion decay constant

$$f_\pi \equiv m_\pi^{-1}\,\langle 0\,|A_0(0)|\,\pi\rangle \tag{1.127}$$

we use two different methods to be able to pick the best determination, because for light quark masses with highly correlated data there is no clear preference for one of the methods. By the first method the amplitude $\langle 0|A_0(0)|\pi\rangle$ is determined from the correlator $C_{AA}(t)$, and the pion mass is the previously obtained one. By the second method [45] the amplitude ratio

$$r_{AP} = \frac{\langle 0\,|A_0(0)|\,\pi\rangle}{\langle 0\,|P_5(0)|\,\pi\rangle} \tag{1.128}$$

is fitted by using the asymptotic behaviour

$$\frac{C_{AP}(t)}{C_{PP}(t)} = r_{AP} \tanh\left(m_\pi \left(\frac{L_t}{2} - t\right)\right). \tag{1.129}$$

Again m_π is fixed at the value from the global fit to $C_{PP}(t)$. The pion decay constant is then obtained by

$$f_\pi = m_\pi^{-1} r_{AP} g_\pi. \tag{1.130}$$

Quark mass definitions

There are many different ways to get an estimate for the quark mass. In the limit of very small quark masses all of them should show a linear behaviour between each other. Most of the definitions for the quark mass make use of the fact that the pion mass-squared m_π^2 in a first approximation goes to zero the same way as the quark mass does:

$$m_\pi^2 = const. \cdot m_q + \mathcal{O}(m_q^2). \tag{1.131}$$

Under the assumption that m_ρ is roughly a constant as a function of the quark mass one widely used way to estimate the quark mass is to consider the ratio $\frac{m_\pi}{m_\rho}$. However, we believe that this is not a good candidate. Apart from the fact that there seems to be no sign of a linear behaviour compared to other quark mass definitions in the range of medium quark masses there is the further complication that the ρ meson may decay into two pions $\rho \to \pi\pi$ once $\frac{m_\pi}{m_\rho} < \frac{1}{2}$. This makes the measurement of the ρ meson mass m_ρ unnecessarily complicated. Another natural way to get a dimensionless quark mass estimate from m_π^2 is to use the Sommer scale parameter and to define

$$M_r \equiv (r_0 m_\pi)^2. \tag{1.132}$$

This definition is going to be prefered in this work. Another definition that seems to work as well comes from the axial Ward identity, the so-called partially conserved axial current (PCAC) relation

$$\partial_\mu A_\mu^a = 2mP^a. \tag{1.133}$$

In the above notation the quark mass can be defined as

$$m_q^{PCAC} = \frac{f_\pi}{2g_\pi} m_\pi^2. \tag{1.134}$$

This is in physical units, but again a dimensionless quantity can by obtained by multiplying with r_0:

$$\mu_r \equiv r_0 m_q^{PCAC}. \tag{1.135}$$

All the given quark mass definitions are dimensionless. This is quite convenient, but we would like to compare the value of M_r with the strange quark mass. This can be done by using unquenched $N_f = 2$ lattice data. The Ω^- baryon mass $m_{\Omega^-} = 1.672$ GeV and $r_0 = 0.49$ fm give $r_0 m_{\Omega^-} = 4.237$. The CP-PACS collaboration gives results for the Δ baryon mass in [46] at their largest β value $\beta = 2.20$ and for $\kappa = 0.1363$ and $\kappa = 0.1368$. Interpolating between these results one can match $r_0 m_\Delta = 4.237$ if their pion mass is $r_0 m_\pi \simeq 1.76$. This gives for the strange quark mass

$$M_{r,strange} \simeq 3.1. \tag{1.136}$$

Slightly different values are possible if $M_{r,strange}$ is matched in another way, but for definiteness we shall stick to this definition. It should be mentioned that this definition is a rather technical one for operational purposes. No attempt has been made to compute the conventionally defined strange quark mass (for instance in dimensional regularization).

1.5.4 Autocorrelations and error analysis

To get meaningful results from the lattice simulations the error of the measured quantities, both the statistical and the systematical one, has to be estimated. Systematical errors can come from finite volume effects, $\mathcal{O}(a)$ errors, not good enough third polynomial, quenching and many other sources. These errors should be kept below the statistical one.

Let us now consider the statistical error of a set of primary quantities with (exact) expectation values $A_\alpha,\ \alpha = 1, 2, \ldots$. In the measurement sequence the observed estimates for A_α are:

$$\bar{a}_\alpha = \frac{1}{N}\sum_{i=1}^{N} a_\alpha^{(i)}. \tag{1.137}$$

With enough statistics $|\bar{a}_\alpha - A_\alpha| \ll 1$ should be true. If the configurations used for the measurement are independent one can use a naive error estimate, i. e. the variance. However, it is usually advisable to measure more often between two independent configurations to reduce the error. If this is done the naive error has to be reweighted with the effective statistics. For this the integrated autocorrelation length τ_{int} of that quantity is needed, and with that the error estimate for the primary quantities can be estimated by

$$\sigma(A_\alpha)^2 = \frac{2\tau_{int}}{N}\left(\overline{a_\alpha^2} - (\bar{a}_\alpha)^2\right). \tag{1.138}$$

The normalized autocorrelation function of a primary quantity is given by

$$C_{A_\alpha A_\alpha}(t) = \frac{\langle a_\alpha^{(i)}(n) a_\alpha^{(i)}(n+t)\rangle}{\langle a_\alpha^{(i)}(n) a_\alpha^{(i)}(n)\rangle}. \tag{1.139}$$

For large t this function typically behaves like

$$C_{A_\alpha A_\alpha}(t) \propto e^{-|t|/\tau}, \tag{1.140}$$

which leads to the definition of the exponential autocorrelation length τ_{exp}:

$$\tau_{exp}(A) = \lim_{t\to\infty} \sup \frac{t}{-\log|C_{A_\alpha A_\alpha}(t)|}. \tag{1.141}$$

However, the more important autocorrelation is the integrated one, because due to slow modes there are usually some long tails in addition to (1.140) in $C_{A_\alpha A_\alpha}(t)$. The integrated autocorrelation is defined as

$$\tau_{int}(A) = \frac{1}{2} + \sum_{t=1}^{\infty} C_{A_\alpha A_\alpha}(t). \tag{1.142}$$

For secondary quantities such as the pion mass, r_0 and any measurement including a reweighting factor, or in general any function $f(A_\alpha)$ of the primary expectation values A_α, one cannot compute the integrated autocorrelation in a straightforward way. But there are several possibilities to get an estimate for the autocorrelation, and therefore for the statistical error. Two of these possibilities shall be discussed in this section.

Jackknife analysis with blocking

If A_α has been measured on a large set of independent configurations, then one can use the distribution of the values $f(\bar{a}_\alpha)$ on different subsamples to get an estimate of the error of the secondary quantity. However, there are usually not enough measurements for this method. In that case a generalization, the jackknife analysis can be applied. Jackknife averages of the primary quantities are obtained by leaving out one measurement in all possible ways:

$$a_\alpha^{(J:j)} \equiv \frac{1}{N-1} \sum_{i \neq j} a_\alpha^{(i)}. \tag{1.143}$$

This leads to the jackknife estimators

$$f_\alpha^{(J:j)} \equiv f(a_\alpha^{(J:j)}) \tag{1.144}$$

of the secondary quantities, with a corresponding average of

$$\overline{f_\alpha^{(J)}} \equiv \frac{1}{N} \sum_{j=1}^{N} f_\alpha^{(J:j)}. \tag{1.145}$$

If we continue to assume that the used configurations are independent, we can use the variance of the jackknife errors

$$\sigma^2_{(J)\bar{f}_\alpha} \equiv \frac{N-1}{N} \sum_{j=1}^{N} \left(f_\alpha^{(J:j)} - \overline{f_\alpha^{(J)}} \right)^2 \tag{1.146}$$

as an estimate of the error.

Usually, however, the used configurations are not independent, and as for the primary quantities we will underestimate the error if we don't account for the correlation between the measurements. This can be done by the technique of blocking. For this n successive measurements are collected together in N/n blocks. Each of these blocks is now considered as a single measurement, and again we can apply the jackknife analysis to the blocked data. For the different blocking levels this leads to different estimates of the error $\sigma_\alpha^{(B:n)}(f(A_\alpha))$. In the limit of infinite statistics, the error $\sigma_{f,\alpha}^{(B:n)}$ should approach an asymptotic value $\sigma_{f,\alpha}^{(B:unc)}$ for increasing n. This value can be considered as the standard deviation for the uncorrelated data. The integrated autocorrelation can then be extracted as

$$\tau_{int} = \frac{1}{2} \left(\frac{\sigma_{f,\alpha}^{(B:unc)}}{\sigma_{f,\alpha}^{(B:1)}} \right)^2. \tag{1.147}$$

This method of the jackknife analysis combined with blocking is very easy to apply no matter how complicated the function $f(A_\alpha)$ is. However, we have found that it becomes unstable already at moderate statistics. This is understandable by realizing that the statistics of the individual blocks are reduced compared to the total sample.

Linearization

We will now discuss an advanced method to estimate the error. As has been proposed in [47] the error estimates and autocorrelations can be obtained from linear combinations of primary quantities. This method is based on the linearization of the deviation of the secondary quantity from its true value. This deviation can be expressed as

$$f(\bar{a}) - f(A) \simeq \sum_\alpha (\bar{a}_\alpha - A_\alpha) \frac{\partial f(A)}{\partial A_\alpha}. \tag{1.148}$$

The values of the derivatives at the true expectation values are constants, and therefore the deviation has been expressed as a linear combination of primary quantities. This linear combination can be handled in the same way as the primary quantities themselves. Since we have the estimate

$$\frac{\partial f(A)}{\partial A_\alpha} \simeq \left.\frac{\partial f(A)}{\partial A_\alpha}\right|_{A=\bar{a}} \equiv \bar{f}_\alpha \tag{1.149}$$

we can express the deviation as

$$f(\bar{a}) - f(A) \simeq \sum_\alpha (\bar{a}_\alpha - A_\alpha)\bar{f}_\alpha = \bar{a}_{\bar{f}} - A_{\bar{f}}, \tag{1.150}$$

where

$$A_{\bar{f}} \equiv \sum_\alpha A_\alpha \bar{f}_\alpha \tag{1.151}$$

is a linear combination of primary quantities. Therefore $A_{\bar{f}}$ is a primary quantity, too. Its estimate is

$$\bar{a}_{\bar{f}} \equiv \sum_\alpha \bar{a}_\alpha \bar{f}_\alpha = \frac{1}{N} \sum_{i=1}^{N} a_\alpha^{(i)} \bar{f}_\alpha. \tag{1.152}$$

The variance of $f(A)$ is

$$\sigma_\alpha^2 \simeq \left\langle (\bar{a}_{\bar{f}} - A_{\bar{f}}) \right\rangle^2, \tag{1.153}$$

which shows, that the error of $f(A)$ can be estimated from the integrated autocorrelation of the primary quantity $A_{\bar{f}}$, i. e. the integrated autocorrelation of the secondary quantity can be defined as the one of $A_{\bar{f}}$. It should be noted, that $\langle \ldots \rangle$ stands for the expectation value in an infinite sequence of identical measurements having the same statistics as the actual measurement.

Examples We now apply the method of linearization to some examples that are typically encountered. An easy but important example is the ratio of two primary quantities as needed for the inclusion of the reweighting factors from section 1.3.3. Let A be the measured primary quantity and r the reweighting factor. Then the reweighted estimate is

$$f = \frac{A_1}{A_2}, \tag{1.154}$$

with $A_1 = (rA)$ and $A_2 = r$. With

$$\frac{\partial f}{\partial A_1} = \frac{1}{A_2}, \qquad \frac{\partial f}{\partial A_2} = -\frac{A_1}{A_2^2} \tag{1.155}$$

we get for the linearized deviation

$$\bar{a}_{\bar{f}} = \frac{1}{N}\sum_{i=1}^{N} \frac{r^{(i)}a^{(i)}\bar{r} - r^{(i)}\overline{ra}}{(\bar{r})^2} = 0. \tag{1.156}$$

The variance is estimated by

$$\sigma_f^2 \simeq \frac{2\tau_{int}^{(\bar{f})}}{N}\overline{a_{\bar{f}}^2}, \tag{1.157}$$

where

$$\overline{a_{\bar{f}}^2} = \frac{1}{N}\sum_{i=1}^{N}\left(\frac{r^{(i)}a^{(i)}\bar{r} - r^{(i)}\overline{ra}}{(\bar{r})^2}\right)^2 \tag{1.158}$$

and

$$\tau_{int}^{(\bar{f})} \simeq \frac{1}{2\overline{a_{\bar{f}}^2}}\sum_{d=1}^{N-1}\frac{1}{N-d}\sum_{i=1}^{N-d}\frac{(r^{(i)}a^{(i)}\bar{r} - r^{(i)})(r^{(i+d)}a^{(i+d)}\bar{r} - r^{(i+d)})}{(\bar{r})^4}. \tag{1.159}$$

Another important example is the case of the effective masses as defined in (1.124). We will therefore consider the following ratio

$$r_t = \frac{C_{XY}(t)}{C_{XY}(t+1)} = \frac{e^{-m_{eff}(t)\tau} + (-1)^{X+Y}e^{-m_{eff}(t)\tau}}{e^{-m_{eff}(t)\tau'} + (-1)^{X+Y}e^{-m_{eff}(t)\tau'}}, \tag{1.160}$$

where the factors are symmetrized around $L_t/2$, and with

$$\begin{aligned} \tau &\equiv \tfrac{L_t}{2} - t \\ \tau' &\equiv \tfrac{L_t}{2} - (t+1). \end{aligned} \tag{1.161}$$

For any function $F(r_t)$ of this ratio we have

$$\frac{\partial F}{\partial C_{XY}(t)} = \frac{\partial F}{\partial r_t}\cdot\frac{1}{C_{XY}(t+1)}, \qquad \frac{\partial F}{\partial C_{XY}(t+1)} = -\frac{\partial F}{\partial r_t}\cdot\frac{C_{XY}(t)}{(C_{XY}(t+1))^2}. \tag{1.162}$$

For the i-th value of the linearized deviation this gives

$$D_t^{(i)} = \left.\frac{\partial F}{\partial r_t}\right|_{r_t=\frac{\overline{C_{XY}(t)}}{\overline{C_{XY}(t+1)}}} \frac{C_{XY}^{(i)}(t)\overline{C_{XY}(t+1)} - \overline{C_{XY}(t)}C_{XY}^{(i)}(t+1)}{\left(\overline{C_{XY}(t+1)}\right)^2}, \tag{1.163}$$

which implies

$$\overline{D_t} = \frac{1}{N}\sum_{i=1}^{N} D_t^{(i)} = 0. \tag{1.164}$$

Varying r_t and $m_{eff}(t)$ in (1.160) gives the derivative

$$\frac{\partial m_{eff}(t)}{r_t} = \frac{e^{-m_{eff}(t)\tau'} + (-1)^{X+Y}e^{m_{eff}(t)\tau'}}{r_t\tau'\left(e^{-m_{eff}(t)\tau'} - (-1)^{X+Y}e^{m_{eff}(t)\tau'}\right) - \tau\left(e^{-m_{eff}(t)\tau} - (-1)^{X+Y}e^{m_{eff}(t)\tau}\right)}, \tag{1.165}$$

which directly leads to the quantities needed for the error estimate in (1.153).

One can apply the linearization method also for slightly more complicated functions than the above two examples, e. g. it has been worked out for the case of a mass fit.

However, a straightforward application of even more complicated functions like the determination of the Sommer scale parameter r_0 from the variational method as described in section 1.5.2 seems to be impossible due to the iterative determination of eigenvalues and eigenvectors. However, the linearization method can also be applied numerically. For this the derivative in (1.148) and (1.149) is determined numerically by slightly varying the primary quantities. The resulting estimate of the derivative $\bar{f}_\alpha$ can then be used for the further determination of error estimate. This numerical implementation is quite convenient, because it allows an error estimate for quantities like M_r defined in (1.132) that is superior to a simple combination of the error bars based on the assumption of uncorrelated Gaussian distributions. But once this numerical linearization method is available for r_0 and m_π it is very little effort to apply this for M_r. This numerical implementation has been compared with the exact implementation in the cases of the effective mass and the mass fit. The resulting error bars of the two different implementations of this method were compatible.

Chapter 2

QCD simulations with light quark masses

Today lattice calculations are limited to a region of unphysical parameters due to huge computational demands that arise if one wants to simulate QCD with quark masses close to zero and if one wants to perform the continuum extrapolation in a large physical volume. For that Kenneth Wilson estimated already in 1989 that one would need $\mathcal{O}(10)$ PetaflopYears [48]. This estimate has been confirmed by Karl Jansen for chirally invariant formulations of lattice QCD [49]. This is completely out of reach at a time where first multi-Teraflop machines are announced [50–53].

However, one can already do many interesting studies of QCD at the parameters that can be reached today. Here we will concentrate on the simulation of light dynamical Wilson fermions.

The volume used these days has a spatial extension of $2-3$ fm. This might not be an extremely large volume, but still it should be large enough to keep finite volume effects under control. What remains is to tune the quark to a light mass and go sufficiently close to the continuum limit. Luckily one doesn't have to go all the way in either direction. One can stay at somewhat larger quark masses than the physical values of the up and down quark masses, because chiral perturbation theory (χPT) can be used to extrapolate the data to smaller quark masses [54]. To allow such extrapolations the simulated quark mass should not be too large. To see the curvature predicted by one loop χPT it is expected that quark masses of $m_{ud} \leq \frac{m_s}{4}$ [55] are needed, with m_s the strange quark mass. In addition there are techniques that assist in the continuum limit. One can either use improved actions to be able to extrapolate to the continuum limit already at larger lattice spacings or one can include the $\mathcal{O}(a)$ effects into χPT [56].

This already sounds much better at first sight, but unfortunately a quarter of the strange quark mass still has to be considered as relatively light and therefore as computationally demanding. This mass has to be compared with the existing simulations, where the quark mass cannot be considered as light enough for χPT, because in most cases the mass of the two dynamical quarks is still above half of the strange quark mass $m_{ud} > \frac{m_s}{2}$, and the third quark is neglected completely. With these simulations the curvature predicted by χPT cannot be seen, i. e. the chiral logarithms are not yet found [57, 58].

In [49, 59–63] the costs of unquenched simulations were discussed. Some of the main statements of these references will be presented in section 2.1, where we also study the

scaling behaviour of the TSMB algorithm with respect to the quark mass. For this the region of light quark masses is explored. In section 2.2 we will turn to the scaling with respect to the lattice size.

Using the data from the study of the costs we analyze the eigenvalue spectrum of the non-hermitean Wilson-Dirac matrix Q. Despite the coarse lattices used for this study this can give interesting physical insights, because the used quark masses are the smallest for Wilson fermions so far.

Furthermore with these light quark masses we can test the appearance of the chiral logarithms. Next-to-leading order (NLO) calculations using χPT indicate a logarithmic behaviour in many quantities when going towards light quark masses. This hasn't been seen in other simulations at larger quark masses, and it is interesting to see if these logarithms appear in our simulations at smaller quark masses.

2.1 Quark mass dependence

The authors of references [49, 59–63] were asked at the Berlin Lattice Conference to give a formula for the expected costs depending on the volume, the quark mass and the lattice spacing. Since it is straightforward all of the authors agreed to include the volume as $\left(\frac{L}{\text{fm}}\right)^z$ into this formula. If the lattice spacing was included it was done according to $\left(\frac{1}{a\ \text{GeV}}\right)^z$. For the mass two different ansätze were used, both using the fact that for very small masses the quark mass will be proportional to the square of the pion mass. The quark mass dependence could then be described as $\left(\frac{1}{am_\pi}\right)^z$ or as $\left(\frac{m_\pi}{m_\rho}\right)^z$ using the widely referenced ratio of the pion and the ρ mass. Here are some of the results in these quantities from some of the above references:

$$\text{Lippert:} \qquad \begin{aligned} \beta = 5.6: &\quad 2.3(7)\cdot 10^7 \cdot \left(\tfrac{L}{a}\right)^5 \left(\tfrac{1}{am_\pi}\right)^{2.8(2)} \\ \beta = 5.5: &\quad 1.6(4)\cdot 10^7 \cdot \left(\tfrac{L}{a}\right)^5 \left(\tfrac{1}{am_\pi}\right)^{4.3(2)} \end{aligned} \tag{2.1}$$

$$\text{Wittig:} \qquad 0.31(7)\cdot 10^9 \left(\frac{L}{a}\right)^{4.55} \left(\frac{1}{am_\pi}\right)^{2.77(40)} \tag{2.2}$$

$$\text{Christ:} \qquad 1.4\cdot 10^{11} \frac{L^3T}{(\text{fm})^4} \left(\frac{m_\pi}{m_\rho}\right)^{-5} \left(\frac{1}{a\ \text{GeV}}\right)^7 \tag{2.3}$$

$$\text{Ukawa:} \qquad 2.8\cdot \left[\frac{m_\pi/m_\rho}{0.6}\right]^{-6} \left[\frac{L}{3\ \text{fm}}\right]^5 \left[\frac{a^{-1}}{2\ \text{GeV}}\right]^7 . \tag{2.4}$$

All of these statements give the cost in units of floating point operations needed for one independent configuration. We are mainly concerned on the expected behaviour with the volume and the mass.

There is a general agreement in the scaling with the volume by most of these authors. In equation (2.3) a fourth power of the lattice extension is assumed which is below the statements of the other authors. However, here have been used only $16^3\cdot 32$ and $24^3\cdot 32$ lattices and the results have been extrapolated to larger volumes. So the difference to the fifth power should be within the uncertainty of this result. In equation (2.2) 4.55 is used as a power for the lattice extension. This, however, was taken from [64], where the latest estimate is now a fifth power in equation (2.1).

To further compare the results of equations (2.1) and (2.2) is difficult, because they have only one further parameter $\left(\frac{1}{am_\pi}\right)^z$. With that the different dependence on the lattice spacing and the quark mass cannot be disentangled. Indeed the different exponents for different β values in equation (2.1) show that the scaling behaviour cannot be described by this simple equation.

In the other two equations (2.3) and (2.4) the dependence on the mass was given in the form $\left(\frac{m_\pi}{m_\rho}\right)^z$. With that they assume that the quark mass is properly described by the square of $\frac{m_\pi}{m_\rho}$. This should be the case for extremely light quark masses. However, in both cases the considered masses were somewhat larger than the ones we consider here and even for our data this does not give a good description of the quark mass, as can be seen from figure 2.1.

For this reason we have not taken the ratio of the pion and the ρ mass as a reference for the quark mass. The problem with that ratio lies strongly in the ρ mass, which cannot be considered to be a constant. This can be seen in table 2.3 in the range we want to consider. In addition we have arrived at the situation $\frac{m_\pi}{m_\rho} = 0.5$ where the ρ may decay in a sufficiently large volume into two pions: $\rho \to \pi\pi$. Therefore we have used

$$M_r \equiv (r_0 m_\pi)^2 \tag{2.5}$$

as a reference for the quark mass. In [29] we have then considered the formula

$$C_{\pi La} = F_{\pi La}(r_0 m_\pi)^{-z_\pi} \left(\frac{L}{a}\right)^{z_L} \left(\frac{r_0}{a}\right)^{z_a} \tag{2.6}$$

as a description of the costs. To compare the results with the previously mentioned results in [49, 59–63] we further used

$$C_U = F_U \left(\frac{m_\pi}{m_\rho}\right)^{-z_{\pi\rho}} \left(\frac{L}{a}\right)^{z_L} \left(\frac{r_0}{a}\right)^{z_a}. \tag{2.7}$$

In this form the results of equation (2.4) can be written as

$$\begin{gathered} F_U = 5.9 \cdot 10^6 \text{ flop} \\ z_{\pi\rho} = 6, \quad z_L = 5, \quad z_a = 2, \end{gathered} \tag{2.8}$$

where F_U is given in units of floating point operations (flop). Since we will restrict ourselves to the situation $\frac{r_0}{a} = const.$ we cannot determine the parameter z_a with these simulations. Anticipating the result $z_\pi = 4$ and making use of the fact that the masses are so light that both $M_r = (r_0 m_\pi)^2$ and $\mu_r = r_0 m_q$ give a good approximation to the quark mass, see figure 2.1, we can set $z_{aq} \equiv \frac{z_\pi}{2} = z_a$. The cost can therefore as well be parametrized as

$$C_{qL} = F_{qL}(am_q)^{-z_{aq}} \left(\frac{L}{a}\right)^{z_L}. \tag{2.9}$$

This way the parameter r_0 drops out which is very convenient. Indeed this parametrization of the costs is in some sense similar to equations (2.1) and (2.2), where $z_\pi = z_a$ was assumed so that r_0 could be removed from those equations. However, the simplification used in (2.9) is based on explicit findings for the powers in equation (2.6).

With equations (2.6), (2.7) and (2.9) we have found different ways in which we will parametrize the costs for a dynamical quark simulation. This will help to estimate the costs and feasability of future simulations. However, when doing so it has to be guaranteed that the given extrapolation still is valid for the new parameters. Usually future simulations will be at smaller masses and larger volumes than previous simulations. Due to the special needs of χPT there is an increasing interest to do simulations at much smaller masses than $m_{ud} \geq \frac{m_s}{2}$ which has been used so far. However, the estimates in equations (2.1), (2.2), (2.3) and (2.4) were made in a region of roughly $m_{ud} > \frac{m_s}{2}$ with the HMC algorithm. As has recently been shown [16] the HMC will produce so-called spikes in the force when going into the region $m_{ud} < \frac{m_s}{2}$. These spikes are probably related with extremely small eigenvalues and correspondingly a very small fermion determinant. This limits the precision of the calculation and therefore violates the reversability condition, which is crucial for the HMC. This does not make simulations at smaller quark masses impossible for the HMC because this problem can be solved by lowering the step size $\Delta\tau$ by an appropriate factor. However, this increases the cost estimates done in a region of $m_{ud} > \frac{m_s}{2}$ by orders of magnitude and the extrapolations in (2.1)-(2.4) become invalid.

Up to now the only algorithm for dynamical Wilson fermions that is known to be able to go to such small masses without further complications is the TSMB. This was explained in [23] by looking at the condition numbers used in the runs of the $N = 1$ Super-Yang-Mills theory [65,66], that are also summarized in section 3.3. The condition numbers that appeared were of $\mathcal{O}(10^5)$. In [23] it was estimated that this would correspond to quark masses of roughly $\frac{m_s}{4}$. Comparing with run (h) from table 2.2 and the results for this run from table 2.3 this estimate was fulfilled quite well and indeed by now with the simulations from this section there are simulations even below this quark mass. These simulation runs will give a reliable cost estimate for a range of quark masses as needed for χPT.

It remains to discuss the definition of cost [47]. Possibilities are to measure autocorrelation lengths of some important quantity or to achieve some given small error for them. Using infinite statistics both definitions should be equivalent for some given lattice action. It is not useful to give these costs in units of computer time, because that is highly dependant on the computer speed and system and the degree of optimization of the program. This would only make sense if the performance of the programs would be different due to intrinsic differences between the algorithms. This is, however, not the case because nearly every algorithm for dynamical quarks is dominated by the fermion-matrix-vector-multiplications (MVMs). Here we give the costs either in floating point operations (flop) or in MVMs with the main advantage that results are independent of the used computer system. It is easy to convert between flops and MVMs by using the following exact formula:

$$1 \text{ MVM} = 1344 \cdot L^3 T \text{ flop}. \tag{2.10}$$

Another possible unit would be the number of update cycles. This may seem to be a more natural choice, but one has to be careful because the number of MVMs for one update cycle is dependent on the polynomial orders and, in the case of global heatbath, on the condition number of the fermion matrix. We will give the conversion factor from cycles to MVMs for all of our runs.

Since the matrix multiplications dominate the computing time it is reasonable to express the costs and autocorrelations in units of MVMs. The part not directly related to MVMs is given by the local updates. However, these are dominated by parts which can

be essentially thought of as pieces of MVMs, too. As a result, the following approximate formula for the total amount of MVMs needed for one update cycle can be obtained:

$$N_{MVM}/\text{cycle} \simeq 6\,(n_1 N_\Phi + N_U) + 2\,(n_2 + n_3) N_C + I_G F_G \ . \tag{2.11}$$

N_Φ is the number of local bosonic sweeps per update cycle, N_U the number of local gauge sweeps, N_C the number of global Metropolis accept-reject correction steps, and I_G and F_G give the number of MVMs and frequency of the global heatbath.

For data from APEmille and Cray the estimate of the cost of the local updates obtained from (2.11) agrees with the actual costs up to 5%. Therefore the final costs in units of MVM based on (2.11) are not much influenced by the approximation. This is not true for the data presented for the P4-1700 system, since in this case the matrix multiplication and the local updates are not treated homogeneously. Indeed the former is written in assembler using SSE/SSE2 instructions while our code for the local updates is written in C++ and compiled with the g++ compiler. As a result, the estimate for the cost of the local updates is in this case underestimated by about a factor of three. Still we take the above formula as a reference when tuning the parameters because the number of MVMs is more generally applicable as it does not depend on implementation details. In addition, in the future the local updates could be rewritten by using SSE/SSE2 instructions, too, so eliminating the non-homogeneity with the MVMs.

So we want to determine the costs by measuring autocorrelations in units of MVM. It remains to decide which are those important quantities to be used for the determination of the autocorrelation. The choice should be such that one gets information about the decorrelation of the gauge field as well as on the fermionic sector. It is a common choice to use the average plaquette Tr $\left(\sum_{x\mu\nu} U_{\mu\nu}(x)\right)$ or its timelike part Tr $\left(\sum_{x\mu} U_{0\mu}(x)\right)$ to monitor the decorrelation of the gauge field, and for the fermionic sector the autocorrelation of the pion mass m_π seems to be a reasonable choice. Unfortunately the pion mass is a secondary quantity (a function of primary expectation values) and its autocorrelation is much harder to determine than that of primary quantities. An alternative is the largest-distance pion correlator. Its autocorrelation is a good estimate of the autocorrelation of the pion mass itself, and it is much easier to determine because the pion correlator is a primary quantity. Due to these problems with the pion autocorrelation another quantity is widely used to monitor the decorrelation of the fermionic sector. This is the smallest eigenvalue λ_{min} of $\tilde{Q}^2$, which is a primary quantity and therefore leads directly to good results. However, with the linearization method as described in section 1.5.4 $\tau_{int}^{m_\pi}$ can be reliably determined as any other autocorrelation.

To summarize we will use the average plaquette Tr $(\sum_x U_{\mu\nu}(x))$, the pion mass or correlator and the smallest eigenvalue of $\tilde{Q}^2$ to compute the autocorrelation.

2.1.1 Scaling behaviour in the light quark mass region

The general strategy to determine the exponents in (2.6), (2.7) and (2.9) is simple. Fix the volume in lattice unites $\frac{L}{a}$, which of course is easy, and fix the lattice spacing. Then set the quark mass to different values and extrapolate the needed costs to some appropriate formula.

In practice the situation is more demanding. There is no explicit mass parameter in the action, the only parameters we have available to set the lattice spacing a and the quark

Table 2.1: *Points of the $N_t = 4$ phase transition line as given by [67–69].*

β	5.4	5.3	5.27	5.2	5.12	5.1	5.0	4.95	4.9	4.76
κ	0.148	0.158	0.16	0.165	0.17	0.172	0.177	0.18	0.182	0.19

Table 2.2: *Bare couplings, parameters of the TSMB algorithm and total statistics in* 1000 *update cycles (U_k) of our runs around the $N_t = 4$ phase transition line on a $8^3 \cdot 16$ lattice.*

run	β	κ	n_1	n_2	n_3	n_4	λ	ε	U_k
(a)	5.28	0.160	20	40	70	100	2.8	$1.75 \cdot 10^{-2}$	80
(b)	5.04	0.174	28	90	120	150	3.0	$5.25 \cdot 10^{-3}$	33
(c)	4.84	0.186	38	190	240	300	3.6	$1.44 \cdot 10^{-3}$	31
(d)	4.80	0.188	44	240	300	300	3.6	$7.2 \cdot 10^{-4}$	12
(e)	4.76	0.190	44	360	380	500	3.6	$2.7 \cdot 10^{-4}$	144
(f)	4.80	0.190	44	360	380	500	3.6	$2.7 \cdot 10^{-4}$	224
(g)	4.72	0.193	52	600	750	800	3.6	$0.9 \cdot 10^{-4}$	196
(h)	4.68	0.195	66	900	1200	1100	3.6	$3.6 \cdot 10^{-5}$	200
(i)	4.64	0.197	72	1200	1500	1400	3.6	$1.8 \cdot 10^{-5}$	110
(j)	4.64	0.1975	72	1200	1350	1400	4.0	$2.0 \cdot 10^{-5}$	4

mass are the $SU(3)$ gauge coupling β and the hopping parameter κ. The bare quark mass am_0 can be set using the hopping parameter $\kappa = \frac{1}{2am_0+8r}$. But the quark mass in the Wilsonian formulation is subject to an additive renormalization, so we have to tune κ towards a critical value $\kappa_{crit}(\beta)$ if we want to lower the quark mass. This, however, will change the lattice spacing due to virtual loops of the fermions. Therefore β and κ have to be tuned simultaneously.

The first thing to do is to fix the desired lattice spacing. It should be so large that the physical volume is still large enough. Since most of our simulations were done on a $8^3 \cdot 16$ lattice and we would like to have a volume with a spatial extension of at least 2 fm this limits a to be larger than 0.25 fm. With the Sommer scale parameter $r_0 \approx 0.49$ fm as reference parameter this translates to $\frac{r_0}{a} \leq 2$. With $\frac{r_0}{a} = 2$ we would not be close to the continuum, something that would be considered to be the case for maybe $a < 0.1$ fm, but this should be no concern for a study of the simulation costs. However, we would prefer to choose the lattice spacing not much smaller than that, because the cost dependence could be different far away from the continuum limit.

There is another important issue to take care of when fixing the lattice spacing. The temperature

$$T = \frac{1}{N_t a}, \tag{2.12}$$

with N_t being the smallest lattice extension, should be such that the fields are in the confined phase. Hence the temperature T should be below the temperature of the finite

Table 2.3: *Results of runs specified in table 2.2 for different basic physical quantities. The values given in lattice units can be transformed to physical units by cancelling the lattice spacing a with the help of the results for $\frac{r_0}{a}$ and using $r_0 = 2.53\ GeV^{-1}$.*

run	r_0/a	af_π	am_π	am_ρ	m_π/m_ρ	M_r	am_q
(a)	1.885(30)	0.3738(50)	1.2089(36)	1.2982(32)	0.9312(17)	5.19(20)	0.2694(39)
(b)	1.715(20)	0.4321(23)	1.0428(41)	1.1805(38)	0.8834(14)	3.20(10)	0.1777(19)
(c)	1.616(110)	0.4171(47)	0.7886(40)	1.0251(48)	0.7693(32)	1.61(24)	0.09244(232)
(d)	1.903(159)	0.4199(75)	0.753(11)	0.999(12)	0.752(11)	2.05(40)	0.0815(20)
(e)	1.697(46)	0.4191(20)	0.7151(20)	0.9941(19)	0.7187(16)	1.473(88)	0.07220(71)
(f)	1.739(33)	0.3658(34)	0.5825(34)	0.9089(47)	0.6431(33)	1.026(51)	0.04773(95)
(g)	1.772(41)	0.3791(39)	0.5695(38)	0.9116(33)	0.6256(31)	1.018(61)	0.04271(126)
(h)	1.765(37)	0.3668(54)	0.5088(51)	0.8983(35)	0.5675(42)	0.806(50)	0.03500(90)
(i)	1.812(46)	0.3575(48)	0.4333(48)	0.8616(80)	0.5002(60)	0.616(45)	0.02367(58)
(j)	1.756(128)	0.3377(48)	0.4205(54)	0.859(12)	0.4894(65)	0.545(47)	0.02027(95)

temperature phase transition T_{crit}. Again we find the restriction that the lattice spacing should not be too small, because otherwise the fields will switch over to the deconfined phase where the dynamics change and, more importantly, something like a pion mass can no longer be defined meaningful.

For the $8^3 \cdot 16$ lattices we have to make sure that we stay below the $N_t = 8$ phase transition line. Indeed it makes sense to go along a phase transition line with $N_t < 8$. Not only we will make sure that we are in the correct phase, this will further fix the lattice spacing for us, because $T_{crit} r_0 \approx const.$, which was found to be valid for the mass region considered in [23]. Both the $N_t = 4$ and the $N_t = 6$ thermodynamical transition lines have the desired properties, as was found in previous simulations with $N_f = 2$ Wilson quarks [70, 71]. As a starting point, we have chosen the $N_t = 4$ phase transition line as given by the points of [67–69] and summarized in [71]. The points of this line as found in the literature are given in table 2.1, and they can easily be extended using the guidance line in [71]. The extrapolation is necessary because the last point of table 2.1 still corresponds to a mass of roughly $\frac{m_s}{2}$.

Following that guidance and retuning while going to new points we went down along that line, increasing κ and therefore going to lighter quark masses while at the same time keeping the lattice spacing constant at about $a \approx 0.27$ fm and $\frac{r_0}{a} \approx 1.8$, as can be seen from the measurement of the basic quantities in table 2.3.

We now turn to the determination of z_π, $z_{\pi\rho}$ and z_{aq} in equations (2.6), (2.7) and (2.9) respectively. This study uses the $8^3 \cdot 16$ lattice simulations as given in table 2.2, and the results were previously reported in [29]. Results for the autocorrelations are given in table 2.4. A first thing to notice is that the autocorrelation of the fermionic sector as described by the smallest eigenvalue λ_{min} or the pion mass m_π and its correlator is smaller by a factor of three to five than that of the gauge field sector. In case of m_π one of the reasons for this is the intrinsic fluctuation of the pion propagator explained by the freedom to randomly choose the position of the source for the inversion. However, this argument does not hold for the smallest eigenvalue. These smaller autocorrelations in the fermionic sector are expected but worthwhile to mention because of different findings in

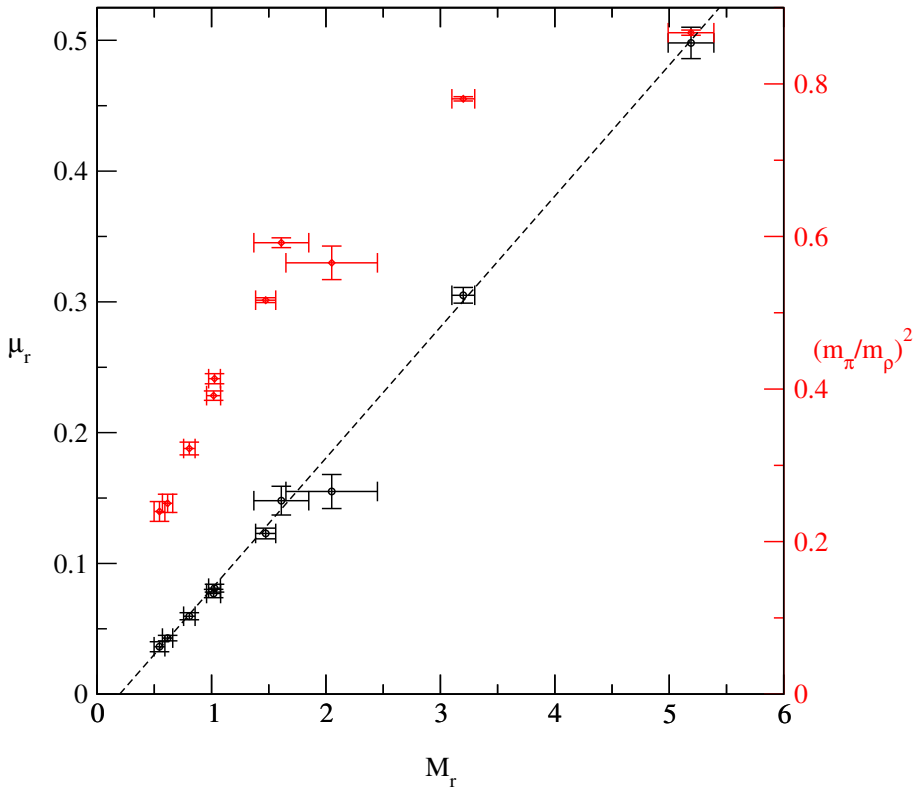

Figure 2.1: *Scaling of different quark mass definitions. A good linear fit is possible for the quark mass from the PCAC relation μ_r and M_r, while the ratio $\frac{m_\pi}{m_\rho}$ doesn't relate that nicely to the other definitions in this mass region.*

the past, where they were larger by a factor of two [72].

Using the values in table 2.4 one can extract the behaviour of τ_{int}^{plaq}, τ_{int}^{min} and $\tau_{int}^{m_\pi}$ as a function of the different dimensionless quark mass parameters M_r leading to z_π, $\frac{m_\pi}{m_\rho}$ leading to $z_{\pi\rho}$ and am_q leading to z_{aq}. Since the different runs are at slightly different values of $\frac{r_0}{a}$ they should be corrected to a common value of e. g. $\frac{r_0}{a} = 1.8$ using the assumed power $z_a = 2$. This small correction is only needed when extracting z_π and $z_{\pi\rho}$, while for z_{aq} there is no direct dependence on $\frac{r_0}{a}$.

The results of this study are collected in the plots of figure 2.2. The linear fits to τ_{int}^{plaq} give $z_\pi \simeq 4$, $z_{\pi\rho} \simeq 6$ and $z_{aq} \simeq 1.8$. For the fermionic sector lower exponents are found, indicating that cost estimates based on the plaquette autocorrelation alone give a too pesimistic result. Altogether we can summarize these results as:

$$z_\pi \simeq 3 - 4, \qquad z_{\pi\rho} \simeq 5 - 6, \qquad z_{aq} \simeq 1.3 - 1.8. \tag{2.13}$$

2.1.2 Determinant breakup

In [24, 25] algorithmic improvements for the simulation of staggered fermions coupled via hypercubic smeared links (HYP) were proposed. This HYP algorithm uses a stochastic estimate in a global Metropolis step similar to the correction step of the TSMB algorithm,

Table 2.4: *Integrated autocorrelations in update cycles obtained from runs specified by table 2.2. The second column gives the number of MVMs per cycle in thousands. The suffix min, plaq and m_π refer to the minimal eigenvalue of $\tilde{Q}^2$, the average plaquette and the pion mass, respectively.*

run	$kMVM$	τ_{int}^{min}	τ_{int}^{plaq}	$\tau_{int}^{m_\pi}$
(a)	1.49		200(20)	
(b)	2.45	340(60)	350(50)	140(20)
(c)	4.35		420(80)	150(20)
(d)	5.05	$\simeq 310$	490(90)	170(90)
(e)	7.34	550(110)	490(40)	207(33)
(f)	7.31	810(110)	800(90)	187(63)
(g)	10.5	320(80)	820(180)	188(13)
(h)	16.2	380(120)	940(330)	186(40)
(i)	20.4	670(210)	1500(300)	153(54)
(j)	17.4	$\simeq 390$	$\simeq 1050$	

see section 1.3.2. However, the acceptance rate for this correction step in the HYP algorithm was found to be very low, and already at small lattice sizes of 10 fm^4, i. e. $L \approx 1.5\,\mathrm{fm}$ it happened, that from 500 sample configurations not a single one was accepted [24]. They identified a large variance in the noisy estimator as the source of the problem. However, the straightforward solution to use several stochastic estimates violates the detailed balance condition [25, 73]. Therefore they came up with an alternative improvement for the noisy estimator, which still reduces the variance but leaves the correction step exact. The idea is to break up the determinant into several pieces by rewriting it as

$$\left|\det(\tilde{Q})\right|^{N_f} = \left\{\left|\det(\tilde{Q})\right|^{\frac{N_f}{N_b}}\right\}^{N_b}. \tag{2.14}$$

The number of breakups N_b can be chosen arbitrarily, corresponding to an arbitrary number of stochastic estimates in the correction step. For the HYP algorithm this leads to a significant improvement using eight to twelve determinant breakups [24, 25]. Something similar was already proposed in [74], where, however, no direct performance gain was found.

This determinant breakup can also be used with the TSMB algorithm [75] by using the extention for many flavours from section 1.3.4. However, a priori it cannot be decided if this will help to reduce the autocorrelations. Of course, the variance will be reduced due to the breakup, and therefore one can expect shorter autocorrelations in units of update cycles. But, on the other side, each update cycle will become more costly because the total number of boson fields $N_b n_1$ is increasing and more MVMs are needed in the correction step.

We have chosen run (b) from table 2.2 to compare different numbers of breakups. For each breakup we fixed the first polynomial order n_1 by requiring a fixed acceptance rate of $55\% - 60\%$. One way of fixing n_2 would be to ask for the same distribution of reweighting

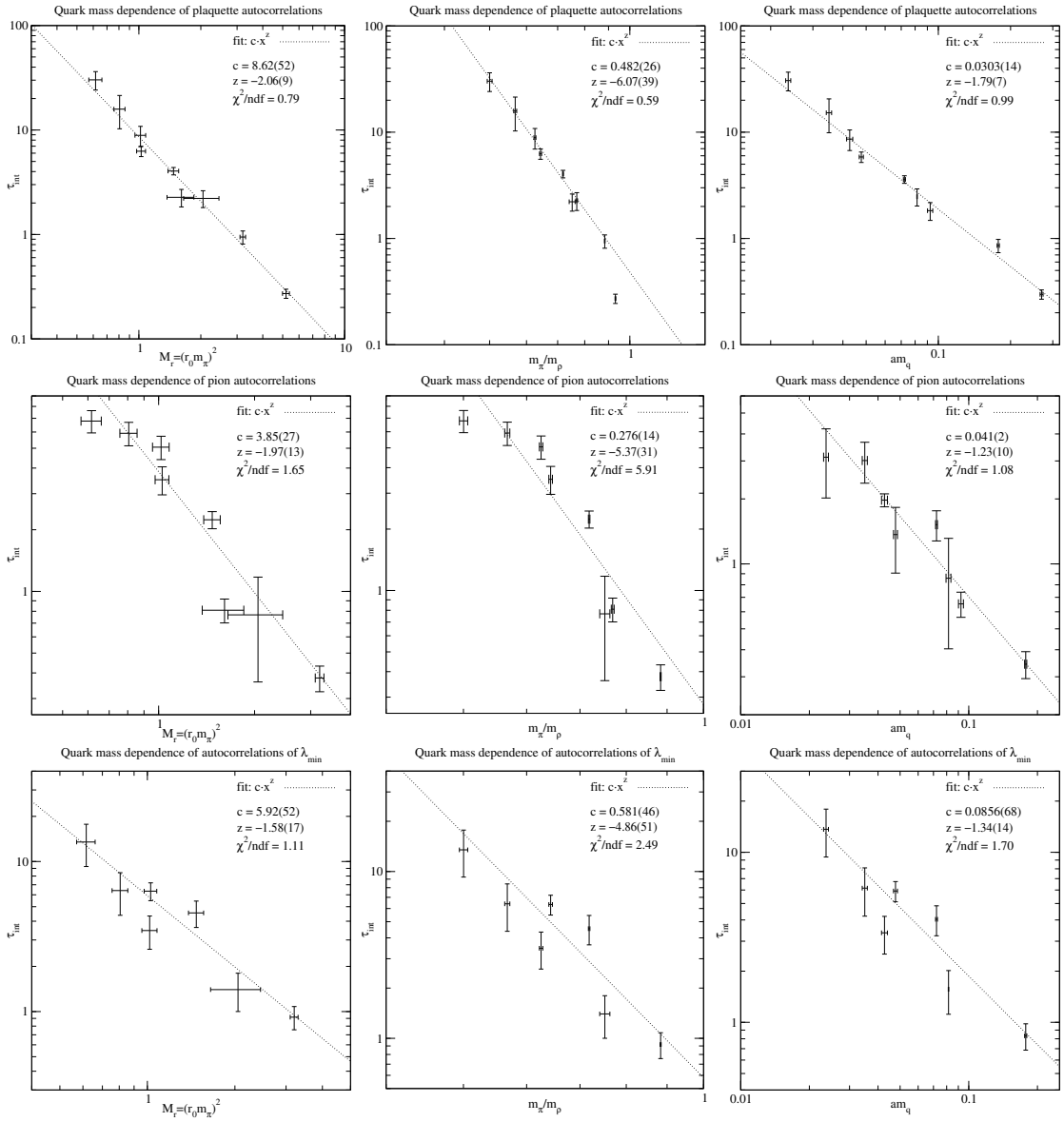

Figure 2.2: *Power fit of the autocorrelation of the plaquette, pion mass and smallest eigenvalue λ_{min} of $\tilde{Q}^2$ respectively given in units of $10^6 \cdot MVM$. The best fit is done using χ^2 minimization with respect to errors in both dimensions.*

factors. However, in this run they are precisely peaked around one anyway. A roughly equivalent way of fixing n_2 is to keep the relative deviation at the interval ends constant. This is how we fixed n_2 and n_3. The results from these simulation tests are given in table 2.5. We were able to validate the expectation that the autocorrelation measured in update cycles is reduced when breaking up the determinant. Furthermore we found that the costs for one update cycle are rising less than expected by just looking at the polynomial orders n_1 and n_2 and scaling (2.11) by them. The reason for this is that in (2.11) the total number of iterations in the global quasi heatbath I_G is not scaling with the

Table 2.5: *Run (b) from table 2.2 with determinant breakup in two, four and eight pieces. All other polynomial and updating parameters are unchanged.*

N_b (flavours)	n_1	n_2	n_3	$kMVM$	$\tau_{int}^{plaq}[MVM]$	$\tau_{int}^{min}[MVM]$	$\tau_{int}^{m_\pi}[MVM]$
$1\,(N_f = 2)$	28	90	120	3.22	$1.13(16) \cdot 10^6$	$1.09(19) \cdot 10^6$	$3.67(48) \cdot 10^5$
$2\,(N_f = 1 + 1)$	20	84	100	4.45	$6.05(53) \cdot 10^5$	$6.45(90) \cdot 10^5$	$2.36(36) \cdot 10^5$
$4\,(N_f = 4 \times \frac{1}{2})$	14	72	80	6.20	$1.55(37) \cdot 10^6$	$1.95(50) \cdot 10^6$	$3.60(56) \cdot 10^5$
$8\,(N_f = 8 \times \frac{1}{4})$	10	64	80	9.79	$1.17(29) \cdot 10^6$	$1.63(39) \cdot 10^6$	$4.77(58) \cdot 10^5$

number of boson fields but remains roughly constant when applying determinant breakup.

For this run with two degenerate quarks at a mass close to the strange quark mass and on a $8^3 \cdot 16$ lattice we found that one can benefit from determinant breakup by almost a factor of two. In this simulation point the optimal breakup seems to be $N_b = 2$. It remains to be seen whether determinant breakup helps at smaller quark masses and larger volumes, too. For smaller quark masses one can expect to gain even more, maybe by splitting the determinant into more than two pieces. There is hope for this further improvement because for the stochastic estimate in the correction step the most important contribution comes from a tiny interval at the lower border ε. In this interval there are only few eigenvalues, and without determinant breakup the variance will grow due to the steeper functional behaviour for larger condition numbers. If the interpretation of the variance is correct, then there is more room for improvement at smaller quark masses and there is a chance that the determinant breakup can help even more. So far there is even less known about the improvements due to determinant breakup at larger volumes. There the eigenvalue spectrum is denser, which already might reduce the variance, but on the other hand there are more important eigenvalues, and hence determinant breakup might still be as efficient. To make a final decision on the use of determinant breakup these simulation tests have to be repeated at other parameters, i. e. at smaller quark masses, larger volumes and closer to the continuum limit. For the moment we have shown that determinant breakup speeds up simulations by about a factor of two for intermediate quark masses and small volumes, and that it has the potential for further improvements at other parameters. Further investigations should be made, because future simulations can benefit from a better knowledge about the determinant breakup.

2.2 Volume dependence

Apart from the scaling with the quark mass the volume dependence of the autocorrelations is interesting. For this the run (f) from table 2.2 was repeated as run $(f12)$ with the same β and κ values on a $12^3 \cdot 24$ lattice, and runs (e) and (h) were repeated as $(e16)$ and $(h16)$ on a 16^4 lattice. When going to a larger lattice the first polynomial order n_1 has to be increased, because otherwise the acceptance rate in the correction step would drop due to a denser eigenvalue spectrum. All other polynomial parameters should remain essentially unchanged assuming no large finite volume effects. If these effects are small, the interval given by ε and λ remains. There is no need to change n_2 and n_3, they might even be slightly reduced due to the increased n_1. This is true for runs $(e16)$ and $(h16)$. For run

Table 2.6: *Simulation parameters for the analysis on larger volumes for run* (e) *at* $\beta = 4.76$, $\kappa = 0.190$, *for run* (f) *at* $\beta = 4.80$, $\kappa = 0.190$, *and for run* (h) *at* $\beta = 4.68$, $\kappa = 0.195$. *Run* $(f12)$ *is on a* $12^3 \cdot 24$ *lattice,* $(e16)$ *and* $(h16)$ *are on* 16^4 *lattices. The lattice extension as given in the last column is deduced from* r_0/a.

run	n_1	n_2	n_3	λ	ε	L[fm]
(e)	44	360	380	3.6	$2.7 \cdot 10^{-4}$	2.31(6)
$(e16)$	72	350	440	3.6	$2.7 \cdot 10^{-4}$	4.57(9)
(f)	44	360	380	3.6	$2.7 \cdot 10^{-4}$	2.25(4)
$(f12)$	72	500	560	3.4	$1.36 \cdot 10^{-4}$	3.02(9)
(h)	66	900	1200	3.6	$3.6 \cdot 10^{-5}$	2.22(5)
$(h16)$	96	860	1100	3.6	$3.6 \cdot 10^{-5}$	4.51(16)

Table 2.7: *Results of runs specified in table 2.6 for different basic physical quantities. The values given in lattice units can be transformed to physical units by cancelling the lattice spacing* a *with the help of the results for* $\frac{r_0}{a}$ *and using* $r_0 = 2.53\ GeV^{-1}$.

run	r_0/a	af_π	am_π	am_ρ	m_π/m_ρ	M_r	am_q
$(e16)$	1.673(43)	0.4250(27)	0.7075(17)	0.9852(23)	0.7181(15)	1.401(79)	0.07210(32)
$(f12)$	1.993(54)	0.3645(31)	0.5866(27)	0.8880(90)	0.6606(67)	1.367(88)	0.04881(59)
$(h16)$	1.742(60)	0.3746(60)	0.5054(33)	0.8582(67)	0.5890(46)	0.773(63)	0.03396(60)

(f) the lower boundary ε was not optimal, which is why we used a better, i. e. smaller one in run $(f12)$. It should be stressed that this is no finite volume effect because the actual smallest eigenvalue of $\tilde{Q}^2$ is roughly the same in the two runs and only the algorithmic parameters have been adjusted to be better suited for this situation. Due to the larger condition number in this run it was necessary to increase n_2 and n_3, too. We give all the parameters together with their values on the $8^3 \cdot 16$ lattice in table 2.6.

In the cost estimates of this work we usually neglect additional costs for parameter tuning and equilibration, i. e. thermalization of the fields. This is reasonable, because usually a configuration thermalized for similar parameters is available, and thermalization starting from that configuration is quite cheap. Furthermore on small lattices this effect is negligible anyway. This situation slightly changes on the 16^4 lattice. We didn't have similar configurations for this lattice size, and thermalization from a random configuration ("hot start") would have taken a substantial time on this lattice size before equilibrium is reached. Therefore we have chosen another strategy. We have taken a configuration from the corresponding $8^3 \cdot 16$ run and doubled each of the spatial extensions. This way we acquired a 16^4 configuration without breaking the gauge, keeping the plaquette value exactly unchanged and keeping the eigenvalues roughly unchanged. This configuration is not thermalized, and furthermore the configuration has an intrinsic periodicity. However, thermalization can be reached much earlier by this method, and the periodicity can be monitored by measuring the different spatial slices of the plaquette. Results are shown

Table 2.8: *Integrated autocorrelations in update cycles obtained from runs specified by table 2.6. The second column gives the number of MVMs per cycle in thousands. The suffix plaq and m_π refer to the average plaquette and the pion mass, respectively.*

run	τ_{int}^{plaq}[flop]	$\tau_{int}^{m_\pi}$[flop]
(e)	$4.59(37) \cdot 10^{13}$	$1.94(31) \cdot 10^{13}$
$(e16)$	$7.5(1.3) \cdot 10^{14}$	$5.02(55) \cdot 10^{13}$
(f)	$7.47(84) \cdot 10^{13}$	$1.76(59) \cdot 10^{13}$
$(f12)$	$2.40(41) \cdot 10^{14}$	$4.52(82) \cdot 10^{13}$
(h)	$1.7(6) \cdot 10^{14}$	$3.3(7) \cdot 10^{13}$
$(h16)$	$1.10(17) \cdot 10^{15}$	$8.3(8) \cdot 10^{13}$

in figure 2.3. It can clearly be seen that the correlation as a remnant of the old $8^3 \cdot 16$ lattice has vanished after roughly 1000 update cycles in run $(e16)$. For run $(h16)$ this took a little longer, here roughly 3000 update cycles were needed. But still this is a very good way to speed up thermalization, since otherwise the costs for reaching a thermalized configuration could have easily been higher by an order of magnitude.

To determine the exponent z_L in (2.6), (2.7) and (2.9) it is needed to repeat some of the runs of table 2.2 on larger lattices, either increasing the physical volume or going closer to the continuum limit. With the simulations in table 2.6 we have chosen to keep the lattice spacings roughly unchanged while increasing the physical volume.

Results for the autocorrelations of these runs in comparison with the corresponding simulations on a $8^3 \cdot 16$ lattice are given in table 2.8. The autocorrelation of the plaquette increases roughly by one order of magnitude when going from a $8^3 \cdot 16$ lattice to a 16^4 lattice, while a factor of 13 could be expected from $z_L = 5$ as given in [62], see (2.8). Therefore our preliminary results seem to be in good agreement with those previous estimates by other collaborations.

However, the more interesting sector is the fermionic one. Here we find that the pion mass autocorrelation increases by less than a factor of three when going from a $8^3 \cdot 16$ lattice to a 16^4 lattice, and our results in this sector would be more consistent with $z_L \simeq 2 - 2.5$. This is remarkable, because it is below the trivial factor of $z_L = 4$, which would be the naive estimate including only the increased number of lattice points. Partly this pleasant scaling behaviour can again be explained through the intrinsic fluctuations of the pion propagator, and the increasing number of timeslices available for fixing the source randomly.

2.3 Behaviour of the eigenvalue spectrum

The eigenvalue spectrum of the Wilson-Dirac fermion-matrix is interesting both physically and for the simulation algorithms. From the physical point of view the low-lying eigenvalues are expected to dominate the hadron correlators [76, 77] and carry information of the topological content of the background gauge field [78–80]. Due to the importance of the question of the behaviour of the eigenvalue spectrum at light quark masses we study

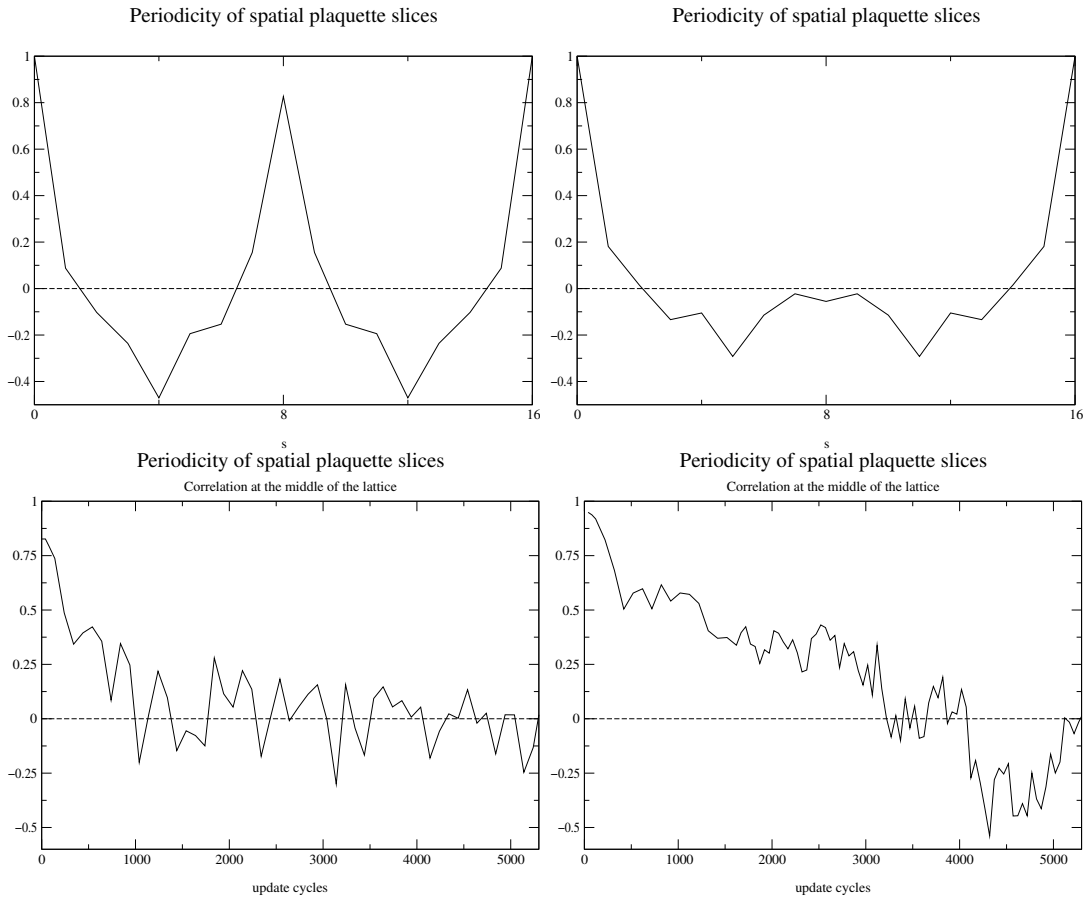

Figure 2.3: *In the upper two panels the correlation of the spatial plaquette of run* ($e16$) *is shown after 40 and after 1540 updates, respectively. In the lower left panel this correlation of run* ($e16$) *at the middle of the lattice, i. e. at* $s = \frac{L}{2}$ *is plotted as a function of update cycles. In the lower right panel the same is plotted for run* ($h16$).

them on the $8^3 \cdot 16$ lattices where light quark masses are reached, although these lattices are rather coarse.

We will first study the eigenvalues of the hermitean fermion-matrix, where the algorithm of Kalkreuther and Simma [81] is used to calculate the smallest eigenvalues. In section 2.3.2 we will study the non-hermitean matrix using the Arnoldi method [82, 83].

We will further study the presence of negative eigenvalues. This is not necessary for $N_f = 2$, but it will give indications on the presence of a sign problem for cases with an odd number of flavours as planned for the future [23].

2.3.1 Eigenvalues of the hermitean fermion-matrix and reweighting factors

The eigenvalues $\tilde{\lambda}_{min}$ of $\tilde{Q}^2$ are among those quantities that are monitored during the runtime of the simulation. It is always an important reference parameter for a gauge configuration, and for multi-bosonic algorithms it is even more important because the

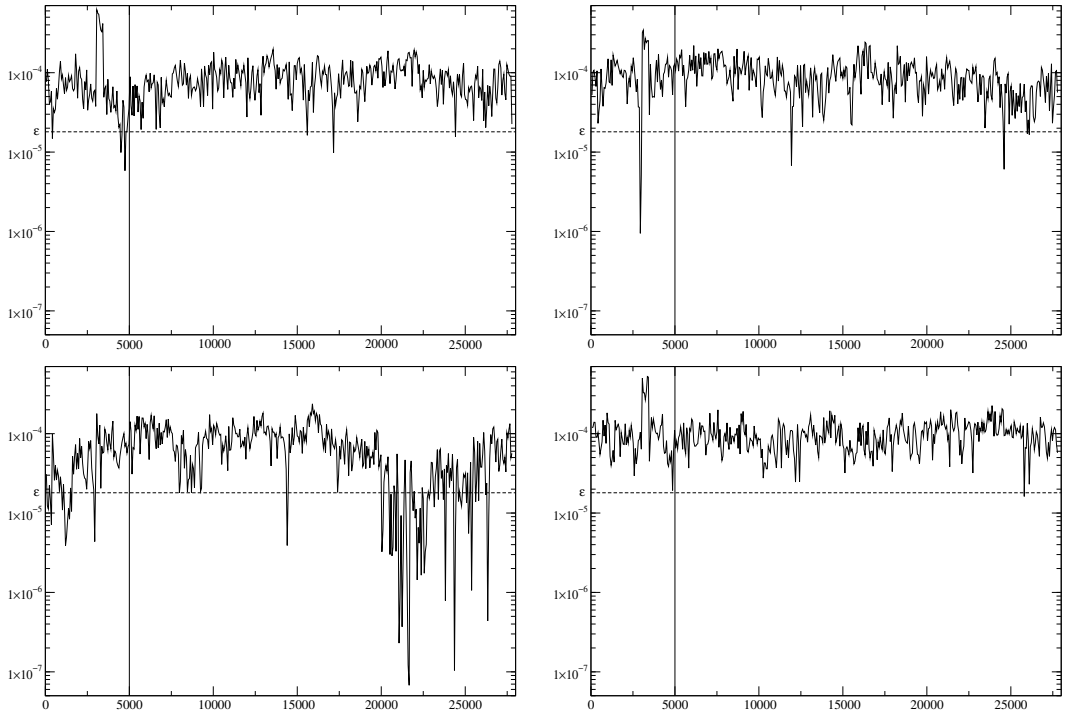

Figure 2.4: *Histories of the smallest eigenvalue* $\tilde{\lambda}_{min}$ *at* $\beta = 4.64, \kappa = 0.197$ *for the four independent lattices. The lower limit of the polynomial* ε *is shown by the dashed line. The measurement of physical quantities was started at the vertical line to exclude thermalization effects. The lower left figure is the history with exceptionally small eigenvalues, while the other three lattices show a typical behaviour.*

polynomial approximation will only be good enough if all of the eigenvalues $\tilde{\lambda}_{min}$ are inside the interval $[\varepsilon, \lambda]$, compare with (1.26). This is no concern for the correctness of the TSMB algorithm, because the ε of the third polynomial is usually set below the ε of the first and second polynomial by a factor of 100, so that there is no systematic error introduced due to the third polynomial. All other errors can be corrected by the reweighting factor. Still it is obvious that for performance reasons we don't want to let the smallest eigenvalue $\tilde{\lambda}_{min}$ go below the ε of the first and second polynomial, which we usually tried to set below the typical smallest eigenvalue by a factor of two or more. However, for small quark masses as in (h) and (i) in table 2.2 the smallest eigenvalue may start to fluctuate alot. These simulations were done on the APEmille installation in Zeuthen, which mainly consists of eight crates. On one crate there always have to run at least four independent $8^3 \cdot 16$ lattice replicas, which is indeed the setup we have chosen. In one of the four independent runs of (i) it happened that the smallest eigenvalue dropped below ε by more than two orders of magnitude. It did stay there for quite some time until it did recover. If this would have been the only run another much better polynomial could have been chosen, which would have pushed $\tilde{\lambda}_{min}$ back to the preferred situation. After that one should have switched back to the original polynomial because this is much cheaper than this better polynomial but still it is good enough in nearly all cases. Since, however, we had four lattices running

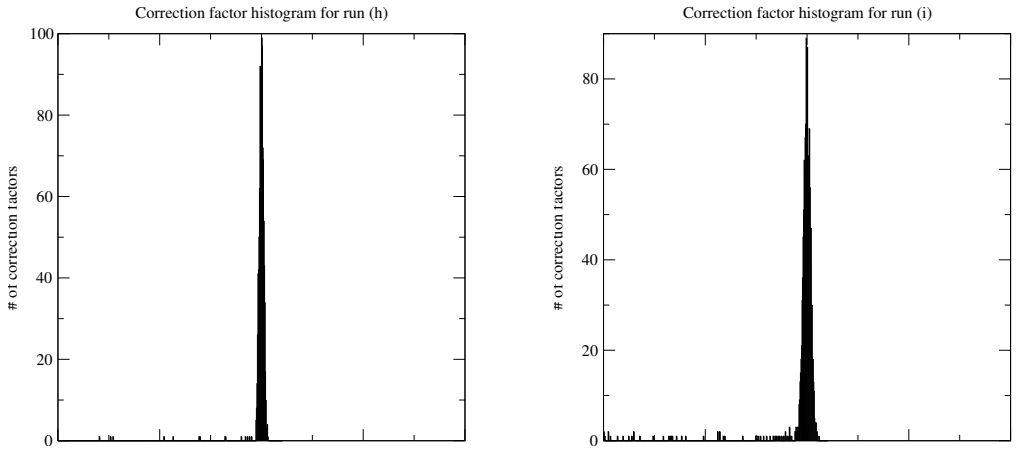

Figure 2.5: *Reweighting factors for run* (h) *(left panel) and* (i) *(right panel).*

in parallel we took the opportunity to keep the polynomial fixed and to see if the expected behaviour, the recovering of the smallest eigenvalue really sets in. As can been seen in figure 2.4 this did happen.

Taking the opportunity to watch the recovering of the smallest eigenvalue did have one drawback. The autocorrelations are completely spoiled by that effect and the reweighting factors become very small. We therefore had to drop this lattice for the study of autocorrelations. This is clearly allowed because we could have used a better polynomial for a very short time and hence this lattice would have continued as the other ones. The reweighting factors for the sum of the four independent lattices are shown in figure 2.5 for runs (h) and (i), which were the only ones where we found something like a flattish tail.

In all other runs than (i) in table 2.2 we did not see eigenvalues staying below ε for such a long time.

2.3.2 Eigenvalues of the non-hermitean fermion-matrix

Other than the eigenvalues of the hermitean fermion-matrix the eigenvalues of the non-hermitean fermion matrix are not looked after during the simulation. However, they are very interesting because they contain more information. Therefore it is worthwhile to study them although it is more expensive to compute them.

The eigenvalues of Q depend trivially on the valence hopping parameter κ_{val}, because

$$Q = 1 - \kappa_{val} D. \tag{2.15}$$

This is not true for the hermitean fermion-matrix $\tilde{Q} = \gamma_5 Q$. The spectrum of D is invariant under complex conjugation and sign change, which can be seen from the symmetries

$$Q^\dagger = \gamma_5 Q \gamma_5, \qquad ODO = -D, \tag{2.16}$$

with $O_{xy} = (-1)^{x_1+x_2+x_3+x_4}\delta_{xy}$. One can therefore gain in speed by choosing an arbitrary value $\kappa_{val} = \bar{\kappa}_{val}$ and recover the results for the original κ_{val} by a shift. However, this

may influence the numerical precision, so the value of $\bar{\kappa}_{val}$ should be chosen such that it gives the best compromise between computation time and precision.

One can further gain in speed by making use of the observation that the Arnoldi algorithm is more efficient on the even-odd preconditioned matrix $\bar{Q}$ than on Q itself. Using an analytic relation the eigenvalues of $\bar{Q}$ can be transformed back to the ones of Q. For that purpose Q is written in the form

$$Q = 1 - \kappa \begin{pmatrix} 0 & D_{eo} \\ D_{oe} & 0 \end{pmatrix}. \tag{2.17}$$

Then $\bar{Q}$ is given by

$$\bar{Q} = 1 - \kappa^2 \begin{pmatrix} 0 & 0 \\ 0 & D_{oe}D_{eo} \end{pmatrix}. \tag{2.18}$$

If $v = (v_e, v_o)$ is an eigenvector of Q with eigenvalue λ then it satisfies

$$(\lambda v_e, \lambda v_o) = (v_e - \kappa D_{eo} v_o, v_o - \kappa D_{oe} v_e). \tag{2.19}$$

Then we get from

$$(1 - \kappa^2 D_{oe}D_{eo})v_o = v_o - (1-\lambda)^2 v_o = \lambda(2-\lambda)v_o \tag{2.20}$$

that the eigenvalues of $\bar{Q}$ are either one (in the even subspace), or they satisfy

$$\bar{\lambda} = \lambda(2-\lambda). \tag{2.21}$$

Because of the symmetries mentioned above, the solutions of (1.89) will give all the eigenvalues of the matrix Q.

We have studied the eigenvalue spectrum of the non-hermitean matrix for the runs labeled with (a) and (c) to (j). In each case samples of ten configurations were analyzed at an auxiliary value of $\bar{\kappa}_{val} = 0.17$. We determined both the 150 eigenvalues of the preconditioned fermion-matrix $\bar{Q}$ with smallest modulus and the 50 eigenvalues of the non-preconditioned matrix Q with smallest real part. The results were then transformed to the eigenvalues of Q at the κ value of the dynamical updates ($\kappa \equiv \kappa_{sea}$) using the above formulas. The results are shown in figure 2.6. The dashed vertical line shows the limit for the computation of the eigenvalues with smallest real part. Only the part of the spectrum to the left of this line is known. In a similar way, by computing the eigenvalues with smallest modulus, we have access to the part of the spectrum inside the dashed circle. The circle is deformed and not centered at the origin because it has been transformed together with the eigenvalues by using (1.89). In summary, the spectrum is not known in those points of the complex plane which are both to the right of the vertical line and outside the circle.

Since the sequence from (a) to (j) corresponds to decreasing quark masses it is not a surprise that the eigenvalues have an increasing tendency to go to the left in the complex plane. At the same time they are pushed away from zero as an effect of including the fermionic determinant in the path integral measure. At very small quark masses a pronounced hole near zero develops. For the continuum Dirac operator the spectrum is expected as a vertical line with some gap near zero. On our coarse lattices there is an additional horizontal spread of the eigenvalues and the picture is strongly deformed.

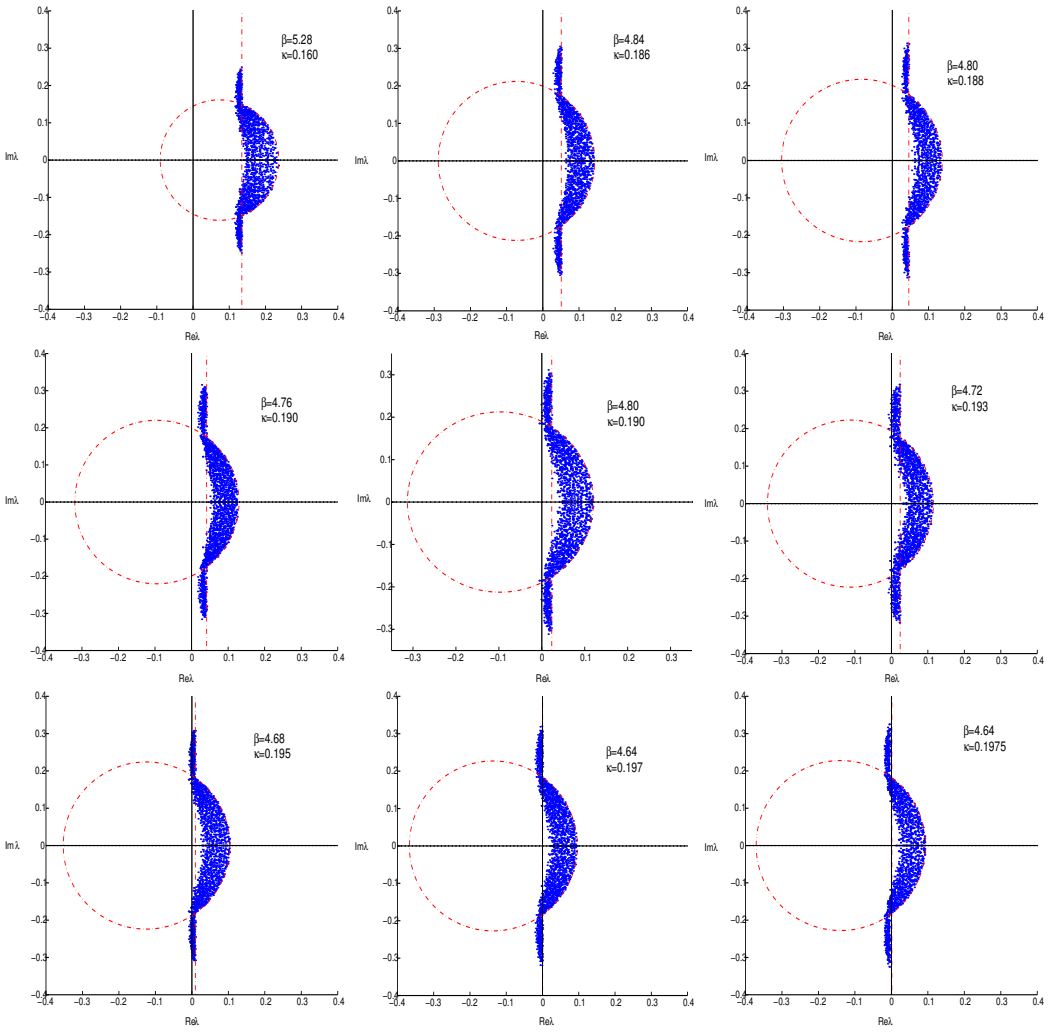

Figure 2.6: *Low-lying eigenvalues from a set of* $\mathcal{O}(10)$ *configurations for runs* (a), (c) *to* (j).

The size of the holes produced by the determinant is very important if we have in mind the possibility of computing observables at a partially quenched valence κ value κ_{val} higher than κ_{sea} used in the update. The distance between the origin and the smallest real eigenvalue determines how much smaller masses (larger κ_{val}) one can reach by partial quenching before encountering exceptional configurations.

2.3.3 Negative eigenvalues

As seen in section 1.3.5 it is important to include the sign of the determinant in the measurement because it had to be neglected in the process of updating. It is, however, unnecessary to calculate the sign of all configurations right from the beginning. A subsample of configurations should be chosen and the sign should be determined. As explained in section 1.3.5 a negative sign is most likely when there are exceptionally small eigenvalues

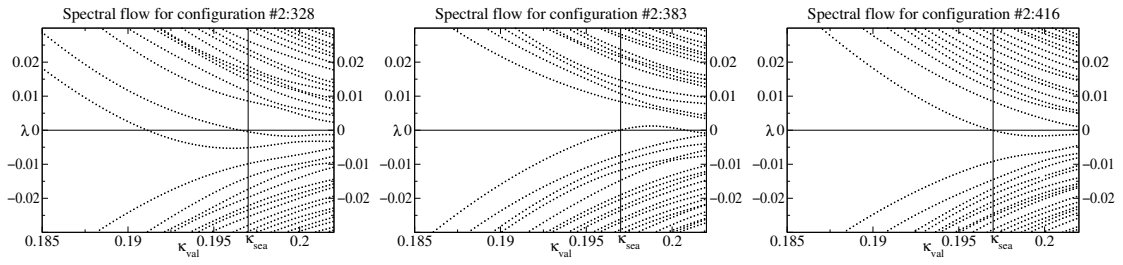

Figure 2.7: *Spectral flow for three configurations of run (i) from table 2.2. These are the only ones where zero-level crossings were found. The vertical line denotes κ_{sea} from the simulation.*

of $\tilde{Q}^2$. Therefore configurations with such eigenvalues should be checked systematically.

In the simulations of this chapter the number of fermion flavours $N_f = 2$ is even, and therefore only the square of the determinant is important. Hence the sign can be ignored. However, this work is considered as preparatory work for later $N_f = 3$ or $N_f = 2 + 1$ simulations. If $N_f = 2 + 1$ is chosen the single quark will be around the strange quark mass, and it is already known and seen again in this work that there is no problem with the sign. Exceptional configurations appear basically never and no sign changes should be expected. If, however, three degenerate quarks ($N_f = 3$) are to be simulated, the aim will be most likely to tune the quark mass to very small values, maybe towards the values reached with the simulations of table 2.2. Although this is not the physical situation such simulations would perfectly make sense, because for use with chiral perturbation theory such an approach might be easier due to fewer parameters. For such runs it is expected that the situation for the sign of the determinant doesn't change drastically from the situation for $N_f = 2$. Therefore it is nice to know if the runs of this chapter give some hint on the appearance of the sign problem.

One of the methods that can be used to find the sign of the determinant on a single configuration is to consider the spectral flow as described in section 1.3.5. Having searched for negative signs in all of the runs of table 2.2 we found a negative sign only on two configurations of run (*i*). Actually we have found three configurations with zero-level crossings, the spectral flow of these configurations is shown in figure 2.7. However, one of these configurations has two zero-level crossings for $\kappa_{val} < \kappa_{sea} = 0.197$ and therefore the sign of the determinant is positive according to equation (1.66).

The two configurations with negative determinant come from the long tail of the reweighting factors as shown in the right panel of figure 2.5, both have reweighting factors of $\mathcal{O}(10^{-4})$. Their relative statistical weight is $\mathcal{O}(10^{-7})$. Clearly the configurations with negative sign of the determinant are statistically insignificant even at such small quark masses as a fifth of the strange quark mass. And although (partially quenched) chiral perturbation theory allows three degenerate quarks at this mass the additional computational costs for pushing a third quark towards such light masses is probably not worth the effort. Therefore, provided the picture will not change dramatically on larger lattices, for all physical circumstances it seems very unlikely that the sign of the determinant could ever become a problem [29].

Since we found at least three configurations with zero-level crossings we want to take the opportunity and compare the method of the spectral flow with some other method.

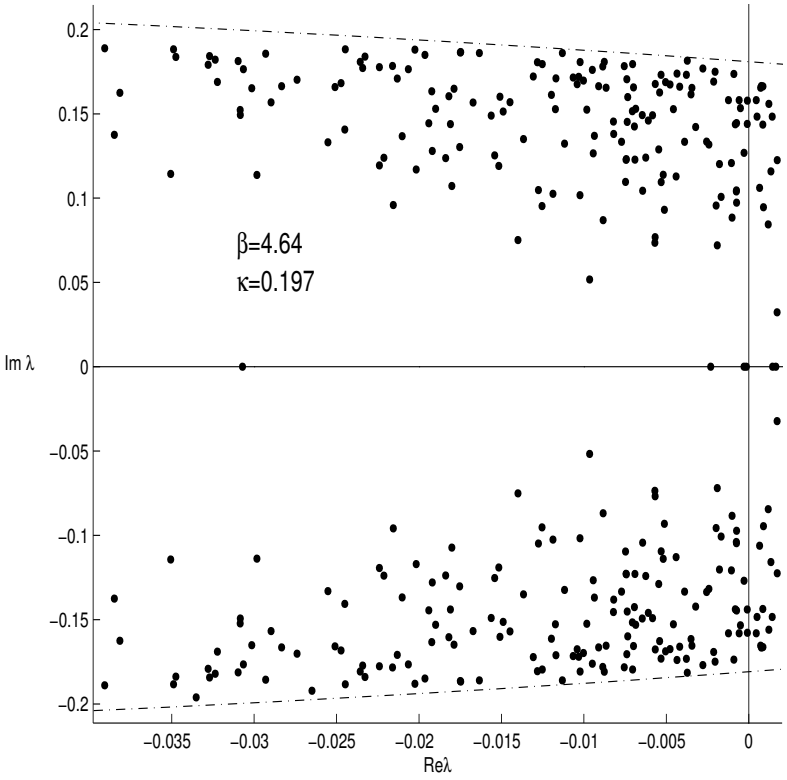

Figure 2.8: *Eigenvalues of the non-hermitean fermion matrix Q for the runs of figure 2.7.*

In section 2.3.2 we were already looking at the smallest eigenvalues of the non-hermitean matrix Q using the Arnoldi algorithm. If we have enough of these eigenvalues we can find out the sign of the determinant by another method. The eigenvalues appear either in complex conjugate pairs or they are real. Therefore $\det Q$ can only have a negative sign if there is an odd number of eigenvalues at the negative side of the real axis. Comparing the method of the spectral flow with the method using the non-hermitean eigenvalues from the Arnoldi algorithm we see a very good agreement. The eigenvalues for the configurations from figure 2.7 are shown in figure 2.8. The configuration that has two zero-level crossings has two real negative eigenvalues, while for the two configurations with one zero-level crossing the determination from the non-hermitean eigenvalues points towards a negative sign.

2.4 Chiral logarithms and the applicability of Chiral Perturbation Theory

As stressed before, lattice simulations do not necessarily have to be done at the costly and so far unreachable physical quark masses. Effective theories, i. e. Chiral Perturbation Theory (χPT) can be used to extrapolate results obtained at larger masses to the physical situation. In this section we will shortly introduce the foundations of χPT and we will see

how well our data is described by it.

2.4.1 Chiral Perturbation Theory (χPT)

At vanishing quark masses the QCD Lagrangian (1.1) can be written as

$$\mathcal{L}^0_{QCD}(x) = -\frac{1}{4}F_{\mu\nu}(x)F^{\mu\nu}(x) + i\bar{q}_L \not{D} q_L + i\bar{q}_R \not{D} q_R. \tag{2.22}$$

It is then invariant under global $SU(N_f)_L \otimes SU(N_f)_R$ transformations of the left- and right-handed quarks in flavour space, the chiral symmetry transformations. Since indeed the up, down and strange quarks are light this should be a good approximation for this part of the hadronic spectrum. However, this kind of chiral symmetry is not seen in nature. Instead the hadrons, e. g. the pseudoscalar meson octet shown in figure 1 in the introduction, can only be classified in $SU(3)_V$ representations, while degenerate multiplets with opposite parity are not found. This leads to the conclusion that the ground state, i. e. the vacuum is not chirally invariant under $SU(3)_L \otimes SU(3)_R$. It is spontaneously broken to $SU(3)_V$, where $g_L = g_R$ for $g_{L,R} \in SU(3)_{L,R}$. The Goldstone bosons that have to appear due to this spontaneous symmetry breaking can be identified as the eight lightest hadronic states: $\pi^{\pm,0}$, η, $K^{\pm,0}$, and $\bar{K}^0$.

The fact that the pseudoscalar mesons can be interpreted as Goldstone bosons implies strong constraints on their interactions. Because the other particles of the hadronic spectrum are heavier than these pseudoscalar mesons this allows to build an effective field theory containing only the particles of the pseudoscalar meson octet.

If we denote the coordinates describing the Goldstone fields as ϕ^a, $a = 1, \ldots, 8$, then the change of the Goldstone coordinates under a chiral transformation is given by

$$U(\phi) \xrightarrow{SU(3)_L \otimes SU(3)_R} g_R U(\phi) g_L^\dagger, \qquad g_{L,R} \in SU(3)_{L,R}. \tag{2.23}$$

The unitary matrix $U(\phi)$ can be written as

$$U(\phi) = \exp\left(\frac{2i\Phi}{f}\right), \tag{2.24}$$

with

$$\Phi(x) \equiv \frac{1}{\sqrt{2}}\vec{\lambda}\vec{\phi} = \begin{pmatrix} \frac{1}{\sqrt{2}}\pi^0 + \frac{1}{\sqrt{6}}\eta_8 & \pi^+ & K^+ \\ \pi^- & -\frac{1}{\sqrt{2}}\pi^0 + \frac{1}{\sqrt{6}}\eta_8 & K^0 \\ K^- & \bar{K}^0 & -\frac{2}{\sqrt{6}}\eta_8 \end{pmatrix}. \tag{2.25}$$

For an effective low-energy chiral field theory we have to write down the most general Lagrangian using the matrix $U(\phi)$ that still respects chiral symmetry. This Lagrangian can be organized in terms of an increasing number of derivatives:

$$\mathcal{L}_{eff}(U) = \sum_n \mathcal{L}_{2n}. \tag{2.26}$$

To lowest order the only non-trivial effective chiral Lagrangian is uniquely given by

$$\mathcal{L}_2 = \frac{f^2}{8}\mathrm{Tr}\left(\partial_\mu U^\dagger \partial^\mu U\right) \tag{2.27}$$

This Lagrangian can be expanded in Φ, which leads to the Goldstone kinetic terms and infinitely many interaction terms between an increasing number of pseudoscalars. We can therefore write:

$$\mathcal{L}_2 = \frac{1}{2}\mathrm{Tr}\left(\partial_\mu \Phi \partial^\mu \Phi\right) + \frac{1}{6f^2}\mathrm{Tr}\left(\left(\Phi \overleftrightarrow{\partial_\mu} \Phi\right)\left(\Phi \overleftrightarrow{\partial^\mu} \Phi\right)\right) + \mathcal{O}\left(\Phi^6/f^4\right). \tag{2.28}$$

Applying perturbation theory to this effective theory allows to compute decay amplitudes between the different pseudoscalar mesons.

The aim of applying this approach to lattice gauge field theory is to estimate the quark mass dependence of the hadronic observables. The quarks can be added as external classical fields to (2.22), leading to

$$\mathcal{L}_{QCD} = \mathcal{L}^0_{QCD} + \bar{q}\gamma^\mu(v_\mu + \gamma_5 a_\mu)q - \bar{q}(s - i\gamma_5 p)q, \tag{2.29}$$

where $v_\mu(x)$, $a_\mu(x)$, $s(x)$ and $p(x)$ are hermitean, colour neutral matrices in flavour space. For $a = v = 0$ the lowest order effective Lagrangian (2.27) then takes the form

$$\mathcal{L}_2 = \frac{f^2}{8}\mathrm{Tr}\left(\partial_\mu U^\dagger \partial^\mu U + U^\dagger \chi + \chi^\dagger U\right), \tag{2.30}$$

where

$$\chi = 2B_0(s + ip). \tag{2.31}$$

This allows to give predictions about the hadronic spectrum and decay constants in terms of the constants f and B_0. For instance for degenerate quark masses the pion mass-squared at tree-level is given by

$$M_\pi^2 = 2m_{ud}B_0, \tag{2.32}$$

and the pion decay constant is

$$f_\pi = f. \tag{2.33}$$

Higher orders in perturbation theory can be calculated [54], where the characteristic chiral logarithms appear. In (one-loop) next-to-leading order (NLO) the above quantities then scale with the quark mass as follows:

$$\frac{M_r}{2\mu_r} = Br_0 - \frac{M_r \cdot Br_0}{16\pi^2(f_\pi r_0)^2}\ln\left(\frac{(\Lambda_3 r_0)^2}{M_r}\right) + \mathcal{O}(M_r^2) \tag{2.34}$$

$$f_\pi r_0 = fr_0 + \frac{M_r}{8\pi^2 f r_0}\ln\left(\frac{(\Lambda_4 r_0)^2}{M_r}\right) + \mathcal{O}(M_r^2). \tag{2.35}$$

In both cases the Sommer scale parameter r_0 has been used to get dimensionless quantities and therefore allow for an easy comparison with lattice data. A more detailed review about the topic of effective field theories and χPT can be found in [84], and a recent summary of lattice results fitted to this formulas is in [85].

2.4.2 Chiral logarithms at light quark masses

So far the application of (2.34) and (2.35) was not crowned with success, because recent results still show that the data is more compatible with a linear fit than with chiral logarithms from the NLO results of χPT, see [57,58]. The reason for this failure is plausible:

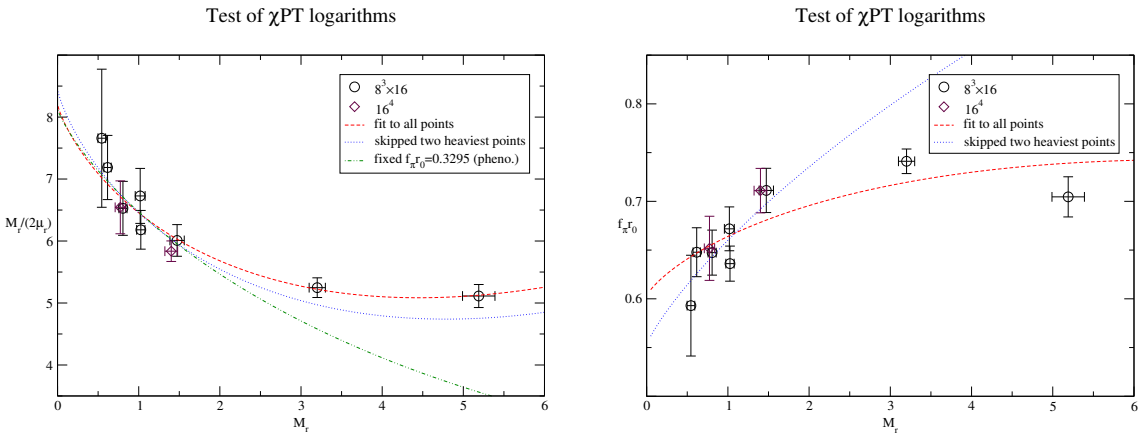

Figure 2.9: *Left panel: Fit of the pseudoscalar meson mass-squared with the one-loop χPT formula (2.34). Right panel: Fit of the pseudoscalar meson decay constant with the one-loop χPT formula (2.35).*

the used quark masses of $m_{ud} \geq \frac{m_s}{2}$ are too heavy, so that the one-loop approximation of χPT doesn't give a reliable description of the data.

With the runs studied in this chapter we have results for smaller quark masses. However, to be precise we are not allowed to directly apply the χPT formulas (2.34) and (2.35) to our data. These formulas should be applied to continuum results, while our results are on rather coarse lattices. This was fine for an algorithmic study, but this should be avoided if χPT is to be applied. Furthermore χPT is an effective theory, i. e. a phenomenological theory. Therefore one has to apply the above formulas to renormalized quantities, while we have given up to now only the unrenormalized ones.

Still it is worthwhile to repeat the fits to (2.34) and (2.35) as in [57, 58], because this can give insights about the region of applicability of χPT, i. e. which quark masses have to be realized on the lattice. And indeed the expectations from [55] would suggest that the quark masses we have reached should be small enough to make the chiral logarithms visible.

Our data together with best fits to (2.34) and (2.35) are shown in figure 2.9. Clearly some curvature can be seen, and the results may be fitted nicely to the formulas of χPT. The results from the fit to (2.34) are $Br_0 = 8.2$, $f_\pi r_0 = 0.27$ and $\Lambda_3 r_0 = 3.5$. The results from the fit to (2.35) are $fr_0 = 0.60$ and $\Lambda_4 r_0 = 4.3$. Further constraint fits are possible, and in any case we get reasonable values, similar to the ones deduced in [85].

The fact that our data in the region of small quark masses with $\frac{m_s}{5} \leq m_{ud} \leq \frac{2m_s}{3}$ qualitatively shows the expected logarithmic behaviour of chiral perturbation theory is quite satisfactory. However, one has to keep in mind the remarks about the coarse lattice and the neglected renormalization factors. Therefore the results shown here should only be taken as a hint to estimate the correct quark mass region and further work is needed to finally deduce the physical values of the fit parameters.

Chapter 3

$N = 1$ Supersymmetric Yang-Mills theory

The TSMB algorithm was originally proposed for the $N = 1$ supersymmetric Yang-Mills theory [19]. This theory is very QCD-like in the sense that there is a $SU(N_c)$ gauge field and a fermion field. In unbroken supersymmetry this fermion, called gaugino or gluino, is massless, while a massive gluino breaks supersymmetry softly. Differences are that the fermion is in the adjoint and not in the fundamental representation and that it is a Majorana and not a Dirac fermion. Due to the Majorana nature of the gluino it can effectively be treated as half a fermion, i. e. $N_f = \frac{1}{2}$. This makes this theory easier to handle for multibosonic algorithms, because the function to be approximated in (1.26) is less singular at $x = 0$. In addition, the symmetry features of this $N = 1$ SUSY theory can be used to test the quality of the dynamical fermion because there have to be the same number of bosonic and fermionic degrees of freedoms. Otherwise the supersymmetry would break down, which could be seen in the Ward identities.

In this chapter we will introduce some basics of this simple supersymmetric model. With that we will discuss some problems of bringing it onto the lattice, and we will have a look at some physical results including the supersymmetric Ward identities.

3.1 Introduction of the theory

It is widely believed that it is possible to describe nature with just one single theory, called GUT (grand unified theory) or TOE (theory of everything). In that theory gravitation and the fundamental forces from elementary particle physics are unified non-trivially.

It was shown early by Coleman and Mandula [86] that it is impossible to unify non-trivially the space-time symmetry, i. e. the Poincaré group with the inner symmetries as known from the theory of electroweak interactions or from QCD. Either the resulting group will be a trivial product of the Poincaré group and the Lie group of inner symmetries, or the arising theory will have a trivial S matrix, i. e. the scattering amplitude will vanish. This is the no-go theorem of Coleman and Mandula.

Soon it could be shown that this no-go theorem could be bypassed by extending the concept of the Lie group. While usually a Lie group is fully described by the commutating relations between its generators it was now tried to include the anti-commutating relations

[87]. This led to two classes of generators that can be classified as bosonic and fermionic. A systematic study showed that the $\mathbb{Z}_2$ graded Lie algebra is the only one that can be used in conjunction with quantum field theory [88]. Applied to the original problem this leads to the Super-Poincaré algebra that is used in supersymmetric theories.

The first supersymmetric toy model is the Wess-Zumino model [89]. It consists out of a real scalar field, a real pseudo-scalar field and a Majorana spinor field.

It would be very complicated to guess the correct symmetries for a theory that includes the correct kinds of particles. To simplify the work with supersymmetric theories the superfield formalism was introduced. These superfields live in a superspace, which is the usual Minkowskian space-time together with additional fermionic dimensions. For further explanations and references see [90–94]. In this notation it is easy to construct non-abilian supersymmetric gauge theories. One of the most simplest non-abilian supersymmetric gauge theories is constructed from the supersymmetric field tensor W_A as:

$$\mathcal{L} = \frac{1}{4} W^A W_A \,|_{\theta\theta} + (h.c.). \tag{3.1}$$

Using the usual non-abilian field strength tensor

$$F_{\mu\nu} = \partial_\mu A_\nu - \partial_\nu A_\mu + [A_\mu, A_\nu] \tag{3.2}$$

and the covariant derivative in the adjoint representation

$$\mathcal{D}_\mu \bar{\lambda} = \partial_\mu \bar{\lambda} + [A_\mu, \bar{\lambda}] \tag{3.3}$$

and going over to Wess-Zumino gauge fixing and Euclidean space-time we get the following Lagrangian:

$$\mathcal{L} = -\frac{1}{2g^2} \mathrm{Tr}\left(F_{\mu\nu} F_{\mu\nu}\right) + \mathrm{Tr}\left(\bar{\lambda} \gamma_\mu \mathcal{D}_\mu \lambda\right) - \mathrm{Tr}\left(DD\right). \tag{3.4}$$

Using the equations of motion $D = 0$ for the auxiliary field D we get the on-shell action of the $N = 1$ supersymmetric Yang-Mills theory:

$$\mathcal{S} = \int \mathrm{d}^4 x \left\{ \frac{1}{4} F^a_{\mu\nu}(x) F^a_{\mu\nu}(x) + \frac{1}{2} \bar{\lambda}^a(x) \gamma_\mu \mathcal{D}_\mu \lambda^a(x) \right\}. \tag{3.5}$$

As mentioned in the introduction of this chapter this action looks alot like the QCD action. Differences are a factor of $\frac{1}{2}$ in front of the fermionic part of the action and the fact that the fermion field isn't a Dirac spinor in the fundamental representation but a Majorana spinor in the adjoint representation.

The action (3.5) is by construction invariant under the SUSY transformations

$$\begin{aligned} \delta A_\mu &= -2g \bar{\lambda} \gamma_\mu \varepsilon \\ \delta \lambda &= -\frac{i}{g} \sigma \cdot F \varepsilon \\ \delta \bar{\lambda} &= \frac{i}{g} \bar{\varepsilon} \sigma \cdot F. \end{aligned} \tag{3.6}$$

The Lagrangian changes only as $\delta\mathcal{L} = \bar{\varepsilon} \partial_\mu j_\mu$ with the supercurrent

$$j_\mu(x) = \mathrm{Tr}\left(\frac{i}{g} F_{\nu\tau}(x) \gamma_\mu \sigma_{\nu\tau} \lambda(x) \right). \tag{3.7}$$

It is possible to break this symmetry softly by adding a gaugino mass term for the fermion to the action:

$$\mathcal{S} = \int \mathrm{d}^4x \left\{ \frac{1}{4} F^a_{\mu\nu}(x) F^a_{\mu\nu}(x) + \frac{1}{2} \bar{\lambda}^a(x) \gamma_\mu \mathcal{D}_\mu \lambda^a(x) + m_0 \bar{\lambda}^a(x) \lambda^a(x) \right\}. \tag{3.8}$$

With this mass term the action is no longer invariant under the supersymmetry transformations (3.6) and supersymmetry is only recovered in the limit $m_0 \to 0$. In section 3.4 we will see more precisely what that means by looking at the Ward identities, which display the consequences of supersymmetry.

3.2 SYM on the lattice

Once knowing how to put QCD on the lattice (see section 1.1) it is easy to put the $N = 1$ supersymmetric Yang-Mills theory (SYM) on the lattice. The action using Wilson fermions can be written as:

$$S = S_g + S_f \tag{3.9}$$

$$S_g = \beta \sum_{pl} \left(1 - \frac{1}{N_c} \mathrm{Re}\,\mathrm{Tr}\, U_{pl} \right) \tag{3.10}$$

$$S_f = \frac{1}{2} \sum_x \left(\bar{\lambda}^a_x \lambda^a_x - \kappa \sum_{\mu=1}^{4} \left[\bar{\lambda}^a_{x+\hat{\mu}} V^{ab}_{x\mu} (1+\gamma_\mu) \lambda^b_x + \bar{\lambda}^a_x V^{ab\,T}_{x\mu} (1-\gamma_\mu) \lambda^b_{x+\hat{\mu}} \right] \right). \tag{3.11}$$

As in QCD the fields were rescaled by a factor of $\sqrt{\frac{1}{2\kappa}}$ with $\kappa = \frac{1}{2m_0+8r}$ and we have fixed the Wilson parameter $r = 1$. The adjoint gauge field is defined as

$$V^{ab}_\mu(x) \equiv 2\mathrm{Tr}\left[U^\dagger_\mu(x) T^a U_\mu(x) T^b \right] = V^{ab}_\mu(x)^* = V^{ab}_\mu(x)^{T^{-1}}, \tag{3.12}$$

with $T^a = \frac{1}{2}\tau^a$, see section A.2.1.

With the fermion matrix

$$Q^{ab}_{xy}[U] = \delta^{ab}\delta xy - \kappa \sum_{\mu=1}^{4} \left(\delta_{y,x+\hat{\mu}} (1+\gamma_\mu) V^{ab}_{x\mu} + \delta_{y+\hat{\mu},x} (1-\gamma_\mu) V^{ab\,T}_{y\mu} \right) \tag{3.13}$$

and the Majorana condition[1]

$$\lambda = \lambda^{\mathcal{C}} = \mathcal{C} \bar{\lambda}^T \tag{3.14}$$

with $\mathcal{C}$ the charge conjugation operator the fermionic action can be rewritten as

$$S_f = \frac{1}{2} \sum_{xy} \lambda^a_x C Q^{ab}_{xy} \lambda^b_y. \tag{3.15}$$

The fermionic path integral can be written as

$$\int \mathcal{D}[\lambda] e^{-S_f} = \mathrm{Pf}(CQ) = \pm \sqrt{\det Q}. \tag{3.16}$$

[1]This definition is based on the analytic continuation of Green's functions from Minkowski to Euclidean space [95, 96].

There is only one integration variable λ and not $\bar{\lambda}$ because of the Majorana condition (3.14).

The soft supersymmetry breaking term vanishes for $m_0 = 0$, and therefore the bare mass parameter κ has to be tuned to κ_{crit}. At κ_{crit} there is a first order phase transition, at least in the continuum limit. At non-zero lattice spacing the effects of this phase transition can be seen in the distribution of the gaugino condensate [97].

The TSMB algorithm makes use of the determinant, and by comparing with (1.37) we see that a Majorana fermion can be simulated using an effective fermion number of $N_f = \frac{1}{2}$. However, this approach does not include the sign of the Pfaffian and it has to be included in the reweighting step. But while in QCD in the confined phase we know that in the continuum limit there should be no sign problem this is less clear in the theory with Majorana fermions, because the Pfaffian in general could have any sign. Luckily there have been no indications for severe problems due to this. Some configurations with negative sign were found on a $6^3 \cdot 12$ lattice at negative gaugino mass [30], but on larger lattices at positive gaugino mass there was none.

3.3 Simulations for the Ward identity

We now turn to the simulation of the $N = 1$ supersymmetric Yang-Mills theory. Here we use the $SU(2)$ gauge group. First numerical studies of SYM with $SU(3)$ were reported in [98]. In section 3.4 we will consider the SUSY Ward identity on the lattice. The dependence of the spectrum on the hopping parameter κ was already studied in [30]. For this κ values up to 0.1925 were studied on a $12^3 \cdot 24$ lattice at $\beta = 2.3$. Going to larger κ values corresponding to smaller gluino masses was not possible in that work because of the shrinking of the physical volume. The reason for this is the renormalization of the lattice spacing by fermionic virtual loops. Once the physical volume is too small the finite size effects will become too large for a study of the mass spectrum. This should be the case for $\kappa > 0.1925$, while for $\kappa \leq 0.1925$ finite size effects should be below the order of the statistical uncertainties of [30]. This should be true despite the fact that $\frac{L}{r_0}$ is smaller than what one would accept in QCD because of the fact that the π-mass in QCD is relatively small, while corresponding masses in the $N = 1$ Super-Yang-Mills theory are expected to be somewhat larger [66, 99].

For this study of the Ward identity we can go further in κ at the same $12^3 \cdot 24$ lattice and the same $\beta = 2.3$ because Ward identities are valid in a finite volume, where their structure remains unchanged but only the coefficients may be volume dependent. These coefficients are, however, essentially renormalizations defined at the scale of the UV cutoff a^{-1}, so any κ value should be fine. Therefore we will use $\kappa = 0.1925$, $\kappa = 0.194$ and $\kappa = 0.1955$ for our simulations. The last point seems to be too close to the critical value of $\kappa_{crit} = 0.1955(5)$ as determined in [22]. However, that value was determined on a $6^3 \cdot 12$ lattice by looking at the vanishing of the gluino mass, so that study includes both $\mathcal{O}(a)$ and finite volume effects that should be non-negligible. Indeed we will see that the Ward identities allow an independent determination of κ_{crit}, and it will turn out that in the absence of finite volume effects and with smaller $\mathcal{O}(a)$ effects the critical hopping parameter is somewhat larger than anticipated in [22]. Nevertheless the simulation points that we have chosen correspond to quite small gluino masses and are well suited for a study of the SUSY Ward identity. The most important run parameters are reported in table 3.1. However, most

Table 3.1: *Parameters of the* $12^3 \cdot 24$ *lattice simulations at* $\beta = 2.3$. *For further details see [66].*

κ	$\varepsilon \cdot 10^4$	λ	n_1	n_2	updates	offset	N_{lat}
0.1925	3.0	3.7	32	150	216000	50	9
0.194	1.0	4.5	28	160	42000	20	9
0.1955	0.125	5.0	32	480	65800	10-15	8

of these runs consist out of several runs with different parameters, mainly due to the fact that an optimal choice of polynomials or a better updating sequence was looked for. Here only the parameters that were used in the majority of the runs are quoted. For more details see [66].

For the updating of the boson fields the local heatbath and overrelaxation algorithms were used. The global heatbath is applicable here, too. However, it was not yet used in these simulations and was only introduced for later runs on a $16^3 \cdot 32$ lattice [100]. For the gauge field the widely usable multihit Metropolis algorithm was used. The more efficient heatbath and overrelaxation algorithms cannot be used, because they require the action to be quadratic in the field to be updated, which is not the case for the action given in (3.9) due to the adjoint representation of the gluino field.

When running the simulation the behaviour of some important observables has to be monitored closely. For the TSMB algorithm one of the most important observables is the smallest eigenvalue λ_{min} of $\tilde{Q}^2$. It should be above the ε of the second polynomial most of the time, and above the ε of the third polynomial all of the time. The latter is especially important in this run because Neuberger's formula [101] was used and not the Newton iteration (1.44). Therefore the approximation of the third polynomial breaks down completely below ε. If, however, the ε of the second polynomial is undercut sometimes this will increase the autocorrelation but otherwise no systematical error is introduced as long as the reweighting factor is calculated properly.

The run at $\kappa = 0.1925$ had been studied in detail in [30]. The histogram for λ_{min} for the other two runs is in figure 3.1. Although the smallest eigenvalue λ_{min} is nearly never below the ε of the second polynomial it is still worthwhile to have a look at the reweighting factors. In the ideal case they should be peaked closely around one. Indeed this is the case as can be seen in figure 3.2.

3.3.1 The sign of the Pfaffian

As described in section 3.2 the updating is done using the measure $|\sqrt{\det(Q)}|$ which might differ from the correct measure, the Pfaffian, by a sign

$$\mathrm{Pf}(CQ) = \left|\sqrt{\det(Q)}\right| \cdot \mathrm{sign}(\mathrm{Pf}(CQ)). \tag{3.17}$$

As seen before this is not necessaryly a problem because we can include the sign in the reweighting process. But again we would like to see that only a negligible sub-sample has negative reweighting factors so that no problems with numerical cancellation arise that

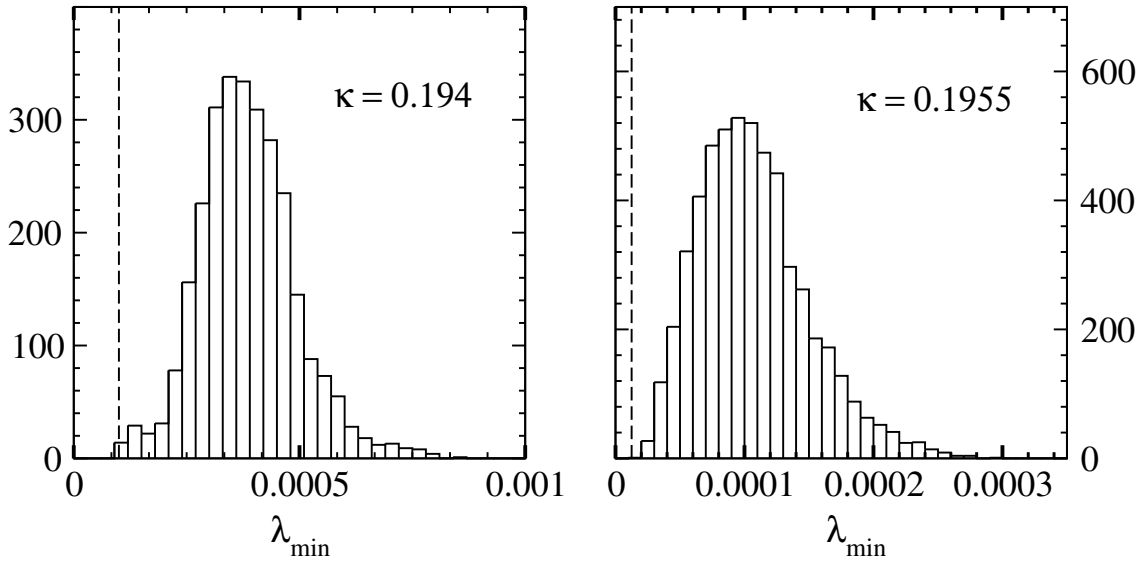

Figure 3.1: *Distribution of the smallest eigenvalue λ_{min} of $\tilde{Q}^2$ for the two simulation points with smaller gluino mass. The dashed line indicates the value of ε used in the simulation.*

would lead to large statistical fluctuations. If it is indeed the case that only a small sub-sample of the configurations is affected by a negative sign then we don't have to calculate the correct sign for all configurations since the effect is negligible and it is enough to show for a sub-sample that indeed all or nearly all configurations have the same sign, usually a positive one.

As explained before odd numbers of negative eigenvalues of $\tilde{Q}$ are responsible for the negative sign of the Pfaffian. A change in the sign therefore has to come with extremely small eigenvalues and hence the configurations with extremely small eigenvalues are the ones where a negative sign of the Pfaffian is most likely. These configurations have been analyzed for a negative sign systematically using the method of the spectral flow. In addition the run with $\kappa = 0.194$ has been analyzed further. Roughly 10% of all the configurations have been taken randomly and were analyzed in the same way. In none of the analyzed configurations we found zero-level crossings at a κ value below the simulation parameter κ_{sea}. Therefore all configurations have a positive sign. In figure 3.3 a few examples of the spectral flow for this simulation point are shown. These examples show the worst case scenarios that we have found, and still it is obvious that none of them has a zero-level crossing before κ_{sea}. Actually even up to $\kappa_{val} = 0.1955$ there is no such crossing, so that these configurations could have been taken to analyze the Ward identity at $\kappa = 0.1955$ using partial quenching. However, in that case important dynamical effects might have been neglected.

3.3.2 The finite temperature phase transition

The situation for the $N = 1$ $SU(2)$ Super-Yang-Mills theory on the lattice is not very different from the situation of QCD concerning the finite temperature phase transition.

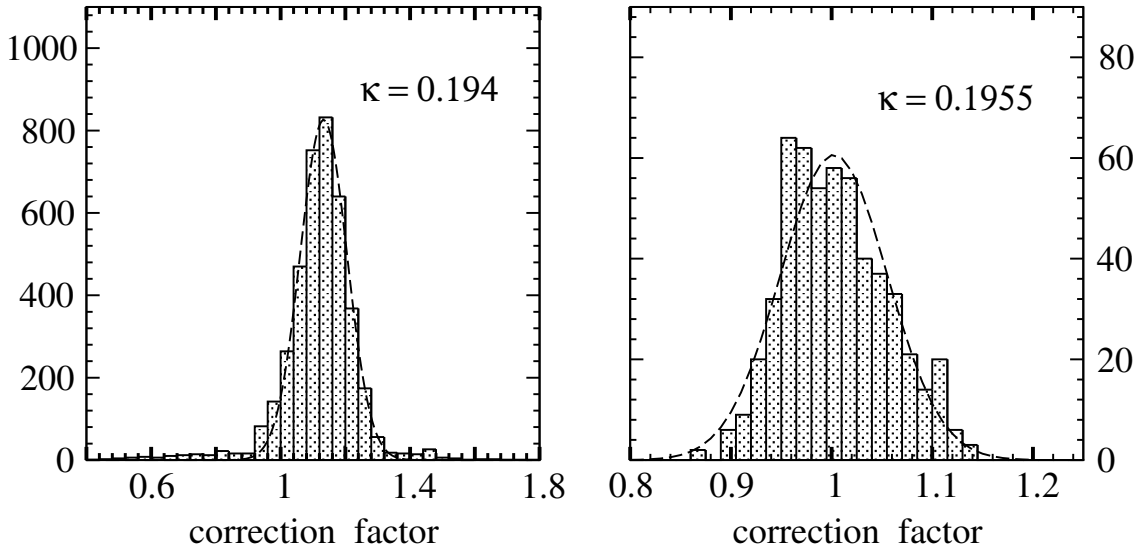

Figure 3.2: *Distribution of the reweighting factors on a sub-sample of the configurations with Gaussian fit.*

Table 3.2: *Phase transition points as determined from figures 3.4 and 3.5 and from [102].*

N_t	β	κ_{phase}
4	2.1	0.2000(25)
4	2.2	0.1730(7)
4	2.25	0.1600(50)
4	2.3	0.0
6	2.3	0.190(2)

For some very small values of β one can be sure that one is in the confined phase everywhere below the critical line $\kappa_{crit}(\beta)$. For large values of β one will be clearly at the deconfined phase for typical values of $N_t = 8, 12, 16$. The situation that is best suited for meaningful simulations due to other limitations like the lattice size and lattice spacing is most likely around the phase transition lines corresponding to the chosen lattice size. It is therefore important to look at the phase transition lines and to make sure that the simulations belong to the confined phase.

If simulations are done on a $12^3 \cdot 24$ lattice the straightforward way of determining the phase would be to look out for the $N_t = 12$ phase transition for a gauge coupling of $\beta = 2.3$ as in the simulations. For this a $24^3 \cdot 12$ lattice would be needed, and simulations would be needed for many different values of κ. So already from these considerations it is obvious that this determination of the phase would require more computer power than the actual simulation. Indeed the situation is even worse. The larger N_t is, the larger is the phase space that has to be considered. With that it becomes exponentially more

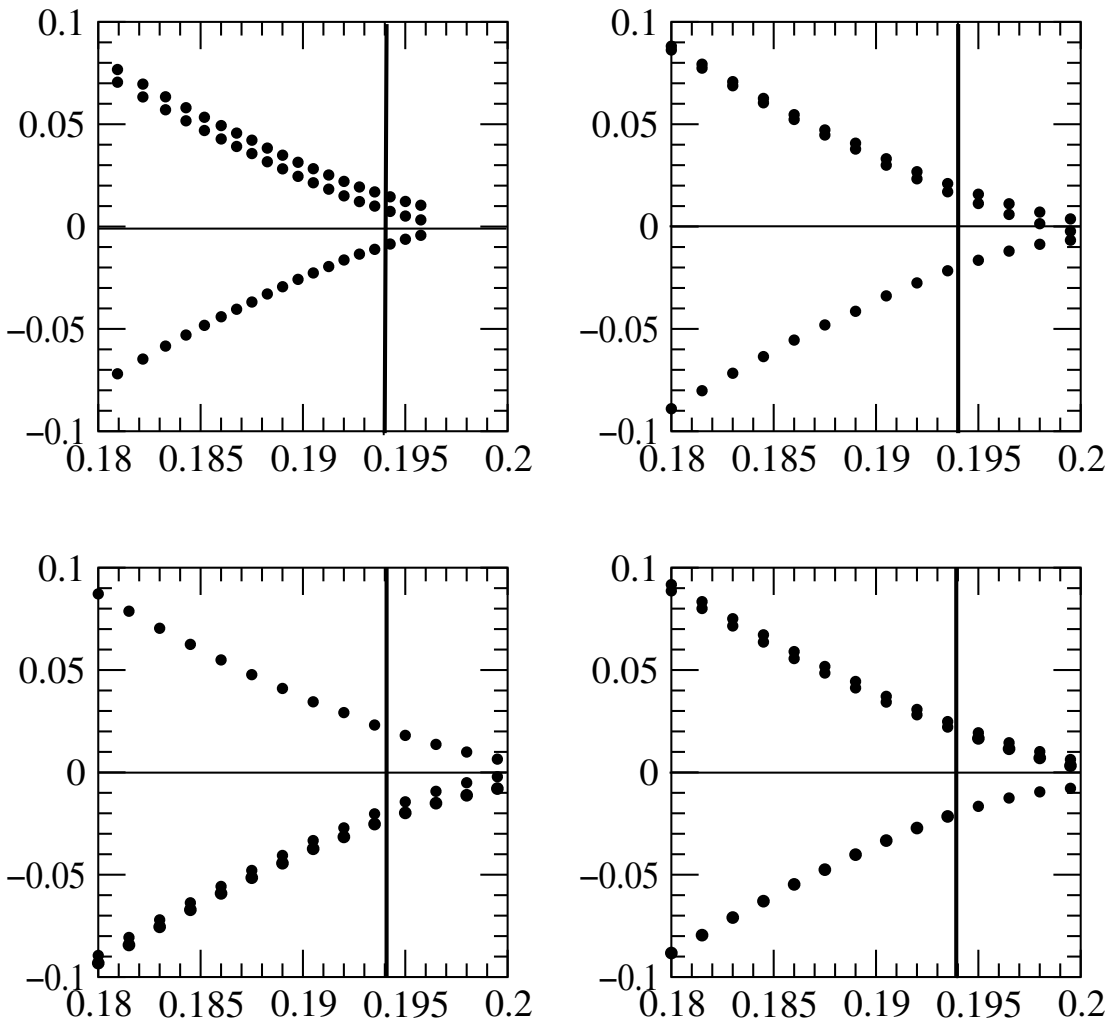

Figure 3.3: *The flow of eigenvalues as a function of the hopping parameter for different configurations produced at* $\beta = 2.3$ *and* $\kappa = 0.194$*. The vertical line indicates the hopping parameter of the simulation.*

difficult to tunnel from one phase to the other and already for $N_t = 12$ it is next to impossible to ever see this phase transition anywhere near the real phase transition point. The determination of the phase transition point would therefore have large errors due to an hysteresis effect. For this it wouldn't even help to start two simulations, one from a cold start and one from a hot start.

It is therefore obvious to determine the phase transition for some smaller values of N_t and then relate the results to $N_t = 12$. The idea behind this is simple, we determine the temperature

$$T_{crit} = \frac{1}{N_t a} \tag{3.18}$$

at the phase transition line for some small value of N_t and assume that the determination of this temperature is not affected by too large $\mathcal{O}(a)$ effects so that T_{crit} in physical units

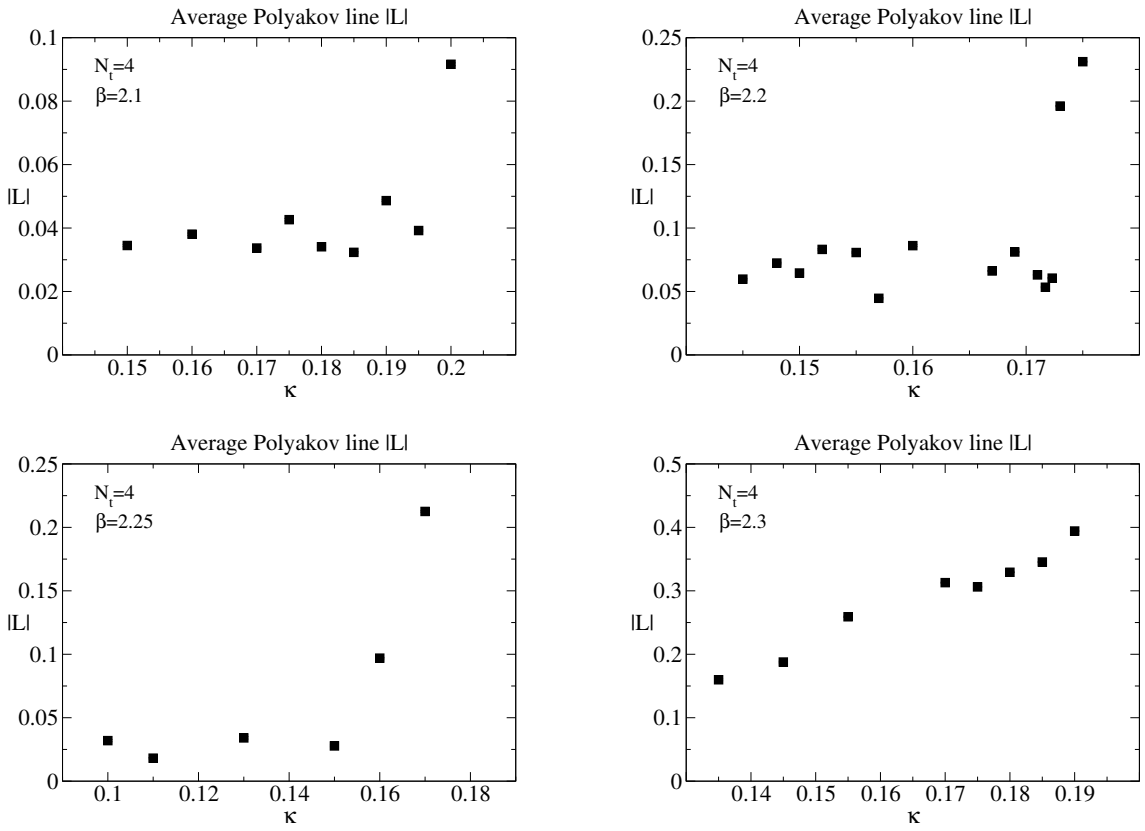

Figure 3.4: *Polyakov lines $|L|$ for different values of β and for $N_t = 4$.*

is roughly the same for a larger lattice, i. e. a larger N_t. This will of course require the connection of the lattice spacing a to some physical scale. As throughout this work the Sommer scale parameter r_0 is a good choice. We can therefore compute $\frac{1}{N_t r_0}$ on the phase transition line for some small lattice and can make a connection to this by measuring r_0 on the larger lattice.

The physical value of r_0 can be determined from effective theories. So far there are no collider experiments or any other occasion where a supersymmetric particle has been observed. Therefore no effective theory can be made up to estimate r_0. One could use the QCD value of 0.49 fm, but this could probably be way off. Nevertheless one can still measure r_0 on the lattice. It can then be used to determine the phase as described above. However, it is not possible to use this value of r_0 to relate the lattice spacing a to some physical scale.

This method by using the Sommer scale parameter to relate different thermal lattices to each other has the obvious disadvantage that $\frac{r_0}{a}$ has to be measured. This is quite tricky on small lattices. We will therefore determine the phase transition line for $N_t = 4$ and $N_t = 6$ and then we will see if we can already decide on which side we are. Only if this is not possible the complicated method of determining r_0 will be applied, for which we need a huge statistics in order to compensate for the small lattice.

Several simulation points for $8^3 \cdot 4$ and $12^3 \cdot 6$ lattices corresponding to $N_t = 4$ and $N_t = 6$ were considered and the phase was determined by measuring the order parameter $|L|$, the

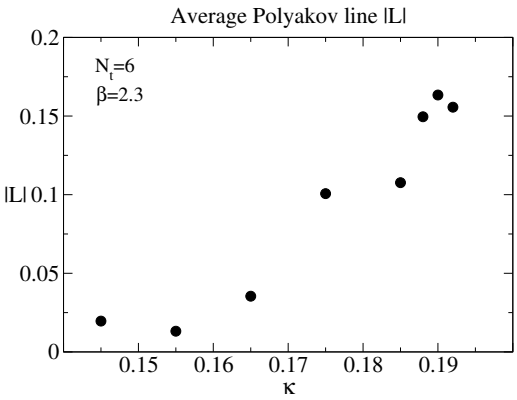

Figure 3.5: *Polyakov lines* $|L|$ *for* $\beta = 2.3$ *and* $N_t = 6$.

absolute value of the Polyakov line in the thermal direction. The plaquette could have been used instead of the Polyakov line, since that observable makes a jump at the phase transition line, too. However, it is theoretical more sound to use the Polyakov line. Results for $N_t = 4$ are shown in figure 3.4 and for $N_t = 6$ in figure 3.5. For $N_t = 4$ and $\beta = 2.3$ no phase transition was found. This is in agreement with the determination of [102], where the phase transition for quenched $SU(2)$ QCD was determined to be $\beta = 2.3$. And since the only difference of this supersymmetric theory and QCD is inside the fermionic sector we can use that determination from a quenched simulation.

The results are given in table 3.2 and figure 3.6. In the figure there are extrapolations for the finite temperature phase transition lines guided by the measured points. For $N_t = 4$ this is a very reliable extrapolation. For $N_t = 6$ we have only one point, but from what is known about phase transition lines in general [71,103] this should be a good extrapolation. Following that general knowledge we have further extrapolated the $N_t = 8$ line, although we have no data at all on this line. This extrapolation is done without taking the critical line κ_{crit} into account.

Previously the DESY-Münster did consider the $8^3 \cdot 16$ lattice at $\beta = 2.3$ and $\kappa = 0.190$ in [30]. Since this is the phase transition point for $N_t = 6$ it can be taken as granted that they were in the confined phase. They further did consider the point of $\kappa = 0.1925$ on that lattice, and $\kappa = 0.1925$ on the $12^3 \cdot 24$ lattice. Both runs were consistent with the results from $\kappa = 0.190$ in the sense that no jump in some observables like the plaquette was found. Indeed this is in good agreement with the extrapolation for $N_t = 8$ in figure 3.6, where the phase transition line is around $\kappa = 0.22$ for $\beta = 2.3$.

We therefore have two strong indications that the runs as given in table 3.1 are in the confined phase. There is no big jump in the results of important quantities like the plaquette compared to points where we are sure that we are in the confined phase, and we are below $\kappa = 0.22$ as determined from the extrapolation in figure 3.6 for $N_t = 8$ while we only have to make sure to be below $N_t = 12$.

Combining these indications leads to a very clear picture of the finite temperature phase transition and it is unnecessary to increase the statistics for a reliable determination of the Sommer scale parameter $\frac{r_0}{a}$.

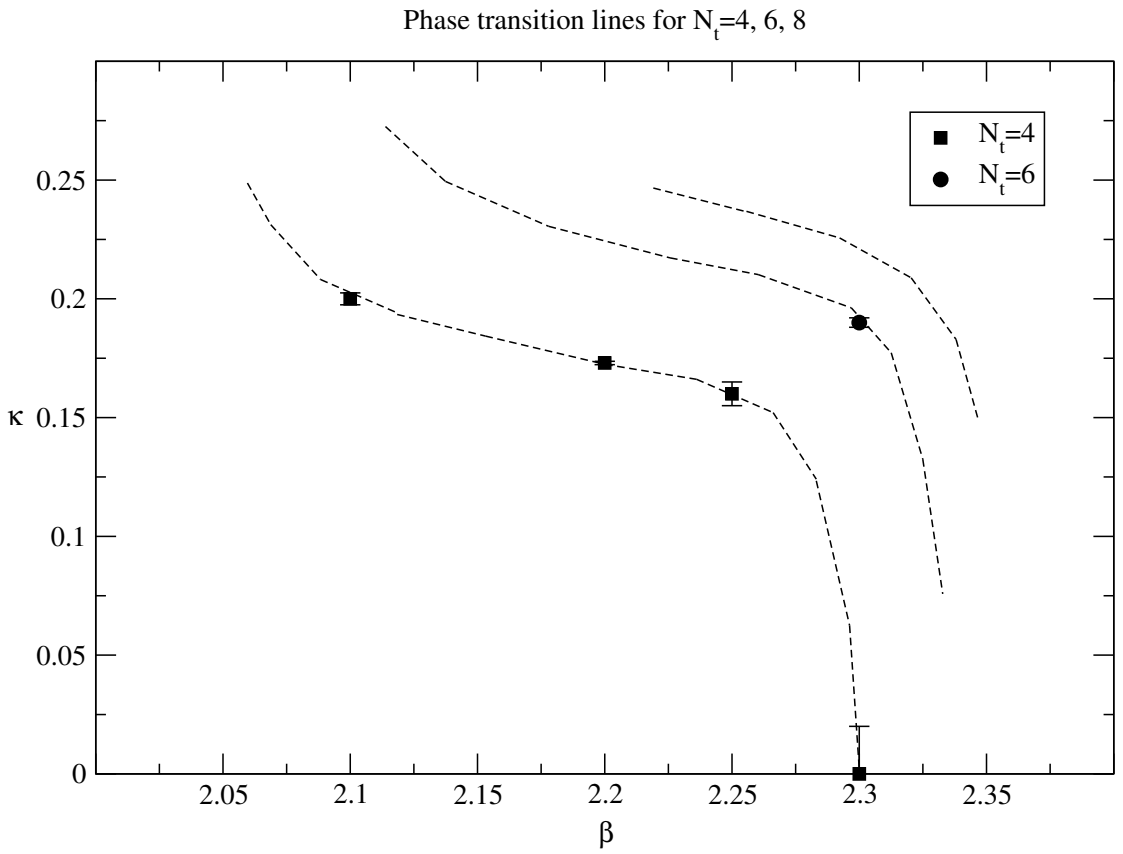

Figure 3.6: *Phase transition points for $N_t = 4$ and $N_t = 6$ from table 3.2. Dashed lines indicate extrapolations for the phase transition line for $N_t = 4$, $N_t = 6$ and $N_t = 8$.*

3.4 The SUSY Ward identity

In this section we will have a look at the supersymmetric Ward identity. As an introduction on this topic we will first have a look at the continuum formulation of the supersymmetric Ward identity in section 3.4.1. In section 3.4.2 we will take a look at the Ward identity on the lattice and discuss how it can be used to monitor the restauration of supersymmetry when performing the continuum limit. The numerical investigation is in section 3.4.3.

3.4.1 The Ward identity in the continuum

For every symmetry of the theory there exists a Noether current which is conserved. Here we are interested in the Noether current corresponding to the supersymmetry transformations (3.6). In these transformations we replace the global parameter ε by a local parameter $\varepsilon(x)$:

$$\begin{aligned} \delta A_\mu &= -2g\bar{\lambda}\gamma_\mu\varepsilon(x) \\ \delta\lambda &= -\frac{i}{g}\sigma\cdot F\varepsilon(x) \\ \delta\bar{\lambda} &= \frac{i}{g}\bar{\varepsilon}(x)\sigma\cdot F. \end{aligned} \tag{3.19}$$

These new transformations are applied to the fields of the path integral for the expectation value of some operator $\mathcal{O}$

$$\langle \mathcal{O} \rangle = \frac{1}{\mathcal{Z}} \int \mathcal{D}[A_\mu] \mathcal{D}[\lambda] \mathcal{O} e^{-S}, \tag{3.20}$$

where $\mathcal{Z}$ is the proper normalization factor. Since the general change of variables of the path integral does not change the value of that integral it follows that the expectation values do not change:

$$\langle \mathcal{O} \rangle = \langle \mathcal{O} \rangle^{\varepsilon} . \tag{3.21}$$

Assuming that the theory is free of a supersymmetric anomaly we can suppose that the measure is invariant under the local supersymmetry transformations (3.19) [104]. This gives

$$0 = - \langle \delta S \mathcal{O} \rangle + \langle \delta \mathcal{O} \rangle . \tag{3.22}$$

With the assumption that the product of operators is localized outside the domain of $\varepsilon(x)$ and

$$\delta S = - \int \mathrm{d}^4 x \, \varepsilon(x) \partial_\mu S \mu(x) \tag{3.23}$$

with the supercurrent, i. e. the Noether current given by

$$S_\mu(x) = -2 \frac{i}{g} \mathrm{Tr} \left(F_{\nu\tau}(x) \sigma_{\nu\tau} \gamma_\mu \lambda(x) \right) , \tag{3.24}$$

we can derive the supersymmetric Ward identity

$$\langle \partial_\mu S_\mu(x) \mathcal{O}(y) \rangle = 0. \tag{3.25}$$

Breaking supersymmetry softly as done in (3.8) by adding a mass term the SUSY Ward identity no longer holds. It is broken by a term coming from the variation of the added mass term. The variation of this term takes the form

$$\chi(x) = 2 \frac{i}{g} \mathrm{Tr} \left(F_{\nu\tau}(x) \sigma_{\nu\tau} \lambda(x) \right) \tag{3.26}$$

and it consequently appears in the Ward identity:

$$\langle \partial_\mu S_\mu(x) \mathcal{O}(y) \rangle = m_0 \langle \chi(x) \mathcal{O}(y) \rangle . \tag{3.27}$$

Now it has become clear why supersymmetry is regained only in the limit $m_0 \to 0$. The SUSY Ward-Takahashi identity (3.25) is broken by a term proportional to m_0. Therefore we are able to tell if supersymmetry is broken or not by looking at the Ward identity. This is something we will use to scrutinize the quality of our lattice approximation with respect to supersymmetry closely. On the lattice supersymmetry is also broken by lattice artifacts, but in the continuum limit this breaking should vanish.

3.4.2 The Ward identity on the lattice

In the action (3.9) SUSY is explicitly broken by the gluino mass term, by the Wilson term, which is also responsible for chiral symmetry breaking, and by the lattice discretization. One can now derive the SUSY Ward identity similar to the calculation in section 3.4.1 but this time starting from the lattice action (3.9) and using a lattice formulation of the

supersymmetry transformations (3.19). These lattice SUSY transformations should of course recover the continuum form in the continuum limit. In addition we want that they commute with the parity $\mathcal{P}$, time reversal $\mathcal{T}$ and charge conjugation $\mathcal{C}$ transformations on the lattice. These requirements are fulfilled by [66, 105, 106]:

$$\begin{aligned}
\delta U_\mu(x) &= -\tfrac{ig_0a}{2}\left(\bar\epsilon(x)\gamma_\mu U_\mu(x)\lambda(x) + \bar\epsilon(x+\hat\mu)\gamma_\mu\lambda(x+\hat\mu)U_\mu(x)\right), \\
\delta U_\mu^\dagger(x) &= \tfrac{ig_0a}{2}\Big(\bar\epsilon(x)\gamma_\mu U_\mu^\dagger(x)\lambda(x) + \bar\epsilon(x+\hat\mu)\gamma_\mu\lambda(x+\hat\mu)U_\mu^\dagger(x)\Big), \\
\delta\lambda(x) &= \tfrac{1}{2}P_{\mu\nu}(x)\sigma_{\mu\nu}\epsilon(x), \\
\delta\bar\lambda(x) &= -\tfrac{1}{2}\bar\epsilon(x)\sigma_{\mu\nu}P_{\mu\nu}(x).
\end{aligned} \tag{3.28}$$

The infinitesimal parameters $\bar\epsilon$ and ϵ satisfy the Majorana condition and $P_{\mu\nu}(x)$ can in general be any lattice representation of the continuum field strength $F_{\mu\nu}(x)$, e. g. as defined from the simple plaquette $U_{\mu\nu}(x)$: $P_{\mu\nu}(x) = \frac{1}{2ig_0a}\Big(U_{\mu\nu}(x) - U_{\mu\nu}^\dagger(x)\Big)$. However, for the numerical analysis we want $P_{\mu\nu}$ to transform under parity and time reversal in the same way as $F_{\mu\nu}$ does in the continuum. Therefore it is convenient to replace the simple plaquette by the clover plaquette [66, 106]:

$$U_{\mu\nu}^{(cl)}(x) = \frac{1}{4}\left(U_{\mu,\nu}(x) + U_{\mu,-\nu}(x) + U_{-\mu,\nu}(x) + U_{-\mu,-\nu}(x)\right) \tag{3.29}$$

$$P_{\mu\nu}^{(cl)}(x) = \frac{1}{2ig_0a}\Big(U_{\mu\nu}^{(cl)}(x) - {U_{\mu\nu}^{(cl)}}^\dagger(x)\Big) \tag{3.30}$$

Repeating the derivation of the Ward identity with the lattice action (3.9) and the SUSY transformations (3.28) we derive the lattice version of the SUSY Ward-Takahashi identity for a gauge invariant operator $\mathcal{O}(y)$:

$$\left\langle\left(\sum_\mu \nabla_\mu S_\mu^{(ps)}(x)\right)\mathcal{O}(y)\right\rangle = m_0\left\langle\chi(x)\mathcal{O}(y)\right\rangle + \left\langle X^{(ps)}(x)\mathcal{O}(y)\right\rangle - \left\langle\frac{\delta\mathcal{O}(y)}{\delta\bar\epsilon(x)}\right\rangle. \tag{3.31}$$

As a lattice derivative the backward derivative

$$\nabla_\mu^b f(x) = \frac{f(x) - f(x-\hat\mu)}{a} \tag{3.32}$$

is used and the SUSY current $S_\mu^{(ps)}(x)$ is the point-split (ps) one

$$S_\mu^{(ps)}(x) = -\frac{1}{2}\sum_{\nu\tau}\sigma_{\nu\tau}\gamma_\mu\mathrm{Tr}\Big(P_{\nu\tau}^{(cl)}(x)U_\mu^\dagger(x)\lambda(x+\hat\mu)U_\mu(x) + P_{\nu\tau}^{(cl)}(x+\hat\mu)U_\mu(x)\lambda(x)U_\mu^\dagger(x)\Big), \tag{3.33}$$

and the operator $\chi(x)$ that we know already from the mass term in the continuum is

$$\chi(x) = \sum_{\nu\tau}\sigma_{\nu\tau}\mathrm{Tr}\left(P_{\nu\tau}^{(cl)}(x)\lambda(x)\right). \tag{3.34}$$

The remaining terms that stem from the breaking of SUSY are collected in the $X^{(ps)}(x)$ term. All we need to know about this term is that in the naive continuum limit it is $X^{(\ldots)}(x) \approx a\mathcal{O}_{11/2}(x)$, where $\mathcal{O}_{11/2}(x)$ is a dimension-$\frac{11}{2}$ operator. The exact expression of $X^{(ps)}(x)$ is given in [105].

The last term in (3.31) is a contact term that vanishes for non-zero distance $|x-y|$ corresponding to the on-shell situation. Since that will be the region where we do the numerical investigation we can safely drop this term from now on. Before having a closer look at the role of the operator $X^{(\dots)}(x)$ in the next paragraph it should be mentioned that the definition of the SUSY current on the lattice is arbitrary up to $\mathcal{O}(a)$ terms since they vanish in the continuum limit. Another choice is the local current

$$S_\mu^{(loc)}(x) = -\sum_{\nu\tau} \sigma_{\nu\tau}\gamma_\mu \mathrm{Tr}\left(P_{\nu\tau}^{(cl)}(x)\lambda(x)\right). \tag{3.35}$$

This definition is more convenient for analytic perturbative calculations [107, 108]. It satisfies a WI similar to (3.31) but with a symmetric lattice derivative $\nabla_\mu^s = \frac{f(x+\hat{\mu})-f(x-\hat{\mu})}{2a}$ and a SUSY-breaking term $X^{(loc)}$ that differs from $X^{(ps)}$ by $\mathcal{O}(a)$ effects.

Renormalization

The Ward identity (3.31) is a relation between bare correlation functions. When switching over to the renormalized Ward identity the operator $X^{(ps)}(x)$ needs a seperate treatment. It follows closely the procedure for the axial WIs in QCD [109, 110], with SUSY-specific topics discussed in [111, 112] and previous presentations of this topic in [66, 106].

Since $X^{(ps)}(x) \approx a\mathcal{O}_{11/2}(x)$ in the naive continuum limit we have to study the renormalization of $\mathcal{O}_{11/2}(x)$. This renormalization will introduce mixing with operators of equal or lower dimensions $d \leq \frac{11}{2}$ and that transform the same as $\mathcal{O}_{11/2}(x)$ under the symmetries of the lattice action. A closer look at the possible operators [66,106] shows that the mixing pattern in the on-shell situation is given by

$$\begin{aligned}\mathcal{O}_{11/2}^R(x) &= Z_{11/2}\left[\mathcal{O}_{11/2}(x) + a^{-1}(Z_S-1)\nabla_\mu S_\mu(x) + a^{-1}Z_T\nabla_\mu T_\mu(x) + a^{-2}Z_\chi\chi(x)\right] \\ &\quad + \sum_i Z_{11/2}^{(i)}\mathcal{O}_{11/2}^{(i)\ R}(x).\end{aligned} \tag{3.36}$$

Depending on the choice between $S_\mu^{(ps)}(x)$ and $S_\mu^{(loc)}(x)$ the lattice derivative has to be the backwards or the symmetric one, and the mixing current $T_\mu(x)$ has to be either

$$T_\mu^{(ps)}(x) = \sum_\nu \gamma_\nu \mathrm{Tr}\Big(P_{\mu\nu}^{(cl)}(x)U_\mu^\dagger(x)\lambda(x+\hat{\mu})U_\mu(x) + P_{\mu\nu}^{(cl)}(x+\hat{\mu})U_\mu(x)\lambda(x)U_\mu^\dagger(x)\Big) \tag{3.37}$$

or

$$T_\mu^{(loc)}(x) = 2\sum_\nu \gamma_\nu \mathrm{Tr}\left(P_{\mu\nu}^{(cl)}(x)\lambda(x)\right). \tag{3.38}$$

Substituting $\mathcal{O}_{11/2}(x)$ in (3.31) with the solution of (3.36) leads to

$$Z_S\left\langle\left(\nabla_\mu S_\mu(x)\right)\mathcal{O}(y)\right\rangle + Z_T\left\langle\left(\nabla_\mu T_\mu(x)\right)\mathcal{O}(y)\right\rangle = m_S\left\langle\chi(x)\mathcal{O}(y)\right\rangle + \mathcal{O}(a), \tag{3.39}$$

with

$$m_S = m_0 - a^{-1}Z_\chi \tag{3.40}$$

being the subtracted gaugino mass.

In the derivation of (3.39) we assumed the vanishing of the correlation

$$a\left\langle\left[Z_{11/2}^{-1}\mathcal{O}_{11/2}^{R}(x)-\sum_{i}Z_{11/2}^{(i)}\mathcal{O}_{11/2}^{(i)\ R}(x)\right]\mathcal{O}(y)\right\rangle=\mathcal{O}(a) \tag{3.41}$$

in the continuum limit, which holds on-shell due to the fact that the multiplicative renormalization factors $Z_{11/2}$ and $Z_{11/2}^{(i)}$ are logarithmically divergent in perturbation theory.

One can now identify the renormalized SUSY current

$$\hat{S}_\mu(x)=Z_S S_\mu(x)+Z_T T_\mu(x), \tag{3.42}$$

and with that the renormalized Ward identity (3.39) formally takes the form of the bare continuum Ward identity (3.27).

In the analogous situation of the axial Ward identity in QCD one can define the renormalized axial current $\hat{J}_\mu^5(x)=Z_5 J_\mu^{5,lat}(x)$ with $J_\mu^{5,lat}(x)$ a generic discretization of the axial current. In this situation a rigorous argument [109, 110] proves that the current $\hat{J}_\mu^5(x)$ coincides with the correctly normalized continuum axial current. Unfortunately this argument cannot be reproduced for the SUSY current $\hat{S}_\mu(x)$ because the proof in QCD relies on some special properties of the axial variation. It leaves the quark field proportional to itself and it leaves the gauge fixing term invariant. Both is not the case for the supersymmetric variation. For the moment it is therefore unclear whether $\hat{S}_\mu(x)$ coincides with the correctly normalized SUSY current up to some possible multiplicative renormalization or not. Some new input on this topic is hoped for from perturbative calculations [105, 113, 114]. If the two currents coincide, then $\hat{S}_\mu(x)$ is conserved when m_S vanishes. This is the restoration of SUSY in the continuum limit.

Insertion operators

We are interested in the numerical investigation of the SUSY Ward identity (3.39). This equation holds for any operator $\mathcal{O}(y)$, but for a large class of operators the Ward identity is trivial because both sides of the equation are zero due to the vanishing of the expectation values if the quantum numbers of $\mathcal{O}(y)$ are not the same as those of $\chi(x)$, $\nabla_\mu S_\mu(x)$ and $\nabla_\mu T_\mu(x)$. We will now try to look out for enough operators $\mathcal{O}(y)$ that don't lead to a trivial statement in the Ward identity. For a more detailed study of this topic see [66, 106]. Before we start we will have a closer look on how the Ward identity (3.39) will be used to get a numerical answer to the question if the SUSY current $\hat{S}_\mu(x)$ is conserved for our simulations when the supersymmetric limit of $m_S=0$ is approached.

Because this will turn out to be convenient for the numerical analysis we will consider the zero spatial momentum Ward identity obtained from the integration (summation) over the spatial coordinates of (3.39):

$$\sum_{\vec{x}}\langle(\nabla_0 S_0(x))\,\mathcal{O}(y)\rangle+\frac{Z_T}{Z_S}\sum_{\vec{x}}\langle(\nabla_0 T_0(x))\,\mathcal{O}(y)\rangle=\frac{m_S}{Z_S}\sum_{\vec{x}}\langle\chi(x)\mathcal{O}(y)\rangle+\mathcal{O}(a). \tag{3.43}$$

For a proper operator $\mathcal{O}(y)$ the correlators in this equation are $4\cdot 4$ matrices in Dirac indices. It is therefore possible to pick a system of two equations and solve it for $\frac{Z_T}{Z_S}$ and $\frac{m_S}{Z_S}$. However, one has to ensure that these two equations are non-trivial and independent. For this it is convenient to replace the generic insertion operator $\mathcal{O}(y)$ by

$$\mathcal{O}(y)\to\bar{\mathcal{O}}^T(y)\equiv\mathcal{C}^{-1}\mathcal{O}(y), \tag{3.44}$$

where we have made use of the Majorana condition (3.14).

With this operator we will have a closer look at the correlator of equation (3.43) that contains the SUSY current. For the other two correlators identical considerations apply. The explicit structure of this correlator is

$$C^{(S,\mathcal{O})}_{\alpha,\beta}(t) = a^{d_{\mathcal{O}}+\frac{9}{2}} \sum_{\vec{x}} \left\langle (\nabla_0 S_0)_\alpha (x) \bar{\mathcal{O}}_\beta(y) \right\rangle, \qquad t = x_0 - y_0. \tag{3.45}$$

The dimensional factor in front of that correlator has been inserted to have a dimensionless correlation, which is what we compute in the numerical calculations.

This correlator can be expanded in the basis of the 16 Dirac matrices Γ:

$$C^{(S,\mathcal{O})}_{\alpha,\beta}(t) = \sum_\Gamma C^{(S,\mathcal{O})}_\Gamma(t) \Gamma_{\alpha,\beta}. \tag{3.46}$$

As it has been shown in [66,106] using discrete symmetries only two contributions survive:

$$C^{(S,\mathcal{O})}_{\mathbb{1}}(t) \equiv \sum_{\vec{x}} \left\langle \overline{\nabla_0 S_0}(x) \mathcal{O}(y) \right\rangle \tag{3.47}$$

$$C^{(S,\mathcal{O})}_{\gamma_0}(t) \equiv \sum_{\vec{x}} \left\langle \overline{\nabla_0 S_0}(x) \gamma_0 \mathcal{O}(y) \right\rangle. \tag{3.48}$$

Both contributions are real due to the Majorana nature of the operators. With them and the still to be specified operators $\mathcal{O}(y)$ we can determine $\frac{am_S}{Z_S}$ and $\frac{Z_T}{Z_S}$ by solving the following system of equations:

$$\begin{aligned} C^{(S,\mathcal{O})}_{\mathbb{1}}(t) + \tfrac{Z_T}{Z_S} C^{(T,\mathcal{O})}_{\mathbb{1}}(t) &= \tfrac{am_S}{Z_S} C^{(\chi,\mathcal{O})}_{\mathbb{1}}(t) \\ C^{(S,\mathcal{O})}_{\gamma_0}(t) + \tfrac{Z_T}{Z_S} C^{(T,\mathcal{O})}_{\gamma_0}(t) &= \tfrac{am_S}{Z_S} C^{(\chi,\mathcal{O})}_{\gamma_0}(t). \end{aligned} \tag{3.49}$$

We will now come back to the question of appropriate operators $\mathcal{O}(y)$. The first thing to notice is that we are looking for gauge invariant operators $\mathcal{O}(y)$ that have spin $\frac{1}{2}$. The operators will have at least dimension $\frac{7}{2}$, and for practical reasons we will restrict ourselves to these kind of operators. An operator with the correct symmetries is

$$\mathrm{Tr}\left(P^{(cl)}_{\mu\nu}(y) \lambda(y) \right). \tag{3.50}$$

From this operator we have to project out spin-$\frac{1}{2}$ components. Some possibilities for that are $S_0(y)$, $T_0(y)$, $\chi(y)$ and

$$\chi^{(sp)}(y) = \sum_{i<j \text{ spatial}} \sigma_{ij} \mathrm{Tr}\left(P^{(cl)}_{ij}(y) \lambda(y) \right), \tag{3.51}$$

where only spacelike plaquettes are used. Since there can be only two independent spin-$\frac{1}{2}$ contributions the above examples are related. This relation is found to be

$$\chi(y) = \gamma_0 T_0(y) - 2\chi^{(sp)}(y), \tag{3.52}$$

$$S_0(y) = 2\gamma_0(\gamma_0 T_0(y) - 2\chi^{(sp)}(y)). \tag{3.53}$$

For the following numerical study one could carry out the analysis for two different sets of operators $\mathcal{O}(y)$. In this way the influence of $\mathcal{O}(a)$ effects could be studied. For the moment we will only use the operators $T^{(loc)}_0(y)$ and $\chi^{(sp)}(y)$ to solve (3.49).

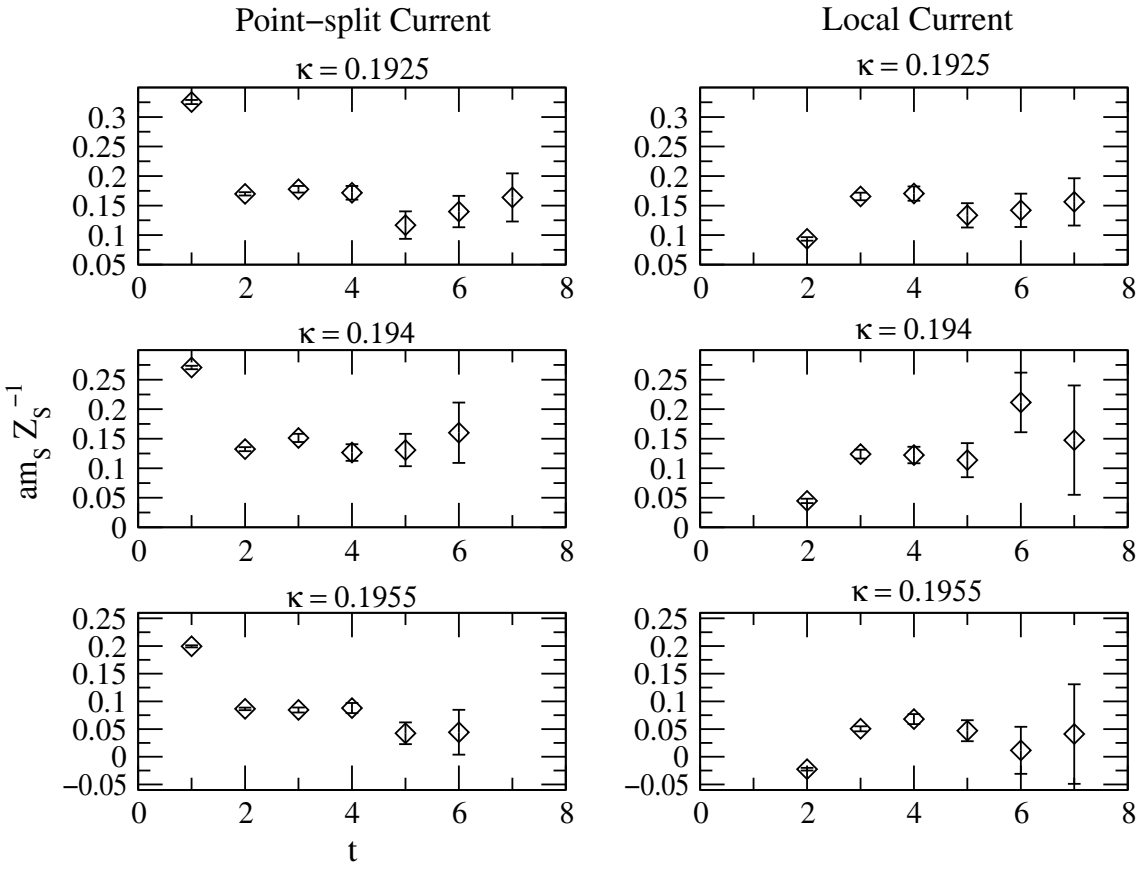

Figure 3.7: $\frac{am_S}{Z_S}$ *as a function of the time-separation* t *with insertion operator* $\chi^{(sp)}(x)$.

3.4.3 Numerical investigation of the Ward identity

We now turn to the numerical determination of $\frac{am_S}{Z_S}$ and $\frac{Z_T}{Z_S}$ by solving (3.49) for the operators $T_0^{(loc)}(y)$ and $\chi^{(sp)}(y)$. Differences between the results for the two operators will signal the effects of $\mathcal{O}(a)$ lattice artifacts.

The experience of [30, 112] tells us that the point-like insertion operators will give a poor signal for the correlations. In these two references this problem was countered by introducing smearing. Therefore we will use APE [35] and Jacobi [36] smearing on the gluon and gluino fields respectively to reduce the statistical fluctuations. The optimal parameters are found on sub-samples of gauge configurations to be $N_J = 18$, $\kappa_J = 0.2$, $N_{APE} = 9$ and $\epsilon_{APE} = 0.5$ [66, 106]. Since APE smearing can only be used on spatial links the smearing is expected to work out less good for $T_0^{(loc)}(y)$.

To be able to measure more often, i. e. to write out the gauge field more often we have chosen the site y of the operator $\mathcal{O}(y)$ randomly for each configuration. In addition we find no correlations between two consecutive measurements which allows to estimate the errors of $\frac{am_S}{Z_S}$ and $\frac{Z_T}{Z_S}$ by a naive jackknife procedure.

On a sub-sample of the configurations reweighting factors were computed. They are shown in figure 3.2. They can be used to repeat the measurement of the ratios $\frac{am_S}{Z_S}$

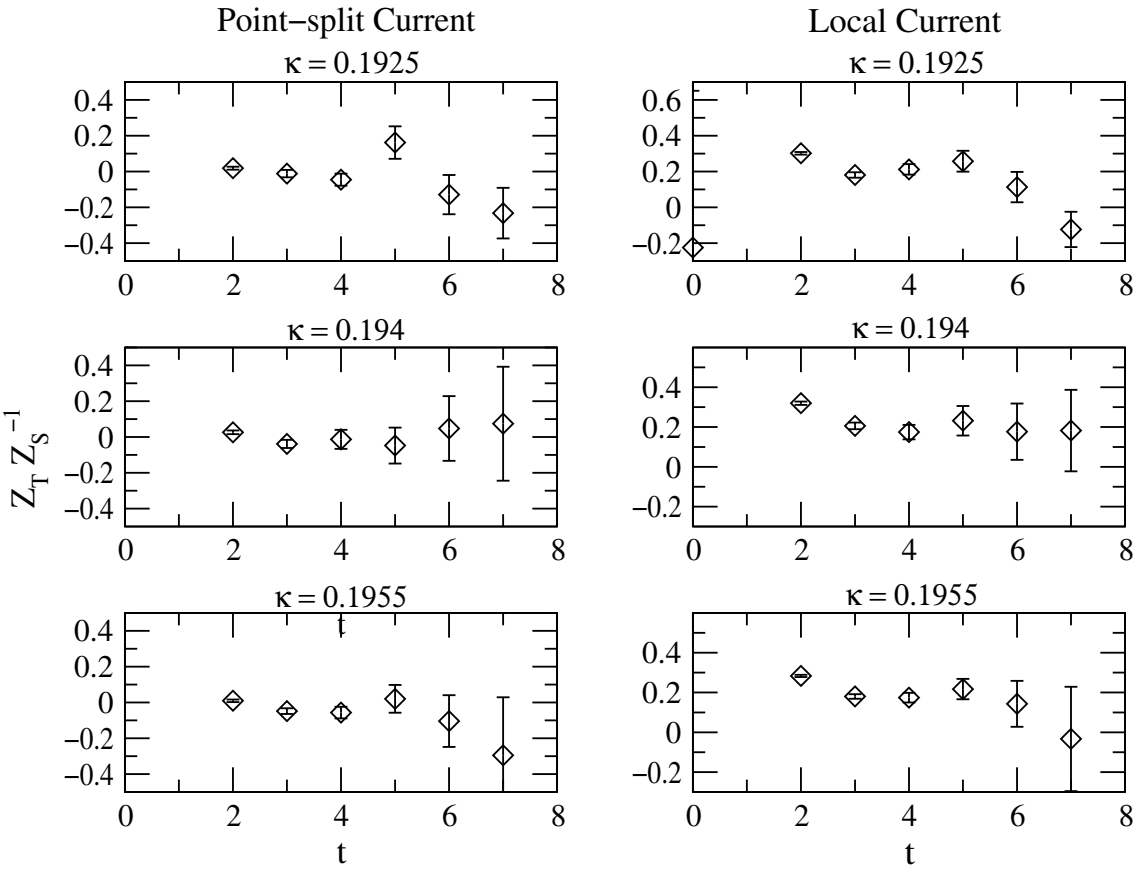

Figure 3.8: $\frac{Z_T}{Z_S}$ *as a function of the time-separation* t *with insertion operator* $\chi^{(sp)}(y)$.

and $\frac{Z_T}{Z_S}$. No significant difference was found when including them, which shows that the approximations of the second polynomials used in these simulation runs are good enough.

A first approximation of the results is achieved by simply solving the system of equations (3.49) for each time-separation t, see figures 3.7 and 3.8. This allows to find a t_{min} above which (3.43) should be valid and contact terms should be absent. Then another method is used to get the final results, where an overdetermined system of equations is constructed and fitting is done for all considered time-seperations $(t_{min}, \ldots, \frac{L_t}{2})$ simultaneously. The results for different t_{min} can be found in the tables 3.3, 3.4, 3.5 and 3.6. The results for $t \geq 3$ seem to be free of effects from the contact term in (3.31). The final results are for $t_{min} = 3$ when $\mathcal{O}(y) = \chi^{(sp)}(y)$ and for $t_{min} = 4$ when $\mathcal{O}(y) = T_0^{(loc)}(y)$.

The dependence on κ can be seen in figures 3.9 and 3.10. It is nice to see that $\frac{Z_T}{Z_S}$ does not show a strong dependence on κ, and through that on m_S. We find for the point-split current

$$\frac{Z_T^{ps}}{Z_S^{ps}} = -0.039(7), \tag{3.54}$$

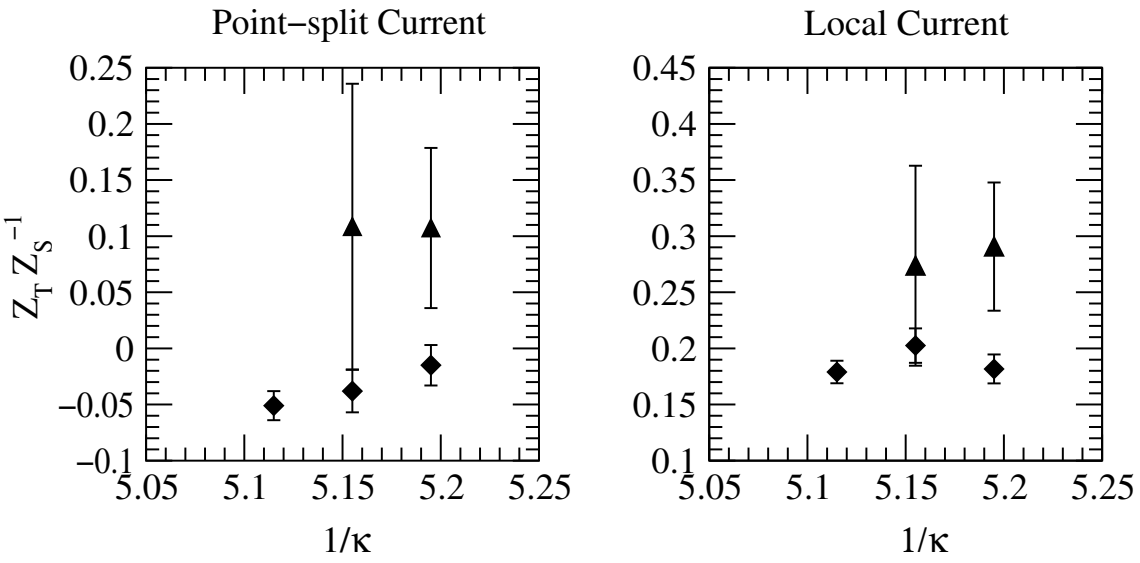

Figure 3.9: $\frac{Z_T}{Z_S}$ *as a function of* $1/\kappa$ *with the insertion operator* $\chi^{(sp)}(x)$ *(filled diamonds) and* $T_0^{(loc)}(x)$ *(filled triangles).*

and

$$\frac{Z_T^{loc}}{Z_S^{loc}} = 0.185(7) \tag{3.55}$$

for the local one. An estimate of this ratio for the point-split current and $\beta = 2.3$ can be obtained from the 1-loop perturbative calculation in [105]. At that order one obtains

$$\frac{Z_T}{Z_S} \equiv Z_T\Big|_{1-loop} = -0.074. \tag{3.56}$$

There is quite a good agreement in the order of magnitude between the numerical and the perturbative estimate. The discrepancies might be contributed evenly to each calculation. For a discussion on the quality of 1-loop unimproved perturbation theory in $N = 1$ Super-Yang-Mills theory see [108]. For the numerical data one has to say that there is some minor dependence on $\frac{Z_T}{Z_S}$ that still could push this value to the perturbative one. In addition there is quite some statistical uncertainty between the results from $\mathcal{O}(y) = \chi^{(sp)}(y)$ and $\mathcal{O}(y) = T_0^{(loc)}(y)$.

For $\frac{am_S}{Z_S}$ the expectation is that it vanishes when κ approaches κ_{crit}. The latter was determined on a $6^3 \cdot 12$ lattice in [22] as $\kappa_{crit} = 0.1955(5)$. The estimate from the point-split current would be $\kappa_{crit} = 0.19750(38)$ and $\kappa_{crit} = 0.19647(27)$ from the local one. The difference between the result from [22] and the determination using the SUSY Ward identity can be explained by systematic effects. The main difference should be due to the fact that in [22] a much smaller $6^3 \cdot 12$ lattice was used, where strong $\mathcal{O}(a)$ and finite volume effects are to be expected. Since the Ward identity holds in any volume there should be no finite volume effect, but of course there will be some $\mathcal{O}(a)$ effect. This and the statistical uncertainty could explain the discrepancy, too.

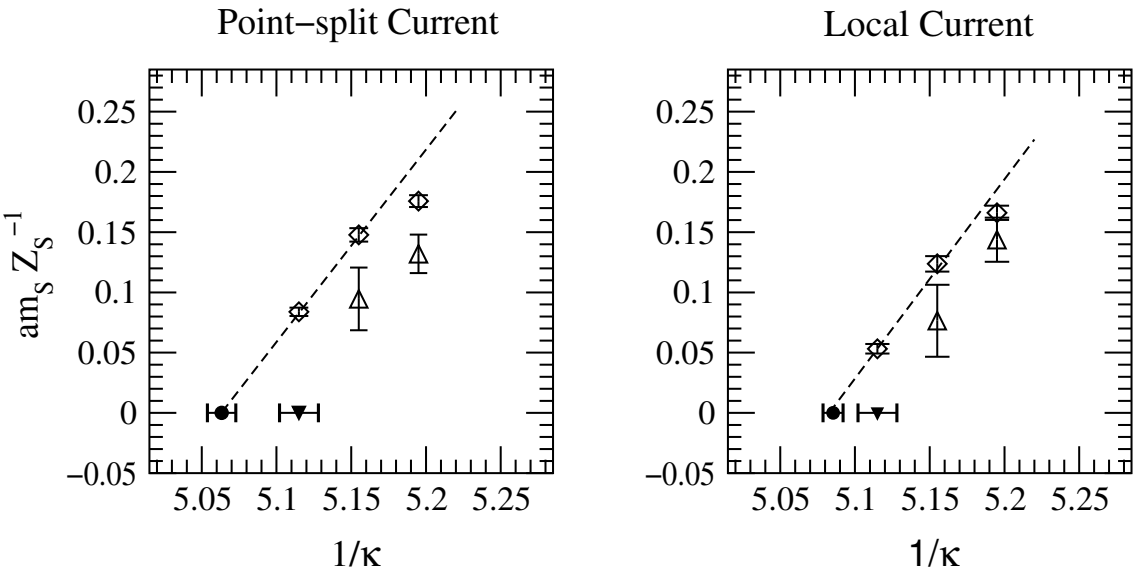

Figure 3.10: $\frac{am_S}{Z_S}$ *as a function of* $1/\kappa$ *with the insertion operator* $\chi^{(sp)}(x)$ *(diamonds) and* $T_0^{(loc)}(x)$ *(triangles). A linear extrapolation is also reported. The filled triangle indicates the determination of* κ_{crit} *from the first order phase transition of [22].*

As a conclusion of this study of the SUSY Ward identity we can say that the results for $\frac{am_S}{Z_S}$ and $\frac{Z_T}{Z_S}$ agree with the Ward identity (3.39) up to $\mathcal{O}(a)$ effects that are comparable in size to the statistical errors. This gives a strong indication that with the parameters chosen for this work it is possible to simulate the $N = 1$ supersymmetric Yang-Mills theory on the lattice in such a way that supersymmetry is recovered in the continuum limit. Of course for a final answer of that question the continuum extrapolation has to be performed, and hence simulations at different β values would be needed.

Table 3.3: *Summary of the results for* $\frac{am_S}{Z_S}$ *at* $\beta = 2.3$ *with point-split currents.*

κ	operator	$t_{min} = 3$	$t_{min} = 4$	$t_{\min} = 5$
0.1925	$\chi^{(sp)}$	0.176(5)	0.166(10)	0.135(14)
0.1925	$T_0^{(loc)}$		0.132(16)	0.124(21)
0.194	$\chi^{(sp)}$	0.148(6)	0.130(11)	0.146(21)
0.194	$T_0^{(loc)}$		0.095(27)	0.090(27)
0.1955	$\chi^{(sp)}$	0.0839(35)	0.0820(7)	0.053(14)

Table 3.4: *Summary of the results for* $\frac{am_S}{Z_S}$ *at* $\beta = 2.3$ *with local currents.*

κ	operator	$t_{min} = 3$	$t_{min} = 4$	$t_{\min} = 5$
0.1925	$\chi^{(sp)}$	0.166(6)	0.166(11)	0.146(16)
0.1925	$T_0^{(loc)}$		0.144(18)	0.143(25)
0.194	$\chi^{(sp)}$	0.124(6)	0.126(12)	0.142(24)
0.194	$T_0^{(loc)}$		0.076(30)	0.098(35)
0.1955	$\chi^{(sp)}$	0.0532(40)	0.064(8)	0.047(15)

Table 3.5: *Summary of the results for* $\frac{Z_T}{Z_S}$ *at* $\beta = 2.3$ *with point-split currents.*

κ	operator	$t_{min} = 3$	$t_{min} = 4$	$t_{\min} = 5$
0.1925	$\chi^{(sp)}$	−0.015(19)	−0.036(31)	0.045(56)
0.1925	$T_0^{(loc)}$		0.11(7)	−0.03(7)
0.194	$\chi^{(sp)}$	−0.038(19)	−0.024(43)	−0.08(7)
0.194	$T_0^{(loc)}$		0.11(13)	0.02(13)
0.1955	$\chi^{(sp)}$	−0.051(13)	−0.064(26)	−0.05(5)

Table 3.6: *Summary of the results for* $\frac{Z_T}{Z_S}$ *at* $\beta = 2.3$ *with local currents.*

κ	operator	$t_{min} = 3$	$t_{min} = 4$	$t_{\min} = 5$
0.1925	$\chi^{(sp)}$	0.183(14)	0.207(27)	0.19(5)
0.1925	$T_0^{(loc)}$		0.29(6)	0.22(6)
0.194	$\chi^{(sp)}$	0.202(15)	0.176(33)	0.186(6)
0.194	$T_0^{(loc)}$		0.27(9)	0.30(11)
0.1955	$\chi^{(sp)}$	0.179(10)	0.170(21)	0.170(45)

Chapter 4

Dynamical domain wall fermions

When putting fermions naively on the lattice the resulting continuum theory has 2^d fermion species for every original one, with d being the dimension of space-time. This is the famous Nielsen-Ninomiya no-go theorem [2], according to which every free fermion lattice Hamiltonian which satisfies some mild assumptions suffers from the effect of fermion species doubling. So far we have treated this problem by giving the unwanted species a heavy mass of the size of the cutoff. This is the approach proposed already by Wilson in his original work [1]. Another approach are staggered fermions proposed by Kogut and Susskind [115]. Both approaches have in common that some parts of the $SU(N_f) \otimes SU(N_f)$ chiral flavour symmetry are broken for any non-zero lattice spacing a. With Wilson fermions this has as a result that the fermion mass aquires an additive renormalization. When going to the continuum limit this makes it necessary to fine tune the fermion mass. This is a complicated and unwanted procedure, but it is generally assumed that we recover the correct continuum target theory so this procedure was accepted for a long time.

However, the price for these kind of fermions is quite high. The degree of restoration of the chiral symmetry is directly related to how close we went towards the continuum. But going a factor of two closer to the continuum is very costly. There is the obvious factor of 2^4 due to the increased number of lattice points, and as seen in chapter 2 there are further costs that are coming from the slowing down of the algorithms. It is usually considered that going down a factor of two in a costs more by a factor of roughly 2^{6-7}.

The situation has changed and there are now many ways to realize fermions with improved chiral properties, see [116] for a list of them. A very interesting approach is to enlarge the four-dimensional lattice in a fifth dimension. The gauge fields are defined independent of this fifth dimension and the fermions can be constructed such that, although all fermion species are heavy, two chiral states appear that are exponentially bounded to the boundaries in the fifth dimension, the so-called domain walls. This approach to the problem of species doubling is called domain wall fermions. With them the continuum limit is disentangled from the chiral limit. For the limit of vanishing lattice spacing in the fifth dimension it has been shown [117–119] that the domain wall fermion formulation is equivalent to the overlap formulation [120–123] where the Ginsparg-Wilson relation [124] for lattice chiral symmetry [125] is fulfilled.

This is a very promising approach. Therefore we want to have a first look at these domain wall fermions in this chapter, although one has to be aware that the computational cost increases by the additional dimension. However, due to the improved chiral properties

the effect on the total costs might be less severe. But even if that is too optimistic the chiral properties make it worthwhile to study this approach. In section 4.1 we will introduce the model as it will be used in our study. The implementation with the TSMB algorithm is discussed in section 4.2 with some exploratory studies started in section 4.3. Domain wall fermions can be used for many other theories, too, e. g. the $N = 1$ Super Yang-Mills theory as discussed in chapter 3. Some of the literature on this topic is discussed in section 4.4.

4.1 Shamir's formulation

We will now construct the fermion action. This is done according to the prescription of Shamir [126]. An outline of this project is given in [127, 128].

The domain walls were originally introduced by Kaplan [129, 130], were further developed by Neuberger and Narayanan [120–123] and then by Shamir and Furman [126, 131]. The fermion fields are defined on a five dimensional space-time lattice with a fifth dimension of even size N_s and free boundary conditions of the Dirac operator along that dimension. With (x, s) being a point on the five dimensional lattice and s being the coordinate in the fifth dimension the link variables obey $U_\mu(x, s) = U_\mu(x)$ independently of s and $U_5(x, s) = 1$. It is therefore natural to interpret the additional dimension as an internal flavour space. The fermion part of the action is given by

$$S_F[U, \bar{\psi}, \psi] = \sum_{x,s;x',s'} \bar{\psi}(x, s) D_F(x, s; x', s') \psi(x', s'), \tag{4.1}$$

with the domain wall fermion Dirac operator

$$D_F(x, s; x', s') = \delta_{s,s'} D_{x,x'} + D^{\perp}_{s,s'} \delta_{x,x'} \tag{4.2}$$

constructed from the standard four dimensional Wilson fermion matrix

$$D_{x,x'} = \delta_{x,x'} (4 - am_0) - \frac{1}{2} \sum_{\mu=1}^{4} \left(\delta_{x',x+\hat{\mu}} (1 + \gamma_\mu) U_{x,\mu} + \delta_{x'+\hat{\mu},x} (1 - \gamma_\mu) U^{\dagger}_{x',\mu} \right) \tag{4.3}$$

and

$$D^{\perp}_{s,s'} = \begin{cases} -\sigma P_L \delta_{s',2} + a m_f P_R \delta_{s',N_s} + \sigma \delta_{s',1} & s = 1 \\ -\sigma P_L \delta_{s+1,s'} - \sigma P_R \delta_{s-1,s'} + \sigma \delta_{s,s'} & 1 < s < N_s \\ +a m_f P_L \delta_{s',1} - \sigma P_R \delta_{s',N_s} + \sigma \delta_{s',N_s} & s = N_s \end{cases} . \tag{4.4}$$

The bare fermion mass of the light boundary fermion is given by m_f, $-m_0$ is a five-dimensional mass representing the "height" of the domain wall and should be chosen as negative. The lattice spacing in the fifth dimension a_s relative to a is given by $\sigma \equiv \frac{a}{a_s}$. Furthermore the right-handed and left-handed chiral projectors are given by

$$P_{R,L} = \frac{1}{2} (1 \pm \gamma_5) . \tag{4.5}$$

The theory with a standard gauge action and this fermion action shows remarkable features. The two chiral components of the Dirac fermion are bound exponentially to the two domain walls, i. e. all correlation functions tend towards their limit like e^{-N_s} [126]. Due to this limiting behaviour small N_s are expected to be enough for a sufficient separation

between the two chiral modes. For $N_s = \infty$ chiral symmetry is exact already at non-zero lattice spacing a. This has the advantage that the continuum limit $a \to 0$ and the chiral limit $N_s \to \infty$ no longer have to be realized simultaneously and the costs to achieve the chiral limit increases only linearly with N_s.

For $m_f = 0$ there is a left-handed fermion near the boundary $s = 1$ and a right-handed fermion near the boundary $s = N_s$. They describe the N_f quarks. If the exponential overlap between the two fermion states is neglected these states describe massless quarks. For finite N_s or when setting $m_f \neq 0$ the right-handed and left-handed components of the quarks are mixed and they get an effective mass

$$m_{eff} = m_0(2 - m_0)\left(m_f + (1 - m_0)^{N_s}\right), \qquad 0 < m_0 < 2 \tag{4.6}$$

in the free theory. Obviously $m_0 = 1$ would be optimal to surpress finite N_s effects to the effective mass. In the interacting theory there might be no optimal value due to fluctuations in m_0, but $m_0 = 1.9$ is a widely used choice.

Besides the wanted light fermion there are $N_s - 1$ four dimensional fields with a heavy mass at the order of the cutoff. As with usual Wilson fermions these heavy fields should decouple from the dynamics in the continuum limit because the effect should be local. This indeed is true for small N_s, but as N_s is increased towards the chiral limit the heavy modes might introduce bulk effects because they could contribute to the effective action $S_{eff}[U]$. Therefore these effects have to be subtracted. This is done by the introduction of bosonic Pauli-Villars type fields [131]. Although their action is non-negative these fields are simply called Pauli-Villars fields in the domain wall fermions literature and we will follow that terminology.

The action for the Pauli-Villars field in case of $N_f = 2$ flavours is given by

$$S_{PV} = \sum_{x,s;x',s';x'',s''} \phi^\dagger_{x'',s''} D^\dagger_{F\,x'',s'';x',s'}(am_f = 1) D_{F\,x',s';x,s}(am_f = 1) \phi_{x,s} \tag{4.7}$$

and the integration over the Pauli-Villars fields results in

$$\int \mathcal{D}[\phi^\dagger]\mathcal{D}[\phi] e^{-S_{PV}} = \frac{1}{\left(\det D_F(am_f = 1)\right)^2}. \tag{4.8}$$

The extention to general fermion flavours N_f goes as for the physical fermions.

The complete action is given by

$$S = S_G[U] + S_F[U, \bar{\psi}, \psi] + S_{PV}[U, \phi^\dagger, \phi]. \tag{4.9}$$

This is the common formulation of domain wall fermions today. Quark operators can be defined as

$$q_x = P_L \psi_{x,s=1} + P_R \psi_{x,s=N_s}, \tag{4.10}$$

$$\bar{q}_x = \bar{\psi}_{x,s=N_s} P_L + \bar{\psi}_{x,s=1} P_R. \tag{4.11}$$

This definition has some finite overlap with the surface states in the chiral limit $N_s \to \infty$ and hence is a possible definition for the quark operators. Indeed this is the simplest possible choice and is used most of the time.

4.2 Domain wall fermions with the TSMB algorithm

We now turn to the use of the TSMB algorithm for domain wall fermions. Most of the simulations done so far are in the quenched regime, and there are few with dynamical fermions. Usually they use the HMC or the HMD-R algorithm. We believe that one can benefit from the good scaling behaviour and the easy extension to odd fermion flavours of the TSMB algorithm. We further believe that it is possible to use dynamical domain wall fermions with the computer power that is available today, because there are arguments that predict the possibility to use coarse lattices (large a_s) and small extensions (small N_s) in the fifth dimension [132]. A detailed description of the TSMB algorithm for domain wall quarks is given in [127].

The domain wall fermion matrix (4.2) satisfies

$$D_F^\dagger = \gamma_5 R_5 D_F \gamma_5 R_5, \tag{4.12}$$

with

$$(R_5)_{s,s'} \equiv \delta_{s',N_s+1-s}\,, \qquad 1 \le s \le N_s \tag{4.13}$$

being the reflection in the fifth dimension. Therefore D_F is not hermitean as needed for the TSMB algorithm. But as with standard Wilson fermions we can define a hermitean version of the fermion matrix

$$\tilde{D}_F = \gamma_5 R_5 D_F. \tag{4.14}$$

With this the fermion measure is

$$\int \mathcal{D}[\bar{\psi}]\mathcal{D}[\psi] e^{-S_F} = \left(\det \tilde{D}_F^2\right)^{\frac{N_f}{2}}, \tag{4.15}$$

and the measure for the Pauli-Villars field can be written in $\tilde{D}_F$ as

$$\int \mathcal{D}[\phi^\dagger]\mathcal{D}[\phi] e^{-S_{PV}} = \frac{1}{\left(\det \tilde{D}_F^2(am_f = 1)\right)^{\frac{N_f}{2}}}. \tag{4.16}$$

Having written both measures in this way it is straightforward to apply the TSMB algorithm along the lines of section 1.3, where the Pauli-Villars fields are described by negative flavour numbers. Actually for even N_f it is very easy to approximate the Pauli-Villars fields, since a polynomial with order $n_1 = \frac{N_f}{2}$ is already exact. An advantage of the TSMB algorithm is that odd flavour numbers can be used without further difficulties, only the polynomial order has to be increased to approximate the requested root.

In general with the TSMB the sign of the determinant needs a special treatment. With domain wall fermions, however, this sign is expected to be irrelevant due to relations between domain wall fermions and the overlap fermions, where a positive determinant is expected for positive mass m_f [117–119].

For some computers it might be a problem that for an implementation of the domain wall fermions all bosonic fields need N_s times more memory due to the fifth dimension and because the memory requirement of the TSMB algorithm is dominated by these fields. However, a closer look reveals that this is no real concern. It is still possible to write the gauge action according to (1.69) and (1.70), see [127]. With this it is possible to keep the

Table 4.1: *Polynomial parameters of the simulations on a $8^3 \cdot 4$ lattice for different lattice spacings and extensions of the fifth dimension.*

σ	N_s	n_1	n_2	n_3	n_4	ε	λ
1.0	8	44	240	300	300	$1.1 \cdot 10^{-2}$	56.0
1.0	12	56	300	450	470	$7.1 \cdot 10^{-3}$	57.0
1.0	16	64	350	470	500	$5.2 \cdot 10^{-3}$	58.0
1.0	24	72	450	640	640	$3.2 \cdot 10^{-3}$	59.0
0.5	6	48	270	350	360	$7.1 \cdot 10^{-3}$	43.0
0.5	12	64	400	570	570	$4.6 \cdot 10^{-3}$	44.0

multi-boson fields on disk reading and writing them one after the other whenever they are updated. In this way memory is no bottleneck for the algorithm, and the time requirement for disk access is negligible compared to the time of the updates. Organized that way the TSMB algorithm has a rather low storage requirement, even for domain wall fermions.

4.3 First exploratory studies

At the beginning of this exploratory study of dynamical domain wall fermions we have chosen to use two degenerate quark flavours on a $8^3 \cdot 4$ lattice, and the parameters are chosen close to the $N_t = 4$ thermodynamic phase transition. The parameters are taken from the set considered in [133]. Typical parameters were $am_0 = 1.9$, $am_f = 0.1$, $\sigma \in \{1.0, 0.5\}$ and $5.2 \leq \beta \leq 5.45$.

In a first step the necessary polynomials have to be found for different values of N_s. Results are shown in table 4.1. Due to the even number of fermion flavours no polynomial is needed for the Pauli-Villars fields. However, their polynomial orders would be much lower than for the boson fields anyway, because for them the mass is fixed at $am_f = 1$. The results from table 4.1 enable a first prediction of the cost dependence on N_s. First of all it has to be noticed that the costs in MVMs for one update cycle increase somewhat faster than $\sqrt{N_s}$. Furthermore the first polynomial order is found to increase like that. With the general experience that the autocorrelation τ_{int} in update cycles increases roughly as n_1 and the fact that the time for one MVM is directly linearly to N_s we find, that the necessary computation work increases roughly as N_s^2 or N_s^3. This fast increase favours settings with small N_s, where the lattice spacing is chosen smaller than usual, namely $\sigma < 1$ [132, 134, 135].

As these test runs show it is possible to simulate dynamical domain wall fermions with the TSMB algorithm. So the next step is to check the improved chiral properties that are claimed to show up in the limit of large N_s. From quenched studies [46] it is known that the improved chiral properties show up only if the four-dimensional fermion matrix D does not have very small eigenvalues, i. e. a gap near zero should be realized in the spectrum of $\tilde{D} = \gamma_5 D$. In our unquenched simulation tests such a gap was not found, see figure 4.1. Maybe the lattice spacing in the fifth dimension is too large, and furthermore larger values of N_s could help. The spectral flow of the domain wall fermion matrix D_F

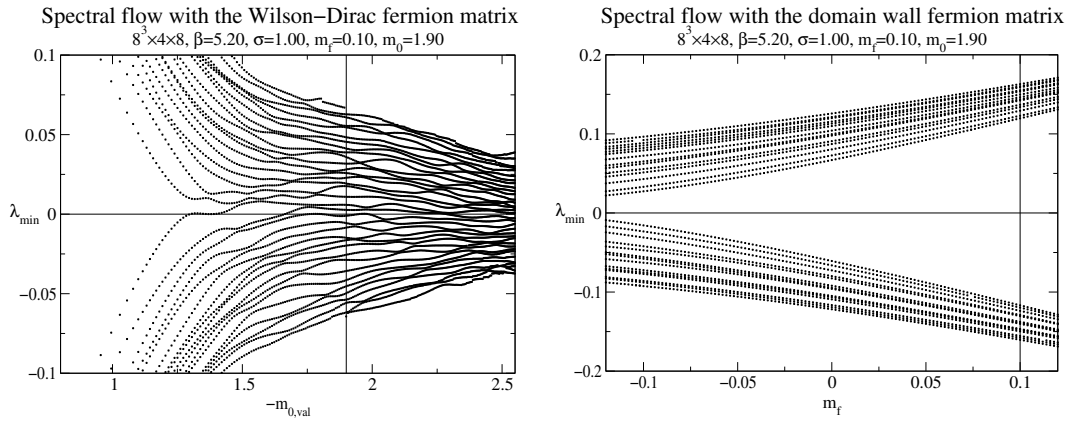

Figure 4.1: *Left panel: Eigenvalue flow for the hermitean Wilson-Dirac matrix. Right panel: Eigenvalue flow for the hermitean domain wall fermion matrix. In both cases the vertical line indicates the mass parameter of the simulation.*

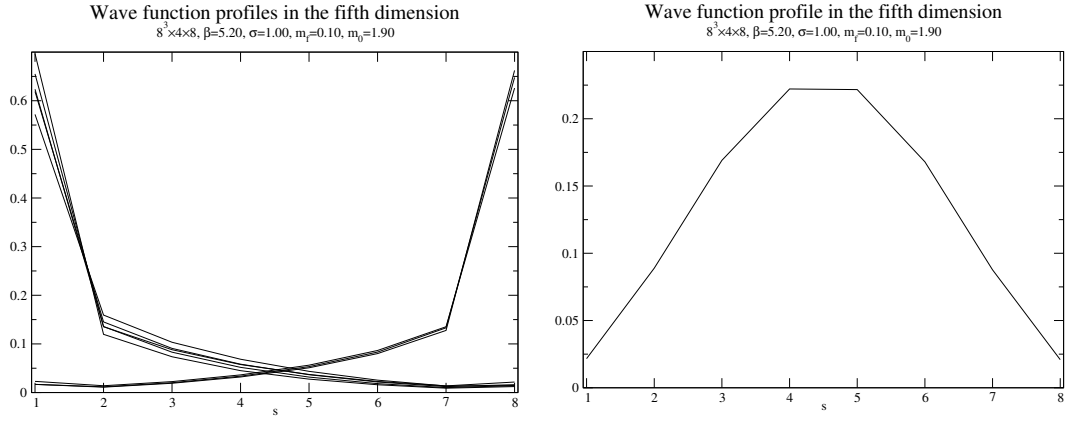

Figure 4.2: *Left panel: Wave function profiles for the eigenstates of D_F corresponding to the eight smallest eigenvalues. Right panel: Wave function profile for the eigenstates of D_F corresponding to the largest eigenvalue.*

is shown in figure 4.1.

Although the parameters of the simulations are obviously not yet tuned properly to see the improved chirality it is still possible to investigate features of the domain wall fermion formulation. In figure 4.2 we can see that the wave function of the largest eigenvalue is concentrated around the middle of the fifth dimension, while the smallest eigenvalues are peaked at the domain walls.

A preliminary conclusion of this exploratory study of dynamical domain wall fermions is, that a simulation is feasable from the algorithmic point of view. But at the same time we find that more work is needed in finding the best way to benefit from the domain wall fermion formulation, with possible improvements over the present situation could come from going closer to the continuum limit, by increasing the extension in the extra dimension or by using improved actions.

4.4 Other applications of domain wall fermions

Apart from zero and finite temperature QCD many other works can benefit from the domain wall fermion formalism. For a recent review on the applications see [116].

In [117,136,137] the use of domain wall fermions for supersymmetric theories has been explored, and these ideas have been applied to the case of the $N = 1$ Super-Yang-Mills theory as discussed in chapter 3. Because of the close relation between the two topics we would like to shortly have a look at the study done in [137]. This SUSY theory is softly broken by a gluino mass term, and we have treated this term by tuning κ towards its critical value. In the limit where we reach the critical value the gluino mass vanishes and in the continuum limit supersymmetry is recovered. In sections 3.4 and 3.4.2 we have considered the Ward identity (3.31) to monitor the restoration of supersymmetry, and indeed we found that SUSY-breaking effects decrease when we get closer to the line of massless gluinos, see figure 3.10.

There is obviously a strong relation between the chiral symmetry breaking and the supersymmetry breaking. If we break chiral symmetry and give the gluino some finite mass, then SUSY is broken proportional to this mass term. As we have seen domain wall fermions can help to improve the chiral properties already at non-zero lattice spacing. It is therefore natural to try this method in the $N = 1$ Super-Yang-Mills theory. At $m_f = 0$ and in the limit $N_s \to \infty$ domain wall fermions ensure that the gluinos are massless and the only remaining supersymmetry breaking operators are irrelevant. Hence no fine-tuning is needed and SUSY is recovered in the continuum limit.

One of the interesting questions is how the breaking of supersymmetry as seen in the Ward identity can be controlled by the domain wall fermions. A first analytic study together with some heuristic argumentations was done in [137]. So far they were unable to do the necessary numerical calculations due to the large computational costs. Afterwards they plan to study the spectrum of the theory. At the end it will be interesting to compare their results with the results from using standard Wilson fermions as in chapter 3 [30].

Conclusions

In this thesis QCD and $N = 1$ Super-Yang-Mills theory have been studied, in both cases with the aim of attaining a relatively small fermion mass.

First of all, we have argued that it is important to include the dynamical fermions in so-called unquenched simulations. The reason is that otherwise not all features of the full theory are visible on the lattice. We have further argued that small fermion masses are an important ingredient when trying to reproduce continuum physics. In QCD Stephen Sharpe and Noam Shoresh have estimated that quark masses of roughly a quarter of the strange quark mass are needed to allow extrapolations to smaller masses using chiral perturbation theory [55]. For the $N = 1$ Super-Yang-Mills theory supersymmetry is explicitely broken by the lattice, and it is only recovered in the massless limit.

In the first chapter we outlined two algorithms, the HMC and the TSMB, which allow for the inclusion of dynamical fermions. Since the TSMB algorithm allows small fermion masses, which we were able to verify in this thesis, we opted for this algorithm. We present new considerations about its implementation, including the use of auxiliary fields to speed up the algorithm and the form of the updating sequence to ensure detailed balance. Furthermore, an extention of the TSMB is discussed which enables the simulation of many fermion flavours with different masses. This can also be used for determinant breakup as inspired by [24, 25].

In the second chapter we studied the costs of QCD simulations with two degenerate quark flavours. The costs are parametrized as a formula depending on the quark mass, the volume and the lattice spacing. Such a formula will be helpfull for future simulations when estimating the costs for some desired simulation parameters and deciding if the simulation is feasable with the available computer power. The existing cost estimates are derived at quark masses around that of the strange quark and thus are not reliable when considering the small quark masses which are required for chiral perturbation theory. We find that the costs with the TSMB algorithms grow roughly quadratically with the inverse quark mass when simulating lighter quarks. This cost estimate is based on the decorrelation of the plaquette, for which we found $z_\pi \simeq 4$, where $\frac{z_\pi}{2}$ gives the power dependence of the costs on the quark mass. Looking at the important fermionic sector the even better behaviour $z_\pi \simeq 3$ is found, indicating a fast decorrelation of the pion mass and the minimal eigenvalue of the fermion matrix. In any case our findings are better than previous estimates for other algorithms, where a cubic dependence was expected, i. e. $z_\pi \simeq 6$. Further algorithmic improvements like the determinant breakup were shown to speed up the simulations by another factor of two in one specific simulation point, and further simulations are proposed at lighter quark masses and larger volumes.

As stressed before, small quark masses are important for chiral perturbation theory,

which, in turn, predicts chiral logarithms coming from the next-to-leading order terms. So far these chiral logarithms haven't been found on the lattice. The explanation given for this are the too heavy quarks above half of the strange quark mass. The results from our simulations for the cost estimate can be used for searching for the chiral logarithms down to a sixth of the strange quark mass, and, indeed, we find the expected behaviour for masses below half of the strange quark mass. These findings are very promising, although one should be aware of the coarseness of the lattice. Thus further simulations are needed to go to the continuum limit. If the results of this thesis can be confirmed for smaller lattice spacings, a region will have been found which is both feasable to simulate with the TSMB algorithm, and which allows a reliable extrapolation using chiral perturbation theory.

Our cost formulas can be used to estimate the costs for obtaining 100 independent gauge configurations in different settings. A physically very interesting simulation point would be a $24^3 \cdot 48$ lattice with lattice spacing $a = 0.125\,\mathrm{fm}$ and two degenerate quark fields at roughly a quarter of the strange quark mass. This would correspond to a lattice extension of 3 fm and $Lm_\pi \simeq 6$. The costs for such a simulation with the TSMB would be roughly $9 \cdot 10^{16} - 3 \cdot 10^{18}$ flop, depending on whether one considers the pion mass or the plaquette autocorrelation as relevant. Another interesting simulation point even closer to the continuum limit would be a $32^3 \cdot 64$ lattice with lattice spacing $a = 0.06\,\mathrm{fm}$ at the same quark mass. This would correspond to a lattice extension of roughly 2 fm and $Lm_\pi \simeq 4$. The costs for this simulation would be $6 \cdot 10^{17} - 4 \cdot 10^{19}$ flop. These simulations can therefore be done with roughly $3 - 1300$ sustained GigaflopYears. Note, however, that in these estimates the costs for parameter tuning and reaching equilibrium are neglected. This is justified by the studies in this work where doubling of the lattice was found to be beneficial for the thermalization. In any case the necessary order of magnitude of computer power for such simulations is expected to be available for the lattice community within the next years.

We furthermore investigated the eigenvalue spectrum of the fermion matrix. This contains alot of physically important informations, however, so far lattice results differ from the expected spectrum, which must be obtained at small quark masses close to the continuum limit. Although the lattices we investigated were very coarse the spectrum is still interesting due to the small masses, and indeed we see the expected dependence on the quark mass.

In chapter three we turned towards the $N = 1$ Super-Yang-Mills theory. By looking at the finite temperature phase transitions for $N_t = 4$ and $N_t = 6$ we have shown that previous simulations of this theory were in the confined phase as required. We proceeded with further simulations at even lighter gluino masses. One of the important questions when simulating this theory on the lattice is, whether, indeed, supersymmetry was realized well enough. This is by no means a trivial question, because supersymmetry is broken explicitly on the lattice due to the gluino mass and by lattice artefacts. The supersymmetric Ward identities as a manifestation of supersymmetric invariance are a good tool to answer the question about the realization of supersymmetry on the lattice. We found that the Ward identities hold up to $\mathcal{O}(a)$ effects, and that it is possible to simulate this supersymmetric theory on the lattice with the algorithms and methods used by the DESY-Münster-Roma Collaboration.

In the last chapter we had a look at other formulations of fermions on the lattice. The chosen formulation, the domain wall fermions, adds a fifth dimension to the four-

dimensional lattice, and at infinite extension in the extra dimension exact chiral symmetry is restored, decoupling the chiral from the costly continuum limit. In this formulation chiral fermions are bound exponentially to the surfaces of the fifth dimension. There have been promising results with this formulation in the quenched approximation, and here we started a first exploratory study to include dynamical domain wall fermions with the TSMB algorithm. We have shown that this is feasable, while, however, the improved chiral properties could not yet be found. Larger extensions in the fifth dimension may be necessary, and improved actions may help further. Studies with dynamical domain wall fermions are at the limit of today's computer capacity, but due to their very good chiral properties it is worthwhile to start these simulations.

In the appendices of this thesis we present details on the computer programs used for the updating, and the performance for some computer platforms used are given.

Appendix A

Notations and conventions

A.1 Gamma matrices

The gamma matrices in the Euclidean are related to those in the Minkowskian:

$$\begin{aligned} \gamma_{1,2,3}^{eucl.} &\equiv -i\gamma_{1,2,3}^{mink.} \\ \gamma_4^{eucl.} &\equiv -i\gamma_4^{mink.} \equiv \gamma_0^{mink.}. \end{aligned} \tag{A.1}$$

In the Euclidean they fulfill

$$\gamma_\mu \equiv \gamma_\mu^{eucl.} = \gamma_\mu^\dagger \tag{A.2}$$

and

$$\{\gamma_\mu, \gamma_\nu\} = 2\delta_{\mu\nu}. \tag{A.3}$$

Furthermore we define γ_5 as

$$\gamma_5 = \gamma_1\gamma_2\gamma_3\gamma_4, \tag{A.4}$$

with vanishing anticommutor with the other gamma matrices:

$$\{\gamma_5, \gamma_\mu\} = 0. \tag{A.5}$$

One possible choice for the gamma matrices is

$$\begin{aligned} \gamma_1 &= \begin{pmatrix} 0 & 0 & 0 & -i \\ 0 & 0 & -i & 0 \\ 0 & i & 0 & 0 \\ i & 0 & 0 & 0 \end{pmatrix} & \gamma_2 &= \begin{pmatrix} 0 & 0 & 0 & -1 \\ 0 & 0 & 1 & 0 \\ 0 & 1 & 0 & 0 \\ -1 & 0 & 0 & 0 \end{pmatrix} \\ \gamma_3 &= \begin{pmatrix} 0 & 0 & -i & 0 \\ 0 & 0 & 0 & i \\ i & 0 & 0 & 0 \\ 0 & -i & 0 & 0 \end{pmatrix} & \gamma_4 &= \begin{pmatrix} 0 & 0 & 1 & 0 \\ 0 & 0 & 0 & 1 \\ 1 & 0 & 0 & 0 \\ 0 & 1 & 0 & 0 \end{pmatrix} \end{aligned} \tag{A.6}$$

This is the chiral representation, in which case γ_5 takes the special diagonal form $\gamma_5 = \mathrm{diag}(1, 1, -1, -1)$.

There is an important relation between the gamma matrices to be noted. When running a simulation most of the time is spent on the application of the fermion matrix Q

as defined through (1.8) and (1.9). This requires the computation of $w_\pm = (1 \pm \gamma_\mu)v$ for some Lorentz vector v. Furthermore the hermitean fermion matrix $\tilde{Q} = \gamma_5 Q$ is used, so $w'_\pm = \gamma_5(1 \pm \gamma_\mu)v$ is needed, too. Due to $\gamma_\mu^2 = \mathbb{1}$ we find $w_\pm = \pm\gamma_\mu w_\pm$ and $w'_\pm = \mp\gamma_\mu w'_\pm$. Therefore the different components of the result are not independent and only half of them have to be calculated. Since the calculation of each component requires some $SU(3)$ matrix multiplications the program is speeded up by nearly a factor of two if this "gamma-trick" is exploited.

A.2 Generators of the $SU(N_c)$

The generators T^a, $a = 1, 2, \ldots, N_c^2 - 1$, are hermitean, traceless matrices generating the $SU(N_c)$. They fulfill

$$[T^a, T^b] = i f_{abc} T^c \tag{A.7}$$

$$\{T^a, T^b\} = \frac{1}{N_c}\delta^{ab} + d_{abc} T^c, \tag{A.8}$$

with f_{abc} the totally antisymmetric structure constant and d_{abc} totally symmetric

$$d_{abc} = 2\mathrm{Tr}(\{T^a, T^b\}, T^c). \tag{A.9}$$

A.2.1 Generators for $N_c = 2$

Usually the Pauli matrices

$$\sigma^1 = \begin{pmatrix} 0 & 1 \\ 1 & 0 \end{pmatrix} \qquad \sigma^2 = \begin{pmatrix} 0 & -i \\ i & 0 \end{pmatrix} \qquad \sigma^3 = \begin{pmatrix} 1 & 0 \\ 0 & -1 \end{pmatrix} \tag{A.10}$$

are used for the generators of $SU(2)$:

$$T^a = \frac{1}{2}\sigma^a. \tag{A.11}$$

Commutator and anticommutator for the Pauli matrices are

$$[\sigma^a, \sigma^b] = 2i\epsilon_{abc}\sigma^c \tag{A.12}$$

$$\{\sigma^a, \sigma^b\} = 2\delta^{ab}. \tag{A.13}$$

ϵ_{abc} is the totally antisymmetric third rank tensor completely defined through its antisymmetry and $\epsilon_{123} = 1$. One can read of

$$\begin{aligned} f_{abc} &= \epsilon_{abc} \\ d_{abc} &= 0. \end{aligned} \tag{A.14}$$

A.2.2 Generators for $N_c = 3$

For $N_c = 3$ the generators are defined as

$$T^a = \frac{1}{2}\lambda^a, \tag{A.15}$$

from the Gell-Mann matrices

$$\begin{aligned}
\lambda^i &= \begin{pmatrix} \sigma^i & 0 \\ 0 & 0 \end{pmatrix}, \quad i = 1,2,3 & \lambda^4 &= \begin{pmatrix} 0 & 0 & 1 \\ 0 & 0 & 0 \\ 1 & 0 & 0 \end{pmatrix} \\
\lambda^5 &= \begin{pmatrix} 0 & 0 & -i \\ 0 & 0 & 0 \\ i & 0 & 0 \end{pmatrix} & \lambda^6 &= \begin{pmatrix} 0 & 0 \\ 0 & \sigma^1 \end{pmatrix} \\
\lambda^7 &= \begin{pmatrix} 0 & 0 \\ 0 & \sigma^2 \end{pmatrix} & \lambda^8 &= \tfrac{1}{\sqrt{3}} \begin{pmatrix} 1 & 0 & 0 \\ 0 & 1 & 0 \\ 0 & 0 & -2 \end{pmatrix}.
\end{aligned} \tag{A.16}$$

Therefore f_{abc} and d_{abc} for $N_c = 3$ are completely defined through

$$\begin{aligned}
1 &= f_{123} = 2f_{147} = 2f_{246} = 2f_{257} = 2f_{345} = -2f_{156} = -2f_{367} = \frac{2}{\sqrt{3}} f_{678} \\
\frac{1}{\sqrt{3}} &= d_{118} = d_{228} = d_{388} = -d_{888} \\
-\frac{1}{2\sqrt{3}} &= d_{448} = d_{558} = d_{668} = d_{778} \\
\frac{1}{2} &= d_{146} = d_{157} = d_{247} = d_{256} = d_{344} = d_{355} = -d_{366} = -d_{377}.
\end{aligned} \tag{A.17}$$

Appendix B

Implementation issues and usage notes on the programs

For the studies in this work programs were needed for QCD, for $N = 1$ SYM and for the domain wall fermions. These three programs differ from each other, but the general organization is somewhat similar[1]. We will now discuss the implementation of the QCD program. It is explained what has to be done when using the program to generate configurations, and how to measure quantities on these configurations. The TSMB algorithm needs polynomials for matrices with large condition numbers. The fastest way for generating these polynomials is by using the program `quadropt`, which uses the CLN library (class for large numbers or class library for numbers) [138].

The program we use both for updating the gauge and boson fields and for measurements is `nf3qcd`[2]. The TSMB updates are done according to the description in section 1.4, and some of the theory for the measurements is explained in section 1.5.

The flow of the program may vary depending on the settings in the file `config.dat`, where one can choose between the UPDATE and the MEASUREONLY mode. For the moment we will concentrate on the UPDATE mode.

At startup of the program the fields are initialized. For the gauge field this means that either a hot start is done, i. e. all gauge links are set to random $SU(3)$ matrices, or the field is read from a file, which allows to continue a previous simulation run[3]. The file for the gauge field is named `L:filename`, where `L` stands for the numerical label of the lattice. Usually this label is zero, but when several lattices are running in parallel this label

[1] For QCD we have another version of the code besides the one written in C++. It is written in TAOmille and runs on the APEmille in Zeuthen. Some details of that program are quite different, but the general structure is similar to the C++ code.

[2] The program for $N = 1$ SYM is called `su2sym`, the one for domain wall fermions is called `dwqcd`. The QCD program for the APEmille is called `mbQcd`.

[3] To be precise there is a further alternative for setting the gauge field. There is a routine `Simulation::SetTestFields()`, which sets both the gauge and the boson fields to some predefined values. These predefined values depend on the site and internal indices like the Lorentz, spinor, colour and boson number indices. They don't depend on pseudo-random numbers, i. e. they are the same whenever this routine is called, and more importantly they are independent of the chosen grid that is used for the parallelization. This routine is valueable when debugging problems of the parallelization. Furthermore it can be used to compare the APE program with the C++ program, and comparisons with yet another independent program `wqcdb` written by István Montvay are possible, too.

allows to distinguish the different replicas. This file furthermore contains the status of the pseudo-random number generator and some information about the run parameters. There is a routine to read the boson field from a file, too. However, with the global heatbath (1.77) it is best to generate a new and completely independent boson field at the beginning of the program. This should be done from time to time anyway, and furthermore this is convenient because this removes the need to store these fields, which takes a non-negligible amount of time and disk space.

After the phase of the initialization a test of the chosen polynomials is run. The first applies the first polynomial to a Gaussian random vector and compares the result for the root representation formula and the recursive formula. A further test applies $(\tilde{Q}^2)^{N_f} \left(P^{(2)}_{n_2}(\tilde{Q}^2) P^{(1)}_{n_1}(\tilde{Q}^2) \right)^2$ (or something slightly different in the case of determinant breakup), which should be close to the identity operator, and another test computes the error of the inverse square root represented by the third polynomial $P^{(3)}_{n_3}(\tilde{Q}^2)$. Furthermore a correction step is run without having changed the gauge field. This gives another test of the third polynomial.

Afterwards the fields are updated according to the settings in `config.dat`. For the gauge field heatbath, overrelaxation and N-hit Metropolis updates are available, and before each of them local heatbath and overrelaxation updates for the boson fields are possible. After some number of update cycles a global quasi heatbath can replace the local boson updates to remove the long tail in the autocorrelation. It is always required to perform an even number of updates of one kind due to the way detailed balance is implemented, namely after one update of one kind is done there has to be another one with the path of updates reversed, see section 1.3.2 for more details.

After some update cycles, set through the variable UPDATINGINMEASURING-CYCLES in `config.dat`, a measurement is performed and typically the gauge field is written. This time the gauge field is written in a file `L:G:filename`, where `L` has the same meaning as above and `G` labels the different gauge field files so that they can be stored and found easily. Possible measurements supported by the latest version of the program are the determination of the extremal eigenvalues of $\tilde{Q}^2$, the reweighting factor, the sign of the determinant, Wilson loops, pion and kaon correlators, eigenvalues of the non-hermitean matrix Q, timeslices and spaceslices of plaquettes and other quantities. Usually not all measurements are done during the process of updating. Switching to the MEASUREONLY mode further measurements can be done on the stored gauge fields.

Before the program exists the run statistics are printed out, including the acceptance rates in the correction step and the global quasi heatbath. Furthermore performance results and runtimes are given.

This program contains quite a number of routines, so that the source code now consists of 21650 lines. While most routines have no strong dependence on other parts of the program this is not true for the parallelization, which is spreaded all over the program. Therefore this part requires some further explanation. The parallelization for the matrix vector multiplication is straightforward. There is no assumption on the present status of the vectors, and the matrix routine calls all necessary routines to get the needed data from neighbouring nodes. For the gauge and the boson field the situation is different. Here it is assumed that all first and second neighbours of the active sites are available on the node at all times. In the local updates the new field therefore has to be communicated to the neighbouring nodes. To minimize the overhead for communication as many sites as

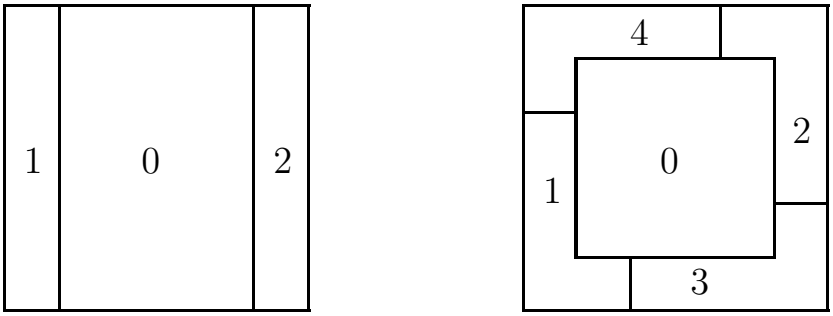

Figure B.1: *Classification of the regions as needed for the local updates. All sites in one region can be updated together, communication with neighbouring nodes is done only when a new region is to be updated. Left panel shows the regions as needed for splitting up one dimension, right panel for two dimensions.*

possible should be communicated together. This is possible by going a path through the lattice with respect to the regions as given in figure B.1.

More details on how to use the program can be found in the subdirectory `doc/`, where a description on how to use the program as a black box is given.

Apart functionality and usability one of the important requirements for a simulation program in lattice field theory is efficiency. As has been discussed in section 2.1 the time needed for the updates and measurements is dominated by the Wilson-Dirac fermion matrix. Performance results for the P4-1700 cluster can be found in tables B.1 and B.2, for the Cray T3E the results are in tables B.3 and B.4. The APE supports only 32 bit precision[4]. Running on one APEmille node the performance is 218 MFlops. This is independent of the lattice size since the APE does not have a cache. When three directions are parallelized, as it is recommended for the APE, the performance due to the overhead from the communication drops to roughly 126 MFlops.

The results for the P4-1700 cluster and the Cray T3E show, that it is always useful to compare the different possibilites of splitting up the lattice before starting a longer simulation in a new setting. Only this way it can be guaranteed that the best performance is achieved. However, there are obviously some guidelines to follow. Of course, the highest performance is achieved if the program runs on only one processor, while the fastest way is usually to run on as many processors as possible. By comparing the times needed for MPI communication, e. g. for 32 bit and 64 bit, we see that the time is roughly proportional to the amount of data to be transfered. This has been achieved by minimizing the latency time of the MPI calls. However, increasing the number of directions to be parallized increases also the latency time. Therefore it is still needed to compare the performance for the different scenarios. This is especially true on the Cray T3E, since the torus structure of the network makes an estimate of the performance more complicated. Furthermore on the Cray the distribution of the program depends on the utilization by programs from other users. This may require several tests before a grid is found that is best on average.

[4]There is an internal type called double on the APEmille which corresponds to 64 bit precision. However, this cannot be used if efficiency is needed. With the double datatype a complex normal operation $a \cdot b + c$ would require four cycles, which has to be compared to just one cycle if the internal 32 bit complex datatype is used. The next version of the APE (apeNEXT) is supposed use 64 bit throughout.

Table B.1: *Performance measurements for the even-odd preconditioned, hermitean Wilson-Dirac fermion matrix $\tilde{\tilde{Q}}$. The lattice size is $12^3 \cdot 24$, results are for the P4-1700 lattice cluster and 64 bit floating point precision. Grid is given in $T[\times Z[\times Y[\times X]]]$.*

CPU grid	Performance [MFlops]	Time for calc. [ms]	Time for MPI [ms]
1	660.6	84.4	0.0
2	526.7	42.2	10.7
3	477.4	28.1	10.8
4	440.9	21.1	10.5
6	383.5	14.1	10.2
8	336.9	10.6	10.1
12	271.4	7.0	10.1
2×2	393.5	21.1	14.3
3×2	358.3	14.1	11.9
2×3	330.5	14.1	14.1
4×2	341.3	10.6	9.9
2×4	293.9	10.6	13.2
3×3	316.4	9.4	10.2
6×2	306.7	7.0	8.1
4×3	298.1	7.0	8.6
8×2	261.4	5.3	8.1
4×4	264.5	5.3	7.9
$2 \times 2 \times 2$	305.7	10.6	12.2
$3 \times 2 \times 2$	288.4	7.0	9.1
$4 \times 2 \times 2$	264.6	5.3	7.9
$2 \times 2 \times 2 \times 2$	240.7	5.3	9.2

Table B.2: *Performance measurements for the even-odd preconditioned, hermitean Wilson-Dirac fermion matrix $\tilde{\tilde{Q}}$. The lattice size is $12^3 \cdot 24$, results are for the P4-1700 lattice cluster and 32 bit floating point precision. Grid is given in $T[\times Z]$.*

CPU grid	Performance [MFlops]	Time for calc. [ms]	Time for MPI [ms]
1	1188.1	46.9	0.0
2	975.1	23.5	5.1
3	855.4	15.6	6.1
4	799.9	11.7	5.7
2×2	710.0	11.7	7.9

Table B.3: *Performance measurements for the even-odd preconditioned, hermitean Wilson-Dirac fermion matrix $\tilde{\tilde{Q}}$. The lattice size is $12^3 \cdot 24$, results are for the Cray T3E-1200 and 64 bit floating point precision. Grid is given in $T[\times Z[\times Y[\times X]]]$.*

CPU grid	Performance [MFlops]	Time for calc. [ms]	Time for MPI [ms]
1	88.9	626.7	0.0
2	80.3	313.4	33.7
3	76.9	208.9	32.6
4	75.2	156.7	28.6
6	70.4	104.5	27.5
8	69.9	78.3	21.3
12	64.4	52.2	19.9
2×2	74.7	156.7	29.7
3×2	71.1	104.5	26.2
2×3	68.2	104.5	31.8
4×2	70.9	78.3	20.0
2×4	65.6	78.3	27.9
3×3	66.3	69.6	23.8
6×2	67.3	52.2	16.8
4×3	65.2	52.2	19.1
8×2	64.5	39.2	14.8
4×4	61.8	39.2	17.2
$2 \times 2 \times 2$	69.4	78.3	22.0
$3 \times 2 \times 2$	66.2	52.2	18.0
$4 \times 2 \times 2$	64.9	39.2	14.5
$2 \times 2 \times 2 \times 2$	63.3	39.2	15.9

Table B.4: *Performance measurements for the even-odd preconditioned, hermitean Wilson-Dirac fermion matrix $\tilde{\tilde{Q}}$. The lattice size is $12^3 \cdot 24$, results are for the Cray T3E-1200 and 32 bit floating point precision. Grid is given in $T[\times Z]$.*

CPU grid	Performance [MFlops]	Time for calc. [ms]	Time for MPI [ms]
1	125.9	442.7	0.0
2	118.1	221.4	14.6
3	110.1	147.6	21.2
4	107.9	110.7	18.4
2×2	104.1	110.7	23.2

Bibliography

[1] K. G. Wilson, Quarks and strings on a lattice, New Phenomena In Subnuclear Physics. Part A. Proceedings of the First Half of the 1975 International School of Subnuclear Physics, Erice, Sicily, July 11 - August 1, 1975, ed. A. Zichichi, Plenum Press, New York, 1977, p. 69, CLNS-321.

[2] H. B. Nielsen and M. Ninomiya, No go theorem for regularizing chiral fermions, *Phys. Lett.* **B105** (1981) 219.

[3] S. Aoki *et al.*, Quenched light hadron spectrum, *Phys. Rev. Lett.* **84** (2000) 238, [*hep-lat/9904012*].

[4] M. Golterman and E. Pallante, On systematic errors due to quenching in ε'/ε, (2002), [*hep-lat/0208069*].

[5] C. J. D. Lin, G. Martinelli, E. Pallante, C. T. Sachrajda and G. Villadoro, Effects of quenching in $\Delta I = 1/2$ kaon decays, (2002), [*hep-lat/0209107*].

[6] N. Metropolis, A. W. Rosenbluth, M. N. Rosenbluth, A. H. Teller and E. Teller, Equation of state calculations by fast computing machines, *J. Chem. Phys.* **21** (1953) 1087.

[7] G. Bhanot, The Metropolis algorithm, *Rept. Prog. Phys.* **51** (1988) 429.

[8] R. T. Scalettar, D. J. Scalapino and R. L. Sugar, New algorithm for the numerical simulation of fermions, *Phys. Rev.* **B34** (1986) 7911.

[9] M. Creutz, Monte Carlo study of quantized $SU(2)$ gauge theory, *Phys. Rev.* **D21** (1980) 2308.

[10] A. D. Kennedy and B. J. Pendleton, Improved heat bath method for Monte Carlo calculations in lattice gauge theories, *Phys. Lett.* **B156** (1985) 393.

[11] S. L. Adler, An overrelaxation method for the Monte Carlo evaluation of the partition function for multiquadratic actions, *Phys. Rev.* **D23** (1981) 2901.

[12] S. L. Adler, Overrelaxation algorithms for lattice field theories, *Phys. Rev.* **D37** (1988) 458.

[13] F. R. Brown and T. J. Woch, Overrelaxed heat bath and Metropolis algorithms for accelerating pure gauge Monte Carlo calculations, *Phys. Rev. Lett.* **58** (1987) 2394.

[14] M. Creutz, Overrelaxation and Monte Carlo simulation, *Phys. Rev.* **D36** (1987) 515.

[15] S. Duane, A. D. Kennedy, B. J. Pendleton and D. Roweth, Hybrid Monte Carlo, *Phys. Lett.* **B195** (1987) 216.

[16] Y. Namekawa *et al.*, Exploring QCD at small sea quark masses with improved Wilson-type quarks, (2002), [*hep-lat/0209073*].

[17] M. Lüscher, A new approach to the problem of dynamical quarks in numerical simulations of lattice QCD, *Nucl. Phys.* **B418** (1994) 637, [*hep-lat/9311007*].

[18] C. Alexandrou, A. Borrelli, P. de Forcrand, A. Galli and F. Jegerlehner, Full QCD with the Lüscher local bosonic action, *Nucl. Phys.* **B456** (1995) 296, [*hep-lat/9506001*].

[19] I. Montvay, An algorithm for gluinos on the lattice, *Nucl. Phys.* **B466** (1996) 259, [*hep-lat/9510042*].

[20] R. V. Gavai, S. Gupta and R. Lacaze, Speed and adaptability of overlap fermion algorithms, (2002), [*hep-lat/0207005*].

[21] R. Frezzotti and K. Jansen, A polynomial hybrid Monte Carlo algorithm, *Phys. Lett.* **B402** (1997) 328, [*hep-lat/9702016*].

[22] R. Kirchner, S. Luckmann, I. Montvay, K. Spanderen and J. Westphalen, Numerical simulation of dynamical gluinos: Experience with a multi-bosonic algorithm and first results, *Nucl. Phys. Proc. Suppl.* **73** (1999) 828, [*hep-lat/9808024*].

[23] F. Farchioni, C. Gebert, I. Montvay and W. Schroers, QCD spectroscopy with three light quarks, *Nucl. Phys. Proc. Suppl.* **106** (2002) 215, [*hep-lat/0110130*].

[24] A. Hasenfratz and A. Alexandru, Evaluating the fermionic determinant of dynamical configurations, *Phys. Rev.* **D65** (2002) 114506, [*hep-lat/0203026*].

[25] A. Alexandru and A. Hasenfratz, Partial-global stochastic Metropolis update for dynamical smeared link fermions, (2002), [*hep-lat/0207014*].

[26] S. Hands *et al.*, Numerical study of dense adjoint matter in two color QCD, *Eur. Phys. J.* **C17** (2000) 285, [*hep-lat/0006018*].

[27] S. Hands, I. Montvay, L. Scorzato and J. Skullerud, Diquark condensation in dense $SU(2)$ matter, *Nucl. Phys. Proc. Suppl.* **106** (2002) 450, [*hep-lat/0110090*].

[28] I. Montvay and G. Münster, Quantum fields on a lattice, Cambridge, UK: Univ. Pr. (1994) 491 p. (Cambridge monographs on mathematical physics).

[29] F. Farchioni, C. Gebert, I. Montvay and L. Scorzato, Numerical simulation tests with light dynamical quarks, *Eur. Phys. J.* **C** (2002), Digital Object Identifier (DOI) 10.1140/epjc/s2002-01057-6, [*hep-lat/0206008*].

[30] I. Campos *et al.*, Monte Carlo simulation of $SU(2)$ Yang-Mills theory with light gluinos, *Eur. Phys. J.* **C11** (1999) 507, [*hep-lat/9903014*].

[31] P. de Forcrand, Monte Carlo Quasi-Heatbath by approximate inversion, *Phys. Rev.* **E59** (1999) 3698, [*cond-mat/9811025*].

[32] B. Jegerlehner, Improvements of the local bosonic algorithm, *Nucl. Phys. Proc. Suppl.* **53** (1997) 959, [*hep-lat/9612013*].

[33] R. Sommer, A new way to set the energy scale in lattice gauge theories and its applications to the static force and α_s in $SU(2)$ Yang-Mills theory, *Nucl. Phys.* **B411** (1994) 839, [*hep-lat/9310022*].

[34] M. Guagnelli, R. Sommer and H. Wittig, Precision computation of a low-energy reference scale in quenched lattice QCD, *Nucl. Phys.* **B535** (1998) 389, [*hep-lat/9806005*].

[35] M. Albanese *et al.*, Glueball masses and string tension in lattice QCD, *Phys. Lett.* **B192** (1987) 163.

[36] C. R. Allton *et al.*, Gauge invariant smearing and matrix correlators using Wilson fermions at $\beta = 6.2$, *Phys. Rev.* **D47** (1993) 5128, [*hep-lat/9303009*].

[37] M. Teper, An improved method for lattice glueball calculations, *Phys. Lett.* **B183** (1987) 345.

[38] E. Eichten, K. Gottfried, T. Kinoshita, K. D. Lane and T.-M. Yan, Charmonium: Comparison with experiment, *Phys. Rev.* **D21** (1980) 203.

[39] J. L. Richardson, The heavy quark potential and the upsilon, J/ψ systems, *Phys. Lett.* **B82** (1979) 272.

[40] C. Michael, Adjoint sources in lattice gauge theory, *Nucl. Phys.* **B259** (1985) 58.

[41] S. Perantonis, A. Huntley and C. Michael, Static potentials from pure $SU(2)$ lattice gauge theory, *Nucl. Phys.* **B326** (1989) 544.

[42] C. R. Allton *et al.*, Effects of non-perturbatively improved dynamical fermions in QCD at fixed lattice spacing, *Phys. Rev.* **D65** (2002) 054502, [*hep-lat/0107021*].

[43] M. Lüscher and U. Wolff, How to calculate the elastic scattering matrix in two-dimensional quantum field theories by numerical simulation, *Nucl. Phys.* **B339** (1990) 222.

[44] R. G. Edwards, U. M. Heller and T. R. Klassen, Accurate scale determinations for the Wilson gauge action, *Nucl. Phys.* **B517** (1998) 377, [*hep-lat/9711003*].

[45] R. M. Baxter *et al.*, Quenched heavy light decay constants, *Phys. Rev.* **D49** (1994) 1594, [*hep-lat/9308020*].

[46] A. Ali Khan *et al.*, Light hadron spectroscopy with two flavors of dynamical quarks on the lattice, *Phys. Rev.* **D65** (2002) 054505, [*hep-lat/0105015*].

[47] R. Frezzotti, M. Hasenbusch, U. Wolff, J. Heitger and K. Jansen, Comparative benchmarks of full QCD algorithms, *Comput. Phys. Commun.* **136** (2001) 1, [*hep-lat/0009027*].

[48] K. G. Wilson, Ab initio quantum chemistry: a source of ideas for lattice gauge theorists, *Nucl. Phys. Proc. Suppl.* **17** (1990) 82.

[49] K. Jansen, Overlap and domain wall fermions: What is the price of chirality?, *Nucl. Phys. Proc. Suppl.* **106** (2002) 191, [*hep-lat/0111062*].

[50] R. Alfieri *et al.*, apeNEXT: A multi-TFlops LQCD computing project, (2001), [*hep-lat/0102011*].

[51] F. Bodin *et al.*, The apeNEXT project, *Nucl. Phys. Proc. Suppl.* **106** (2002) 173, [*hep-lat/0110197*].

[52] D. Chen *et al.*, QCDOC: A 10-teraflops scale computer for lattice QCD, *Nucl. Phys. Proc. Suppl.* **94** (2001) 825, [*hep-lat/0011004*].

[53] P. A. Boyle *et al.*, Status of the QCDOC project, *Nucl. Phys. Proc. Suppl.* **106** (2002) 177, [*hep-lat/0110124*].

[54] J. Gasser and H. Leutwyler, Chiral perturbation theory to one loop, *Ann. Phys.* **158** (1984) 142.

[55] S. R. Sharpe and N. Shoresh, Physical results from unphysical simulations, *Phys. Rev.* **D62** (2000) 094503, [*hep-lat/0006017*].

[56] G. Rupak and N. Shoresh, Chiral perturbation theory for the Wilson lattice action, *Phys. Rev.* **D66** (2002) 054503, [*hep-lat/0201019*].

[57] S. Aoki *et al.*, Exploration of sea quark effects in two-flavor QCD with the $O(a)$-improved Wilson quark action, *Nucl. Phys. Proc. Suppl.* **106** (2002) 224, [*hep-lat/0110179*].

[58] S. Hashimoto *et al.*, Chiral extrapolation of light-light and heavy-light decay constants in unquenched QCD, (2002), [*hep-lat/0209091*].

[59] N. H. Christ, Dynamical fermion simulations, *Nucl. Phys. Proc. Suppl.* **106** (2002) 187.

[60] S. Gottlieb, Cost of dynamical quark simulations with improved staggered quarks, *Nucl. Phys. Proc. Suppl.* **106** (2002) 189, [*hep-lat/0112039*].

[61] T. Lippert, Cost of QCD simulations with $n_f = 2$ dynamical Wilson fermions, *Nucl. Phys. Proc. Suppl.* **106** (2002) 193, [*hep-lat/0203009*].

[62] A. Ukawa, Computational cost of full QCD simulations experienced by CP-PACS and JLQCD Collaborations, *Nucl. Phys. Proc. Suppl.* **106** (2002) 195.

[63] H. Wittig, Cost of dynamical quark simulations: $\mathcal{O}(a)$ improved Wilson fermions, *Nucl. Phys. Proc. Suppl.* **106** (2002) 197, [*hep-lat/0203021*].

[64] T. Lippert, S. Gusken and K. Schilling, About the costs of simulating two-flavour QCD in the deep chiral regime, *Nucl. Phys. Proc. Suppl.* **83** (2000) 182.

[65] F. Farchioni *et al.*, Lattice supersymmetric Ward identities, *Nucl. Phys. Proc. Suppl.* **106** (2002) 938, [*hep-lat/0110110*].

[66] F. Farchioni *et al.*, The supersymmetric Ward identities on the lattice, *Eur. Phys. J.* **C23** (2002) 719, [*hep-lat/0111008*].

[67] R. Gupta *et al.*, QCD with dynamical Wilson fermions, *Phys. Rev.* **D40** (1989) 2072.

[68] K. Bitar, A. D. Kennedy and P. Rossi, The chiral limit and phase structure of QCD with Wilson fermions, *Phys. Lett.* **B234** (1990) 333.

[69] K. M. Bitar *et al.*, Hadron thermodynamics with Wilson quarks, *Phys. Rev.* **D43** (1991) 2396.

[70] Y. Iwasaki, K. Kanaya, S. Sakai and T. Yoshie, Chiral properties of dynamical Wilson quarks at finite temperature, *Phys. Rev. Lett.* **67** (1991) 1494.

[71] T. Blum *et al.*, QCD thermodynamics with Wilson quarks at large kappa, *Phys. Rev.* **D50** (1994) 3377, [*hep-lat/9404006*].

[72] W. Schroers, Advanced algorithms for the simulation of gauge theories with dynamical fermionic degrees of freedom, PhD thesis, University of Wuppertal (2001).

[73] F. Knechtli and U. Wolff, Proof of detailed balance for stochastic Metropolis acceptance, unpublished notes (2002).

[74] M. Hasenbusch, Speeding up finite step-size updating of full QCD on the lattice, *Phys. Rev.* **D59** (1999) 054505, [*hep-lat/9807031*].

[75] F. Farchioni, C. Gebert, I. Montvay and L. Scorzato, Lattice QCD with light dynamical quarks, (2002), [*hep-lat/0209038*].

[76] T. L. Ivanenko and J. W. Negele, Evidence of instanton effects in hadrons from the study of low eigenfunctions of the Dirac operator, *Nucl. Phys. Proc. Suppl.* **63** (1998) 504, [*hep-lat/9709130*].

[77] H. Neff, N. Eicker, T. Lippert, J. W. Negele and K. Schilling, On the low fermionic eigenmode dominance in QCD on the lattice, *Phys. Rev.* **D64** (2001) 114509, [*hep-lat/0106016*].

[78] T. DeGrand and A. Hasenfratz, Density peaks and chiral peaks of fermion eigenmodes in QCD, *Phys. Rev.* **D65** (2002) 014503.

[79] T. G. Kovacs, The topological susceptibility with dynamical overlap fermions, (2001), [*hep-lat/0111021*].

[80] R. Horsley, T. G. Kovacs, V. Linke, D. Pleiter and G. Schierholz, Low-lying fermion modes of $N_f = 2$ improved Wilson fermions, *Nucl. Phys. Proc. Suppl.* **106** (2002) 569, [*hep-lat/0111030*].

[81] T. Kalkreuter and H. Simma, An accelerated conjugate gradient algorithm to compute low lying eigenvalues: A study for the Dirac operator in $SU(2)$ lattice QCD, *Comput. Phys. Commun.* **93** (1996) 33, [*hep-lat/9507023*].

[82] R. B. Lehoucq, D. C. Sorensen and C. Yang, ARPACK Users Guide, (1997), [`http://www.caam.rice.edu/~kristyn/parpack_home.html`].

[83] K. Maschhof and D. C. Sorensen, P_ARPACK, (1996), [`http://www.caam.rice.edu/~kristyn/parpack_home.html`].

[84] A. Pich, Effective field theory, (1998), [*hep-ph/9806303*].

[85] S. Dürr, M_π^2 versus m_q: Comparing CP-PACS and UKQCD data to chiral perturbation theory, (2002), [*hep-lat/0208051*].

[86] S. R. Coleman and J. Mandula, All possible symmetries of the S matrix, *Phys. Rev.* **159** (1967) 1251.

[87] Y. A. Golfand and E. P. Likhtman, Extension of the algebra of Poincaré group generators and violation of P invariance, *JETP Lett.* **13** (1971) 323.

[88] R. Haag, J. T. Lopuszanski and M. Sohnius, All possible generators of supersymmetries of the S matrix, *Nucl. Phys.* **B88** (1975) 257.

[89] J. Wess and B. Zumino, Supergauge transformations in four-dimensions, *Nucl. Phys.* **B70** (1974) 39.

[90] D. Bailin and A. Love, Supersymmetric gauge field theory and string theory, Bristol, UK: IOP (1994) 322 p. (Graduate student series in physics).

[91] J. Bagger and J. Wess, Supersymmetry and supergravity, JHU-TIPAC-9009.

[92] I. L. Buchbinder and S. M. Kuzenko, Ideas and methods of supersymmetry and supergravity: Or a walk through superspace, Bristol, UK: IOP (1998) 656 p.

[93] P. Fayet and S. Ferrara, Supersymmetry, *Phys. Rept.* **32** (1977) 249.

[94] M. F. Sohnius, Introducing supersymmetry, *Phys. Rept.* **128** (1985) 39.

[95] H. Nicolai, A remark on higher order of perturbation theory in Euclidean (super ϕ^3) in four-dimensions, *Nucl. Phys.* **B140** (1978) 294.

[96] P. van Nieuwenhuizen and A. Waldron, On Euclidean spinors and Wick rotations, *Phys. Lett.* **B389** (1996) 29, [*hep-th/9608174*].

[97] R. Kirchner, I. Montvay, J. Westphalen, S. Luckmann and K. Spanderen, Evidence for discrete chiral symmetry breaking in N = 1 supersymmetric Yang-Mills theory, *Phys. Lett.* **B446** (1999) 209, [*hep-lat/9810062*].

[98] A. Feo, R. Kirchner, S. Luckmann, I. Montvay and G. Münster, Numerical simulations of dynamical gluinos in $SU(3)$ Yang-Mills theory: First results, *Nucl. Phys. Proc. Suppl.* **83** (2000) 661, [*hep-lat/9909070*].

[99] I. Montvay, Supersymmetric Yang-Mills theory on the lattice, *Int. J. Mod. Phys.* **A17** (2002) 2377, [*hep-lat/0112007*].

[100] R. Peetz, F. Farchioni, C. Gebert and G. Münster, Spectrum of $SU(2)$ SUSY Yang-Mills theory with a light gluino, (2002), [*hep-lat/0209065*].

[101] H. Neuberger, A practical implementation of the overlap-Dirac operator, *Phys. Rev. Lett.* **81** (1998) 4060, [*hep-lat/9806025*].

[102] J. Engels, F. Karsch, H. Satz and I. Montvay, Gauge field thermodynamics for the $SU(2)$ Yang-Mills system, *Nucl. Phys.* **B205** (1982) 545.

[103] S. Aoki, Phase structure of lattice QCD with Wilson fermion at finite temperature, *Nucl. Phys. Proc. Suppl.* **60A** (1998) 206, [*hep-lat/9707020*].

[104] K. Fujikawa, Path integral measure for gauge invariant fermion theories, *Phys. Rev. Lett.* **42** (1979) 1195.

[105] Y. Taniguchi, One loop calculation of SUSY Ward-Takahashi identity on lattice with Wilson fermion, *Phys. Rev.* **D63** (2001) 014502, [*hep-lat/9906026*].

[106] R. Kirchner, Ward identities and mass spectrum of $N = 1$ Super Yang-Mills Theory on the lattice, PhD thesis, University of Hamburg (2000).

[107] T. Galla, Supersymmetrische und Chirale Ward-Identitäten in einer diskretisierten $N = 1$-SUSY-Yang-Mills-Theorie, Diploma thesis (in german), University of Münster (1999).

[108] C. Gebert, Störungstheoretische Untersuchungen der $N = 1$ supersymmetrischen Yang-Mills-Theorie auf dem Gitter, Diploma thesis (in german), University of Münster (1999).

[109] M. Bochicchio, L. Maiani, G. Martinelli, G. C. Rossi and M. Testa, Chiral symmetry on the lattice with Wilson fermions, *Nucl. Phys.* **B262** (1985) 331.

[110] M. Testa, Some observations on broken symmetries, *JHEP* **04** (1998) 002, [*hep-th/9803147*].

[111] G. Curci and G. Veneziano, Supersymmetry and the lattice: a reconciliation?, *Nucl. Phys.* **B292** (1987) 555.

[112] A. Donini, M. Guagnelli, P. Hernandez and A. Vladikas, Towards $N = 1$ Super-Yang-Mills on the lattice, *Nucl. Phys.* **B523** (1998) 529, [*hep-lat/9710065*].

[113] F. Farchioni *et al.*, On the 1-loop lattice perturbation theory of the supersymmetric Ward identities, *Nucl. Phys. Proc. Suppl.* **94** (2001) 791, [*hep-lat/0011030*].

[114] F. Farchioni *et al.*, SUSY Ward identities in 1-loop perturbation theory, *Nucl. Phys. Proc. Suppl.* **106** (2002) 941, [*hep-lat/0110113*].

[115] J. B. Kogut and L. Susskind, Hamiltonian formulation of Wilson's lattice gauge theories, *Phys. Rev.* **D11** (1975) 395.

[116] P. M. Vranas, Domain wall fermions and applications, *Nucl. Phys. Proc. Suppl.* **94** (2001) 177, [*hep-lat/0011066*].

[117] H. Neuberger, Vector like gauge theories with almost massless fermions on the lattice, *Phys. Rev.* **D57** (1998) 5417, [*hep-lat/9710089*].

[118] Y. Kikukawa and T. Noguchi, Low energy effective action of domain-wall fermion and the Ginsparg-Wilson relation, (1999), [*hep-lat/9902022*].

[119] Y. Kikukawa, Low energy effective action of domain-wall fermion and the Ginsparg-Wilson relation, *Nucl. Phys. Proc. Suppl.* **83** (2000) 630.

[120] R. Narayanan and H. Neuberger, Infinitely many regulator fields for chiral fermions, *Phys. Lett.* **B302** (1993) 62, [*hep-lat/9212019*].

[121] R. Narayanan and H. Neuberger, Chiral fermions on the lattice, *Phys. Rev. Lett.* **71** (1993) 3251, [*hep-lat/9308011*].

[122] R. Narayanan and H. Neuberger, Chiral determinant as an overlap of two vacua, *Nucl. Phys.* **B412** (1994) 574, [*hep-lat/9307006*].

[123] R. Narayanan and H. Neuberger, A construction of lattice chiral gauge theories, *Nucl. Phys.* **B443** (1995) 305, [*hep-th/9411108*].

[124] P. H. Ginsparg and K. G. Wilson, A remnant of chiral symmetry on the lattice, *Phys. Rev.* **D25** (1982) 2649.

[125] M. Lüscher, Exact chiral symmetry on the lattice and the Ginsparg- Wilson relation, *Phys. Lett.* **B428** (1998) 342, [*hep-lat/9802011*].

[126] Y. Shamir, Chiral fermions from lattice boundaries, *Nucl. Phys.* **B406** (1993) 90, [*hep-lat/9303005*].

[127] I. Montvay, Unquenched domain wall quarks with multi-bosons, *Phys. Lett.* **B537** (2002) 69, [*hep-lat/0204019*].

[128] F. Farchioni, C. Gebert, I. Montvay and L. Scorzato, Unquenched domain wall quarks with TSMB, (2002), [*hep-lat/0208064*].

[129] D. B. Kaplan, A method for simulating chiral fermions on the lattice, *Phys. Lett.* **B288** (1992) 342, [*hep-lat/9206013*].

[130] D. B. Kaplan, Chiral fermions on the lattice, *Nucl. Phys. Proc. Suppl.* **30** (1993) 597.

[131] V. Furman and Y. Shamir, Axial symmetries in lattice QCD with Kaplan fermions, *Nucl. Phys.* **B439** (1995) 54, [*hep-lat/9405004*].

[132] Y. Shamir, Dynamical domain-wall fermions with larger a_5 and smaller N_5, unpublished notes (2001).

[133] P. Chen *et al.*, The finite temperature QCD phase transition with domain wall fermions, *Phys. Rev.* **D64** (2001) 014503, [*hep-lat/0006010*].

[134] Y. Shamir, Reducing chiral symmetry violations in lattice QCD with domain-wall fermions, *Phys. Rev.* **D59** (1999) 054506, [*hep-lat/9807012*].

[135] Y. Shamir, New domain-wall fermion actions, *Phys. Rev.* **D62** (2000) 054513, [*hep-lat/0003024*].

[136] D. B. Kaplan and M. Schmaltz, Supersymmetric Yang-Mills theories from domain wall fermions, *Chin. J. Phys.* **38** (2000) 543, [*hep-lat/0002030*].

[137] G. T. Fleming, J. B. Kogut and P. M. Vranas, Super Yang-Mills on the lattice with domain wall fermions, *Phys. Rev.* **D64** (2001) 034510, [*hep-lat/0008009*].

[138] B. Haible, CLN - Class Library for Numbers, [*http://www.ginac.de/CLN*].

Acknowledgments

I would like to thank my supervisor, Dr. István Montvay, for proposing such an interesting topic of this work to me, for his help and encouragement throughout this project, and for the many interesting discussions.

Many thanks go to the members of the DESY-Münster-Roma Collaboration and the qq+q Collaboration, namely Dr. István Montvay, Prof. Dr. Gernot Münster, Prof. Dr. Anastassios "Tassos" Vladikas, Dr. Federico Farchioni, Dr. Robert Kirchner, Dr. Luigi Scorzato, Tobias Galla, Roland Peetz and Enno Scholz, for the numerous discussions and the fruitful collaboration.

It is a pleasure to thank the members of the INFN at the University Tor Vergata at Rome 2 for their hospitality, especially Prof. Dr. Anastassios "Tassos" Vladikas and Prof. Dr. Gian Carlo Rossi for the stimulating discussions around tea (cappuccino) time.

I also like to thank the APE group DESY Zeuthen for their hospitality. I specially thank Hubert Simma and Dirk Pleiter for their friendly help on coding for the APEmille.

Further, I would like to thank all my colleagues at the DESY Theory Group for the pleasant atmosphere, especially Dr. Robert Kirchner, Huitzu Tu and Prof. Dr. Barbara Schrempp, who shared the office with me, and Hartmut Wittig for useful discussions on various topics.

The numerical simulations of this thesis have been performed on the Cray-T3E computers at NIC Jülich, the APEmille installation at DESY Zeuthen and the PC clusters at DESY Hamburg. I thank the respective staff for their kind and competent support.

I am grateful to Jutta Gebert, Nicole Lüdecke, Jan Gleitze, Wilfried Gleitze and Roland Peetz for carefully proofreading first drafts of the manuscript.

I will always remember the great time I had with my teammates at the inofficial DESY-football team, namely Dr. Markos Maniatis, Stefan Berge, Dr. Benedikt "Benno" Plümper, Dr. Stefan Dittmaier, Andre Utermann, Andreas von Manteuffel, Xiang Liu, Asset Barakbaev, Dr. Mauricio Barbi, Dr. Sven Heinemeyer, Dr. Matthias Moritz, Huitzu Tu, Dr. Dominik Stöckinger, Erik Maddox, Dr. Oscar Gonzalez and many others who had time to drop by.

I am grateful to my parents for their continuing support.

Finally, I would like to thank Nina Gleitze for her constant encouragement and support at all stages of the thesis.

Financial support by Deutsches Elektronen-Synchrotron (DESY) is gratefully acknowledged.